

SYNTHESIS AND CHARACTERIZATION OF TiO₂ BASED NANOMATERIALS AND THEIR APPLICATIONS IN WATER PURIFICATION

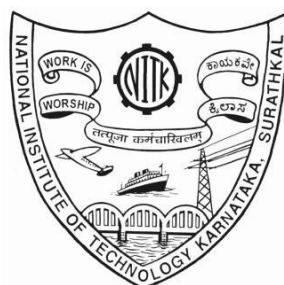
Thesis

Submitted in partial fulfilment of the requirements for the degree of

DOCTOR OF PHILOSOPHY

by

ABHINAV K NAIR



DEPARTMENT OF CHEMICAL ENGINEERING
NATIONAL INSTITUTE OF TECHNOLOGY KARNATAKA,
SURATHKAL, MANGALURU - 575025

September, 2018

DECLARATION

I hereby *declare* that the Research Thesis entitled “Synthesis and characterization of TiO₂ based nanomaterials and their applications in water purification” which is being submitted to the National Institute of Technology Karnataka, Surathkal in partial fulfilment of the requirements for the award of the Degree of Doctor of Philosophy in the Department of Chemical Engineering, is a *bonafide report of the research work carried out by me*. The material contained in this Research Thesis has not been submitted to any University or Institution for the award of any degree.

Place: NITK, Surathkal

Date:

Name: Abhinav K Nair

Register Number: 135020CH13F01

Department of chemical Engineering

CERTIFICATE

This is to certify that the Research Thesis entitled “Synthesis and characterization of TiO₂ based nanomaterials and their applications in water purification” submitted by Mr. Abhinav K Nair (Register Number: 135020CH13F01) as the record of the research work carried out by him, is *accepted as the Research Thesis submission* in partial fulfillment of the requirements for the award of degree of Doctor of Philosophy.

Research Guide

Dr. P E Jagadeesh Babu
Asst. Professor
Dept. of Chemical Engineering
NITK, Surathkal

Chairman - DRPC

ACKNOWLEDGEMENT

Doctorate has been a dream for many years and now after four long years when I stand one step closer to fulfilling that dream my heart fills with gratitude for all those who helped me to endure and live this dream. First and foremost I would like to express my deepest gratitude to my Research Guide Dr. Jagadeesh Babu, Asst. Professor, Department of Chemical Engineering, NITK Surathkal. It was his trust and constant support that enabled me to pursue research with ease. He was not only a research guide but also a kind mentor who always kept his cool even in my failures. It was only because of his genuine consideration that I could balance my research and family life; I thank him from the bottom of my heart.

Secondly, I would like to express gratitude to my RPAC member and former head of department Dr. B. Raj Mohan, for his constant and prompt support even in his busy schedule. I would also like to thank my RPAC member from chemistry department Dr. Udaya Kumar D for his kind and generous support. I thank both my RPAC members for their constructive comments during my presentations which enabled me to speed up my research work.

I humbly express my sincere gratitude to the past and present HODs of Chemical Engineering; Dr Vidya Shetty K, Dr. B. Raj Mohan and Dr. Hari Mahalingam for providing me necessary research facilities. Special thanks to Dr. D. V. R. Murthy and Dr. M. B. Saidutta for their kindness and encouragement. I would also like to thank all the faculty members of the Chemical Engineering Department for their valuable support and encouragement.

I express my sincere gratitude to Prof. K. Narayan Prabhu, Metallurgical and Materials Engineering Department, NITK for providing contact angle measurement facility. I also thank Dr. Anandhan Srinivasan, Metallurgical and Materials Engineering Department, NITK for providing ATR-IR facility. Special thanks to Ms. Rashmi B for SEM analysis.

I take this opportunity to express my sincere gratitude to Mr. Sadashiva, Mrs. Shashikala, Mrs. Thrithilla Shetty, Mr. Suresh, Mr. Ramesh, and all other non-teaching staffs of the department for their support.

I am thankful to all former and current research scholars and PG students of the department for their timely help and support. I owe special thanks to Mr. Rajashekara S, Mr. Gopinath K and Mr. Pragadeesh K S for their wholehearted support and encouragement.

I would like to thank my M.Tech project guide Dr. Arun M Isloor, Department of Chemistry, NITK and his then Ph.D student Dr. Rajesha Kumar for igniting the membranologist in me.

This list of acknowledgement can only capture a small fraction of the people who supported my work, I express my deepest thanks to all, your contribution to my doctoral work was vital.

I am always indebted to my family who encouraged my studies. A big thank you goes to my wife and my grandmother for their great moral support.

Above all, I owe it all to Almighty for giving me the strength, wisdom, and health to carry out and accomplish this research work.

Abhinav K Nair

***DEDICATED TO MY
GURUS***

ABSTRACT

TiO₂ nanoparticles have received great amount of research interest due to their interesting properties like photocatalysis, self-cleaning, super hydrophilicity etc. This work focuses on TiO₂ nanofibers (TNF) and nanosheets (TNS). Hydrothermal technique was used for synthesising both the nanostructures. The nanostructures were used for water purification via two modes: - nanocomposite membrane and photocatalytic hierarchical membranes. As such synthesised TiO₂ nanostructures were blend with polysulfone to form nanocomposite ultrafiltration membranes. Polysulfone (PSF) is a good polymer for membrane synthesis but its hydrophobicity results in greater fouling. The addition of hydrophilic TiO₂ nanostructures can improve the hydrophilicity and enhance the membrane performance. TNF were incorporated in PSF along with polyethylene glycol as a pore former. The novel membranes showed high flux and superior antifouling properties. Highest performance was observed at 10 wt% addition of TNF. TNS was also incorporated in PSF and the membranes were used for rejection of dyes. Best performance for congo red dye rejection was observed at 12-15 wt% addition of TNS. For rhodamine-B dye best performance was observed at 7-10 wt% addition of TNS. Apart from ultrafiltration membranes, the photocatalytic activity of the TiO₂ nanostructures were also studied and applied for water treatment. Hierarchical membranes (HM) were synthesised using these nanostructures along with modifiers like silver (Ag) & graphene oxide (GO). TNF was doped with Ag to improve their photocatalytic activity and used for synthesizing hierarchical membrane for dye degradation. The Ag-TNS membranes showed good degradation for rhodamine-B dye.

TNS had shown better photocatalytic activity during preliminary studies, hence they were used extensively for making photocatalytic hierarchical membranes. TNS was modified with GO to form a composite and used for hierarchical membrane synthesis. The membranes exhibited very good dye removal capabilities. Similarly Ag was also used as a modifier for TNS and applied in hierarchical membranes. The membranes showed good congo red dye removal capacity and also exhibited potential to work under solar radiation. The capability to photo degrade under solar radiation was further explored by synthesising a floating photocatalyst by coating low density polyethylene beads with a composite film of Ag-TNS in PSF. The beads showed appreciable photo degradation of congo red dye under sun light.

Keywords: TiO₂ nanofibers, TiO₂ nanosheets, Polysulfone, Silver, Graphene oxide, Nanocomposite membrane, Photocatalysis, Hierarchical membrane

CONTENTS

1. INTRODUCTION	1
1.1. POLYMER NANOCOMPOSITE MEMBRANES	4
1.1.1 Types of membrane filtration	4
1.1.2 Membrane fouling	5
1.1.3 Polysulfone	6
1.1.4 Improving hydrophilicity	7
1.1.5 TiO ₂ nanomaterials as membrane additives	7
1.2. PHOTOCATALYTIC MEMBRANE REACTORS	7
1.2.1 Nanocatalyst based membrane reactor	8
1.2.2 TiO ₂ nanomaterials based hierarchical membranes	9
2. LITERATURE REVIEW	11
2.1 SYNTHESIS OF TiO ₂ BASED MEMBRANES	11
2.2 HIERARCHICAL ASSEMBLY OF PHOTOCATALYST ON POLYMER MEMBRANES	18
2.3 ENHANCED PHOTOCATALYTIC ACTIVITY OF TITANIA OF TiO ₂ NANOMATERIALS	21
2.4 POLYMER COMPOSITE MEMBRANES	22
2.5 SCOPE AND OBJECTIVES OF THE RESEARCH WORK	26
3. SYNTHESIS OF TiO₂ NANOSTRUCTURES	27
3.1 INTRODUCTION	27
3.2 SYNTHESIS OF TNF	27
3.2.1 Materials	27
3.2.2 Hydrothermal synthesis of TNF	27
3.3 SYNTHESIS OF TNS	28
3.3.1. Materials	28
3.3.2. Hydrothermal synthesis of TNF	28
3.4 CHARACTERISATION OF TiO ₂ NANOMATERIALS	28
3.4.1. Photocatalytic activity	28
3.5 RESULTS AND DISCUSSION	29

4. TNF/PSF NANOCOMPOSITE UF MEMBRANE	32
4.1 INTRODUCTION	32
4.2 EXPERIMENTAL	33
4.2.1 Materials	33
4.2.2 Preparation of TNF incorporated PSF membranes	33
4.3 CHARACTERIZATION	34
4.3.1. ATR-IR analysis	34
4.3.2. XRD analysis	34
4.3.3. SEM analysis	34
4.3.4. Contact angle measurement	34
4.3.5. Permeation properties	34
4.3.6. Antifouling properties	35
4.4 RESULTS AND DISCUSSION	35
4.4.1. Membrane characterization	35
4.4.1.1. ATR-IR analysis	35
4.4.1.2. XRD analysis	38
4.4.1.3. Morphology of the membrane	38
4.4.1.4. Hydrophilicity of membranes	42
4.4.1.5. Membrane permeability and antifouling properties	43
4.5 CONCLUSION	46
5. Ag-TiO₂ NANOFIBER MEMBRANE FOR PHOTOCATALYTIC DEGRADATION OF DYES	47
5.1 INTRODUCTION	47
5.2 EXPERIMENTAL	48
5.2.1 Materials	48
5.2.2 Synthesis of Ag-TNF composite	48
5.2.3 Synthesis of Ag-TNF hierarchical membrane	48
5.3 CHARACTERIZATION	49
5.4 RESULTS AND DISCUSSION	50
5.5 CONCLUSION	57
6. TiO₂ NANOSHEET INCORPORATED PSF NANOCOMPOSITE UF MEMBRANES FOR DYE REMOVAL	59
6.1 INTRODUCTION	59

6.2 EXPERIMENTAL	60
6.2.1 Materials	60
6.2.2 Preparation of TNS incorporated PSF membranes	60
6.3 CHARACTERIZATION	60
6.3.1. XRD analysis	60
6.3.2. SEM analysis	61
6.3.3. TEM analysis	61
6.3.4. Contact angle measurement	61
6.3.5. Permeation properties	61
6.3.6. Antifouling properties	61
6.3.7. Dye rejection study	62
6.4 RESULTS AND DISCUSSION	62
6.4.1. Membrane characterization	62
6.4.1.1. XRD analysis	62
6.4.1.2. Morphology of the membrane	63
6.4.1.3. Hydrophilicity of membranes	68
6.4.1.4. Membrane permeability and antifouling properties	69
6.4.1.5. Dye rejection	73
6.5 CONCLUSION	76
7. TNS-GO PHOTOCATALYTIC HIERARCHICAL MEMBRANE FOR WATER PURIFICATION	77
7.1 INTRODUCTION	77
7.2 EXPERIMENTAL	77
7.2.1 Materials	77
7.2.2 Synthesis of TNS-GO	78
7.2.3 Synthesis of photocatalyst coated HM	78
7.2.4 Characterization	78
7.2.5 Performance study of membranes	78
7.3 RESULTS AND DISCUSSION	79
7.3.1 Characterization of TNS	79
7.3.2. Characterization of TNS-GO HM	81
7.3.3 Performance study of TNS-GO membranes	82
7.4 CONCLUSION	86

8. Ag-TiO₂ NANOSHEET PHOTOCATALYTIC HIERARCHICAL MEMBRANE FOR SOLAR WATER TREATMENT	87
8.1 INTRODUCTION	87
8.2 MATERIALS AND METHODS	88
8.2.1 Materials	88
8.2.2 Synthesis of Ag-TNS composite	88
8.2.3 Synthesis of Ag-TNS HM	88
8.3 CHARACTERIZATION	88
8.3.1. XRD analysis	88
8.3.2. SEM analysis	89
8.3.3. TEM analysis	89
8.3.4 Performance study of membranes under UV radiation	89
8.3.5 Performance study of membranes under solar radiation	89
8.4 RESULTS AND DISCUSSION	90
8.4.1 Characterization of Ag-TNS	90
8.4.2. Characterization of Ag-TNS HM	94
8.5 CONCLUSION	101
9. Ag-TNF/PSF NANOCOMPOSITE FLOATING PHOTOCATALYSTS FOR SOLAR DEGRADATION OF POLLUTANTS	102
9.1 INTRODUCTION	102
9.2 EXPERIMENTAL METHODS	102
9.2.1 Materials	102
9.2.2 Preparation of Ag-TNS/PSF floating photocatalyst	103
9.3 CHARACTERIZATION	103
9.3.1. XRD analysis	103
9.3.2. FESEM analysis	103
9.3.3. Dye degradation studies	103
9.4 RESULTS AND DISCUSSION	104
9.4.1. Characterization of Ag-TNS	104
9.4.2. XRD analysis	106
9.4.3. Characterization of Ag-TNS/PSF coated LDPE bead	107
9.5 CONCLUSION	111

SUMMARY AND CONCLUSIONS	112
SCOPE FOR FUTURE WORK	113
APPENDIX	114
REFERENCES	116
PUBLICATIONS	126
BIO-DATA	128

LIST OF FIGURES

Figure No.	Title	Page No.
Figure 1.1	Schematic representation of membrane fouling	6
Figure 1.2	Schematic representation of photocatalytic membrane reactor	8
Figure 3.1	The schematic diagram of the experimental setup of the photocatalytic reactor	29
Figure 3.2	SEM image of TNF	30
Figure 3.3	TEM image of TNS	30
Figure 3.4	Photocatalytic dye degradation studies of various TiO ₂ nanostructures	31
Figure 4.1	ATR-IR spectra. (a) TNF; (b) M-0; (c) M-10.	36
Figure 4.2	XRD patterns of TNF, PSF, and M-10.	37
Figure 4.3	Cross-sectional SEM images of membranes. (a) M-0; (b) M-1; (c) M-3; (d) M-5; (e) M-10.	38
Figure 4.4	Contact angle measurements of the membranes.	41
Figure 4.5	Permeation and antifouling studies of the membranes. (a) PWF; (b) flux during BSA rejection; (c) flux recovery ratio.	43
Figure 5.1	Schematic representation of membrane testing unit	47
Figure 5.2	Schematic representation of UV irradiated membrane cell	47
Figure 5.3	Sem images of a) Ag-TNF and b) Ag-TNF HM	49
Figure 5.4	XRD of TNF and Ag-TNF	50
Figure 5.5	FTIR spectrum of TNF and Ag-TNF	50
Figure 5.6	EDS spectra of Ag-TNF	51
Figure 5.7	Flux of various membranes	52
Figure 5.8	Dye removal (DR) in presence of UV radiation by various membranes	53
Figure 5.9	Dye removal (DR) in absence of UV radiation by various membranes	53
Figure 5.10	Reuse cycles of the in presence of UV radiation membranes	54
Figure 5.11	Reuse cycles of the in absence of UV radiation membranes	54
Figure 6.1	XRD patterns of S-0, S-10, and TNS.	60

Figure 6.2	SEM images of the membranes. a) S-0, b) S-1, c) S-3, d) S-5, e) S-7, f) S-10, g) S-12, and h) S-15.	64
Figure 6.3	Contact angle measurement of membranes	65
Figure 6.4	PWF of membranes.	66
Figure 6.5	BSA rejection flux of membranes.	67
Figure 6.6	BSA rejection by the membranes.	68
Figure 6.7	Percentage FRR of membranes	69
Figure 6.8	Congo red dye rejection flux of membranes.	69
Figure 6.9	Congo red dye rejection by the membranes.	70
Figure 6.10	Rhodamine B dye rejection flux of membranes.	70
Figure 6.11	Rhodamine-B dye rejection by the membranes.	71
Figure 7.1	a) FESEM image of TNS b) Magnified image FESEM image of TNS	75
Figure 7.2	XRD pattern of TNS	76
Figure 7.3	a) FESEM image of TNS-GO b) SEM image of G-100 membrane cross section	77
Figure 7.4	Tauc plots for band gap estimation of photocatalysts	78
Figure 7.5	Flux of various membranes	79
Figure 7.6	Dye removal (DR) of various membranes in presence of UV radiation	80
Figure 7.7	Dye removal (DR) of various membranes in absence of UV radiation	80
Figure 7.8	Reuse cycles (RC) of the membrane for Dye removal	81
Figure 8.1	Schematic representation of solar water purification setup	86
Figure 8.2	a) SEM image of Ag-TNS b) TEM image of Ag-TNS	87
Figure 8.3	EDS of Ag-TNS	88
Figure 8.4	XRD pattern of Ag-TNS	88
Figure 8.5	Tauc plots for band gap estimation of TNS and Ag-TNS.	89
Figure 8.6	Dye degradation by various powder photocatalysts under solar radiation	90
Figure 8.7	a) Digital image of Ag-TNS hierarchical membrane b) SEM image of Ag-TNS hierarchical membrane surface	91
Figure 8.8	Permeate flux of membranes.	92

Figure 8.9	Dye removal by membranes under UV radiation.	93
Figure 8.10	Dye removal by membranes in absence of UV radiation.	94
Figure 8.11	Reuse cycles (RC) of various membranes for dye removal under UV radiation.	95
Figure 8.12	Dye removal in multiple passages of feed recycles through membranes under UV radiation	96
Figure 8.13	Dye removal in multiple passages of feed recycles through B-200 membrane under solar radiation.	97
Figure 9.1	FESEM image of TNS	100
Figure 9.2	EDS of Ag-TNS	101
Figure 9.3	Tauc plots for band gap estimation of Ag-TNS and TNS.	101
Figure 9.4	XRD patterns of TNS, Ag-TNS and Ag-TNS/PSF.	102
Figure 9.5	FESEM image a) Ag-TNS/PSF coated bead b) Magnified image of Ag-TNS/PSF coating	103
Figure 9.6	Schematic representation of Ag-TNS/PSF floating photocatalyst	104
Figure 9.7	% Dye degradation at different dye concentrations.	105

LIST OF TABLES

Table. No.	Title	Page No.
Table 2.1	Synthesis of Titanium Dioxide Based Membranes literature summary	17
Table 2.2	Hierarchical assembly of photocatalyst on polymer membranes literature summary	24
Table 2.3	Enhanced photocatalytic activity of titanium dioxide nanomaterials literature summary	27
Table 2.4	Polymer nanocomposite membranes literature summary	33
Table 3.1	Table 3.1 BET Surface area analysis of various TiO ₂ nanostructures	32
Table 4.1	Blending compositions of Membranes	35
Table 5.1	Photocatalyst loading of various membranes	50
Table 6.1	Blending compositions of Membranes	62
Table 7.1	Photocatalyst loading of various membranes	80
Table 8.1	Photocatalyst loading of various membranes	90

LIST OF APPENDICES

Appendix. No.	Title	Page No.
Appendix I	Congo red dye calibration curve	113
Appendix II	BSA calibration curve	114

NOMENCLATURE

J_w	- Flux of pure water (L/m^2h)
A	- Cross section area of membrane (m^2)
Q	- Amount of permeate collected (L)
Δt	- Time duration (h)
FRR%	- Flux recovery ratio (%)
R%	- Percentage rejection
%DR	- Percentage dye rejection
Wt.%	- Weight percentage
C_p	- Permeate concentration (mg/mL)
C_f	- Feed concentration (mg/mL)

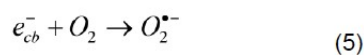
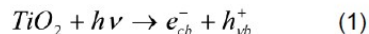
CHAPTER 1

INTRODUCTION

Titanium dioxide (TiO_2) is a versatile material due to its remarkable properties like photocatalytic activity, hydrophilicity, and chemical inertness. Titanium dioxide has extensive applications in various fields like paints, sunscreens, food coloring, catalysis, ceramic membranes, photovoltaic cells, and sensors. The applications of TiO_2 were further widened through the synthesis of nanoscale TiO_2 . Macroscale to a nanoscale reduction in particle size has significantly improved the material property and increased the specific surface area multifold. Enhancement in the material property has further broadened its applications in many domains like photocatalysis, renewable energy, electronics, environmental remediation and chemical engineering. Shape and morphology of the titanium dioxide nanomaterials have an important role in deciding its application and performance. Different shapes of nanosized TiO_2 have been synthesized by many researchers. Some of the common types of TiO_2 nanomaterials are nanoparticles, nanotubes, nanofibers, and nanosheets. Titanium dioxide nanoparticle (TNP) is the commonly used type of nanoscale titanium dioxide. Their small size imparts enormous specific surface area and hence they were extensively used in photo-degradation of organic contaminants (Akpan and Hameed, 2009). The anatase form of TiO_2 is deemed as the most active phase, and has an energy gap (EG) of 3.2 eV and is active under ultra violet radiation. To improve the photocatalytic activity, many modifiers/additives were developed. Noble metals, ceramic oxides, carbon nanotubes and graphene oxide are the commonly used modifiers (Fujishima et al., 2008). Researchers have thus developed visible light active TiO_2 , which is a big break through, since sun light could be efficiently used for photocatalytic degradation of pollutants.

Titania based photocatalytic degradation is widely used to degrade toxic organics and pollutants from water. The distinctive aspect of the photocatalysis is that it breaks down the harmful compounds into simple molecules. By absorbing a light of energy higher or equal than EG, an electron (e^-) gets promoted to conduction band and

creates a hole (h^+). The e^- and h^+ move to the catalyst surface and involve oxidation and reduction. Holes can react with H_2O or OH^- to give hydroxyl radical OH^\bullet . Electron can react with oxygen and produce superoxide radical anion $O_2^{\bullet-}$. The hydroxyl radicals (OH^\bullet) and superoxide radical anions ($O_2^{\bullet-}$) are presumed as the major reactive species in the reaction (Fujishima et al., 2000).



Apart from photocatalytic activity, TiO_2 nanoparticles also exhibit high hydrophilicity, self-cleaning properties and antibacterial traits in presence of ultra violet radiation. These properties are of special interest in developing polymer nanocomposite membranes, since the hydrophobicity of the polymer membrane is a major drawback. For the last two decades titanium dioxide nanoparticles have been studied by many researchers and the following disadvantages are noteworthy: -

- The smaller size of the nanoparticles makes catalyst recovery very difficult from the reaction mixture after its use.
- Studies on occupational diseases and research in nanotoxicology indicate that nano- TiO_2 is carcinogenic in nature. Affirming these findings, in 2010, the International Agency for Research on Cancer (IARC) has categorised titanium dioxide as "Group 2B carcinogen: potentially harmful".
- Use of high quantity of nanoparticles in polymer composites results in particle agglomeration and loss of desired properties.

TiO_2 nanofibers (TNF), nanotubes, and nanorods are 1-D nanostructures of TiO_2 . In TiO_2 photocatalyst, the photo induced charge carriers tend to drift to the surface to initiate surface redox reactions. In spherical particles, the advantages from high surface to volume ratio owing to reducing size are considerably lessened due to

more charge carriers recombination at surface defects. Whereas, in nanofibers and rods, the increased delocalization of charge carriers, enabling them to freely move about the whole length of the crystal and can significantly reduce the probability of charge carrier recombination on the heterogeneous boundary and get better photocatalytic activity. Among the size and shape, the shape of the nanocrystals offers more flexibility in escalating the multiplicity of electronic states than merely decreasing the size of the system (Xie and Shang, 2007). 1-D structures of TiO₂ have been applied to water-splitting, environmental remediation, self-cleaning, and sensors. Recent reports suggest that alkaline hydrothermal method can produce good nanofibers of TiO₂. The nanofibers have mechanical robustness and can be bundled to form networks and webs (Wu et al. 2011).

TiO₂ nanosheets (TNS) are 2D nanostructures with a thickness of a few nanometers and its length and breadth in near micro scale. The ultra-thin sheet structure provides very good specific surface area and the larger size enables easy catalyst recovery from the reaction mixture. These nanostructures are difficult to synthesize with effective size control. Hydrothermal methods have been proved to produce good quality nanosheets (Hu et al., 2014). TiO₂ nanosheets show improved photocatalytic activity than TiO₂ nanoparticles (Chen et al., 2014). Very few literatures are available about the applications of TiO₂ nanosheets (Nakata and Fujishima, 2012). Although TiO₂ nanosheets have exhibited substantial photoactivity and gained interest among researchers, there are relatively lesser reports on the photocatalytic activity of TNS. High specific surface area, nano-scale thickness, and low defect density prevents e⁻/h⁺ recombination at surface defects (Zou et al., 2014).

1.1 POLYMER NANOCOMPOSITE MEMBRANES

A membrane is an inter-phase between two phases acting as a selective barrier. In many processes, during the separation of gaseous or liquid mixtures, semipermeable membranes are used which can allow one or more constituents of the mixture to pass through more readily than the others. Membranes can have typical pore sizes that can give rise to retention of certain species. Separation using membranes is isothermal and can be operated at low temperatures with lesser energy in comparison to thermal separation processes. Also, up scaling of membrane processes and their incorporation

along with other reaction processes is easier. Polymeric membranes are easy to synthesize, possess separation selectivity, and are inexpensive. The use of polymer membranes is gaining interest because of the broad variety of applications.

1.1.1 Types of Membrane Filtration

Membranes are basically categorized into 4 classes, depending on the size of their pores.

Microfiltration (MF): The mean pore size varies between 0.1 to 10 microns and operates at lower pressure 0.1–2 bar. MF is commonly used for pre-treatment. They reject particulates by sieving mode.

Ultrafiltration (UF): UF rejects particles and large molecules by size exclusion or sieving mode. Ultrafiltration membrane is characterized depending on its molecular weight cut-off. Molecular weight cutoff is the molecular mass of a solute having 90 % rejection. Solutes having molecular mass higher than the cut-off have high rejection. The cut-off for Ultrafiltration is in the range of 1000 Da to 100000 Da. Ultrafiltration removes high macromolecules, colloidal particles, organic and inorganics. Lower molecular weight organics and ions such as Na^+ , Ca^{2+} , Cl^- , and sulfate cannot be removed. In UF, a low operating pressure is required to achieve high flux. Ultrafiltration process is considered as pre-treatment process prior to RO.

Nanofiltration (NF): The property of NF is in the middle UF and RO. NF membrane originated in 1970 in the form of modified reverse osmosis membrane possessing high flux. They need a lesser operating pressure (2-20 bar) when compared to reverse osmosis. Moreover, NF combines high permeability with good rejection of dissolved organics ($\text{MM} > 200$ Da). Their cut-off lies in the range of 150 to 1000 Da.

Reverse osmosis (RO): RO is mainly used for desalination. This process employs dense membrane with higher hydrodynamic resistance. Good permeability is obtained only at very high pressure (10–70 bar). Separation occurs because of sorption and diffusion.

1.1.2 Membrane Fouling

The deposition of the impurities on membrane surface during filtration is called fouling. As filtration process progresses, large size pollutants get rejected and thus

the amount of these pollutants deposited on membranes active surface gradually increases. This phenomenon is called cake formation (Fig. 1).

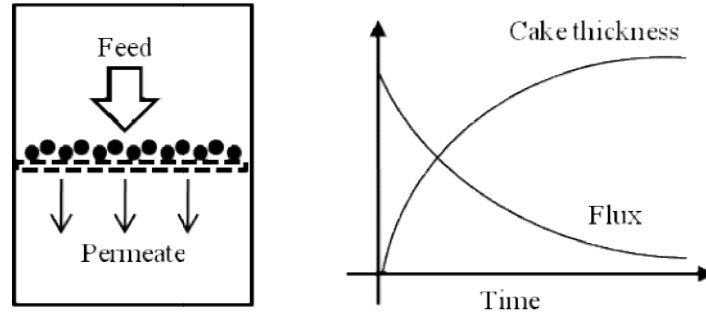


Fig. 1 Schematic representation of membrane fouling

As the cake gains more thickness, it tends to resist the flow. Thus, the flux starts to decline with time. Finally, the flux drops to a minimum and the membrane surface needs to be cleaned. The most common disadvantage of the membrane separation in water purification is fouling. Fouling causes flux reduction. In membrane processes several substances can cause fouling, such as organics, particulates, colloids, and microbes. Even after much development in membrane processes, particulate and colloidal fouling is still the major factor causing flux drop. Fouling degrades the membrane via to the development of extra barrier layer on the membrane surface. Other process conditions also influence fouling.

1.1.3 Polysulfone

Polysulfone (PSF) membrane is widely used due to its good thermal resistance, mechanical properties and chemical stability. The main drawback of polysulfone is its hydrophobicity, whereas for better performance a membrane should have hydrophilicity to counter membrane fouling. The lower permeate flux and higher fouling is due to low hydrophilicity.

1.1.4 Improving hydrophilicity

Several methods are reported in literature to increase the hydrophilicity of a membrane. The main methods are surface treatment and incorporation of hydrophilic materials. Inorganic nanoparticles, when incorporated in the membrane, are found to enhance hydrophilicity and they modify the transport properties without introducing gross defects in the membrane. There have been several reports on nanocomposite

membranes, wherein nano additives like carbon nanotubes, graphene oxide, nano clay etc., have shown very good property enhancement. Addition of inorganic nanoparticles like Al_2O_3 , Fe_2O_3 , SiO_2 , CaCO_3 , TiO_2 etc., have also resulted in better hydrophilicity and antifouling properties. These inorganic nanoparticles are highly hydrophilic in nature and thus improve the hydrophilicity of the membranes. Improved hydrophilicity enables better interaction with water than the foulant, thus the membrane gains better antifouling property.

1.1.5 TiO_2 nanomaterials as membrane additives

TiO_2 nanomaterials possess catalytic activity, super-hydrophilicity, self-cleaning property, and bacterial resistance which makes them best material for membrane modifiers. Researchers have tried blending TiO_2 nanoparticles in polymers and the results have shown improvement in surface hydrophilicity of membrane resulting in greater flux recovery (Yang et al., 2007). Titanium dioxide nanofiber and nanosheets are some of the different morphological forms of titanium dioxide nanomaterials. TNF and TNS fiber have an edge over the nanoparticles due to its higher dimensions; which in turn results in greater interfacial interaction in composites. Also, they are less prone to agglomeration than the small size nanoparticles. TNF and TNS can hence serve as a better reinforcing material in composites due to greater interface interaction.

1.2 PHOTOCATALYTIC MEMBRANE REACTORS

Membrane reactor (MR) is a piece of equipment which merges membrane separation along with chemical reaction as a single unit. Combination of reaction and separation can bring down the processing cost. Also membrane reactors are capable of selectively removing only the product thus shifting the reaction equilibrium towards the product side and enabling a faster rate of reaction. In a membrane reactor (Fig. 2), the active layer of the membrane has been coated with a photocatalyst. On irradiating with photons of suitable energy this catalyst layer gets activated. Initially, films of pollutant get adsorbed on to the catalyst, and subsequently get degraded to smaller molecules like water and CO_2 and pass out along with permeate. The next layer gets adsorbed and the same process goes on as long as photons are incident on the active layer. Thus ideally a membrane reactor does not get choked due to fouling.

The layer of pollutant remains adsorbed on the surface gets degraded in the process. The cake never gains sufficient thickness to decline the flux drastically. The major advantage of a membrane reactor is that the pollutant not only gets separated but also gets degraded.

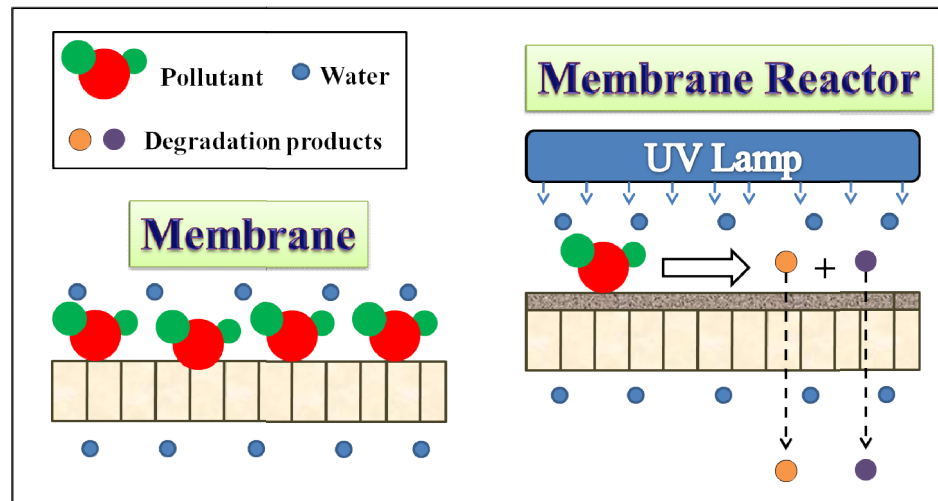


Fig. 2 Schematic representation of photocatalytic membrane reactor mechanism.

1.2.1 Nanocatalyst based membrane reactor

Nanomaterials have received much attention due to their enhanced catalytic activity. But their small size makes catalyst recovery a challenge. Most of the nanomaterials are toxic and potential carcinogens. Due to their high catalytic activity, researchers have developed various methodologies to use these nanocatalysts in membrane reactors. Some of the common methodologies seen in literature are composite membranes, self-assembly, hierarchical physical assembly and sputtering. In case of nanocomposite membranes, the nano additive is directly added to the polymer cast solution, thereby giving a uniform dispersion of additive throughout the membrane. Although an overall enhancement of performance with regard to flux and antifouling properties can be seen in the membrane, with regard to photocatalytic activity the encapsulation of the nanomaterials in the polymer matrix reduces the effective exposed catalyst surface area and thereby the catalytic property cannot be completely exploited. In the case of self-assembly of nanomaterials on top of membranes, the

major drawback is the narrow thickness of the self-assembly layer. The weak mechanical stability of the assembly layer is also a disadvantage. Weak attachment puts the assembly layer at risk during back washing after rejection. Sputtering is a good method to obtain uniform layers but it is an energy intense method, expensive and also it is difficult to make catalyst undergo phase transformation since polymer membranes cannot be calcined at high temperature. Recently synthesis of polymer membranes with a photocatalyst deposited on top via pressurized filtration to form a hierarchical structure or hierarchical membrane have been reported. Hierarchical assembly of nanomaterials on membranes have shown much better results due to the achievement of adequate thickness of photocatalyst layer and complete exposure of the feed to the photocatalyst layer.

1.2.2 TiO₂ nanomaterials based hierarchical membranes

Assembly of photocatalytic nanomaterials on top of polymeric support membranes forming a hierarchically structured membrane has been developed by researchers. These Hierarchical membranes have shown to have better prospects for being developed into membrane reactors. Initially, a well-dispersed suspension of the nanomaterial in water is prepared. This suspension is filtered through a membrane of suitable pore size. When pressurized from the top the water gets filtered away and the nanomaterial gets compressed and coated over the membrane. One of the significant reports on hierarchical membranes using TiO₂ nanomaterials is by Bai et al. (2010). They successfully synthesized a hierarchically multifunctional TiO₂ nano-thorn sphere layer on top of a cellulose acetate membrane (Dia 4.7 cm, pore size 200 nm). This membrane was compared with a similar membrane synthesized using commercial TiO₂ P25 powder. The water permeation and dye removal rates of methyl blue and humic acid and their degradation under UV light using hierarchical TiO₂ nano-thorn membrane were far superior when compared to commercial P25 coated membrane. The base membrane of the hierarchical membrane should have a pore size lower than the size of nanomaterial being loaded on top of it. When nanoparticles are used instead of other shapes, the membranes should have very low pore sizes, and this result in lower flux and greater operating pressure. So in terms of catalyst recovery and in terms of application in hierarchical membrane, nanoparticles are not a good choice. TiO₂ nanosheets and nanofibers have better prospects in this regard since their

structure imparts good mechanical stability to the top layer and also overcome the above-mentioned problems.

1.3 SCOPE AND OBJECTIVES OF THE RESEARCH WORK

Based on the literature survey carried out the following observations were made. Addition of TiO₂ nanomaterials can improve hydrophilicity and enhance membrane performance. Addition of TiO₂ nanoparticle in polymers is restricted due to additive agglomeration. Addition of TiO₂ nanofibres and nanosheets in polymer ultra-filtration membranes has not been reported. TiO₂ nanoparticles have shown toxicity and are considered potential carcinogens. In the field of photocatalysis using TiO₂ nanoparticles, no much emphasis has been given to catalyst recovery. Immobilization of photocatalyst in polymer matrixes as composites largely decreases catalyst activity due to lower exposed catalyst area. Hierarchical membranes having a hierarchical assembly of photocatalyst on their top layer are a good option to improve exposed catalyst area. Little work has been done on hierarchical membrane based on TiO₂ nanosheets and nanofibers.

Accordingly, the following are the objectives of this research work:

1. To synthesize and characterize TiO₂ nanofibres and nanosheets.
2. To study the photocatalytic activity of TiO₂ nanofibres and nanosheets using dye degradation.
3. To study the effect of modifiers, like silver (Ag) and graphene oxide (GO) on the photocatalytic activity of the nanomaterials.
4. To synthesize and characterize polymer nanocomposite ultrafiltration membranes incorporated with TiO₂ nanomaterials.
5. To synthesize and characterize TiO₂ nanomaterial based photocatalytic hierarchical membranes.

CHAPTER 2

LITERATURE REVIEW

2.1 SYNTHESIS OF TiO₂BASED MEMBRANES

Anderson et al. (1988) reported about the synthesis of titania and alumina ceramic membranes using alkoxide as starting materials via sol-gel technique. Crack-free unsupported membranes with thicknesses up to 120 μm were prepared on α -alumina supports. Supported TiO₂ membranes were fabricated with thicknesses up to 0.5 μm . Chang et al. (1994) investigated the thermal and hydrothermal stability of titania, Al₂O₃ membranes. It was observed that at temperatures more than 450 °C (titania) and 900°C (alumina) meta stable to stable transition occurred with modifications in pore structure. Unsupported titania, alumina or zirconia membranes of about 20 μm in thickness could be fabricated via sol-gel method. The supported titania, alumina, and zirconia membranes were synthesized via dip coating using alumina support disks.

Wu et al. (2000) studied effects of sol characteristics and calcination temperature on TiO₂ tubular membranes. Tubular TiO₂/Al₂O₃ membrane was produced with thickness of 1.5 mm by the colloidal method using sol-gel method. Water permeability of the synthesized membrane improved with higher calcination temperature.

Titania membranes on Al₂O₃ support were synthesized by sol-gel technique. The titania sol used had a mean size of 55.6 nm. TiO₂ membrane of thickness of 1 μm was obtained and exhibited homogeneity with a defect free surface. It also had lower pore size of 4.7 nm, larger specific surface area (75m²/g), and lesser crystalline size (8.3 nm) (Puhlfürß et al. 2000).

Benfer et al. (2001) produced Zirconia and titania nanofiltration membranes using a polymeric sol gel technique. They prepared nanofiltration (NF) membranes, polymeric sols were poured into tubular supports consisting of an ultrafiltration membrane. Due to capillary action, a part of the products of the polycondensation reaction gets absorbed into the membrane. This leads to faster polycondensation

reaction at the support surface. A polymeric gel layer forms and the excess sol was poured away. The gel layer was dried over a period of 3 days and then pyrolyzed at 500 °C to form the ceramic top coat.

A novel type of thin-film-composite (TFC) membrane was developed using TiO₂ nanoparticles, to address biofouling problem in membranes. The photocatalytic bactericidal and anti-fouling effect was studied. Introduction of TiO₂ nanoparticles on commercial TFC membrane and its application in reverse osmosis showed significant resistance to microbial fouling and lesser loss of RO permeability (Ho et al. 2003).

In 2003, Kim et al. studied about the synthesis of TNP self-assembled on a TFC membrane made of aromatic polyamide. This work devised the photocatalytic destructive capability of TiO₂ against microbes as an effective tool to reduce biofouling. The self-assembly of TiO₂ nanoparticles was formed by coordinate and hydrogen bonds with COOH groups of the polymer. The novel membrane showed enhanced photo-bactericidal effect on E. coli under ultra-violet radiation.

Bosc and Guizard(2005) developed mesoporous anatase coatings for photocatalytic membrane separation. These coatings exhibited comparatively higher photocatalytic efficiency than the conventional coatings prepared by sol-gel technique. The photocatalytic activity was analyzed using organic dye degradation. Experiments on separation coupled photo-oxidation indicated larger scope of such functionalized membranes.

Ding et al. (2006) developed titania ultrafiltration membranes by a novel method. Directly from nanoparticle suspension by a wet chemical routine, this was the transitional product before drying and calcination during the synthesis process. The thickness of membrane layer is directly proportional to the square root of dipping time. 30 seconds of dipping time was essential to form a crack-free TiO₂ coating. This yielded a TiO₂ layer of 5.9 μm thickness and a mean pore size of 60 nm.

Patterson et al. (2006) derived a method for direct coating of a TiO₂ layer on the centrifugally casted tubular ceramic support. The coating was prepared by dip coating the tubular ceramic support in a homogeneous sol of TiO₂. A thin crack free TiO₂ membrane in anatase phase was obtained. The membranes were found to be in the nanofiltration range.

Bosc et al. (2006) synthesized anatase TiO_2 membranes with hierarchical porosity and evaluated their performance. The TiO_2 coating was synthesized using an inorganic-inorganic hybrid suspensions made by mixing polystyrene latex, a TiO_2 hydrosol, and triblock copolymer. This suspension was coated on to porous alumina substrates via dip coating and subjected to heat treatment to remove the organic content. They reported that hierarchical porosity has increased the flux and selectivity.

Wang et al. (2006) manufactured tubular titania microfiltration (MF) membranes synthesized by dip-coating technique and investigated their corrosive resistances. The anatase layers of titania membranes were more stable than alumina supports in a boiling corrosive medium.

Wang et al. (2007) prepared an asymmetric pure TiO_2 membranes by repeated sol-coating method coupled with a joint drying method and customized sintering procedure. The results showed that the novel membranes with pore size of $0.10\ \mu\text{m}$ and active layer thickness of $15\text{-}20\ \mu\text{m}$ were synthesized with desired fluid permeation properties and incredible in situ photocatalytic activity.

In 2007, Madaeni and Ghaemi studied the self-cleaning properties of TiO_2 nanoparticles assembled on a reverse osmosis membrane. The procedure for self-assembly was similar to Kim et al (2003). It was observed that on UV irradiation, the TiO_2 coated membranes showed greater flux and fouling resistance than the nascent membrane. It was observed that at higher TiO_2 content, the flux started to decline due to blockage of pores. The effect of SiO_2 particles along with TiO_2 was also studied. Addition of SiO_2 in TiO_2 leads to the formation of binary oxide with charge imbalance, which imparts Lewis acidity, and thus the surface acidity increases. With increased acidity, the surface can now strongly absorb hydroxyl radicals. This has increased the hydrophilicity, self-cleaning property, and photocatalytic activity of the membranes. They also briefly discussed the about the effect of membrane roughness the coatings. The rise in roughness of the membrane results in lower contact angle and increased the flux.

Hong et al. (2008) prepared complete TiO_2 membranes for separation and in situ photocatalysis on a porous rutile support by dip-coating method. The membranes were synthesized using an aqueous suspension of TiO_2 nanoparticles via dip coating method and further sintered via calcination. Special emphasis was given to the

coating suspension stability and sintering control. It was reported that the anatase coated membranes exhibited good potential for detoxification of industrial effluents.

In 2008, Rahimpour et al. reported a work similar to Madaeni and Ghaemi (2007), but the membrane used was polyethersulfone ultrafiltration membrane. Compared to nascent membrane the TiO₂ entrapped membranes showed lower flux but better fouling resistance and flux stability. Under UV illumination, TiO₂ entrapped membrane showed a slightly better performance. Superior performance was exhibited by the TiO₂ coated membrane. Extended immersion of membranes in the TiO₂ suspension resulted in pore blockage. They concluded that coating TiO₂ is a better way to modify the membrane than making a composite.

Zhang et al. (2008) synthesized a TiO₂ nano wire membrane. Nanowires were synthesized using the alkaline hydrothermal method. A suspension of the nanofibers was made with a suitable surfactant and they were vacuum filtered on a glass filter having a pore size 0.45 μm. The substrate membrane was uniformly coated by the TiO₂ nanowires and on subsequent drying, a free standing nanowire membrane was synthesized. The membrane was calcined at 700°C with a controlled heating ramp of 2°C/min. This work was one of its kind, they could successfully synthesize a complete membrane out of a TiO₂ nanomaterial effortlessly. The membrane was flexible and could be shaped as flat sheet or cylinder. The pore size was estimated to be 0.05 μm. The photocatalytic activity of TiO₂ nanowires was similar to that of commercial P25 TiO₂. The humic acid removal rate of the membrane increased from 57% to 100% on UV exposure. The study on the increasing resistance of the membrane due to fouling was assessed in terms of increasing transmembrane pressure for a fixed value of flux. The novel membranes showed no elevation in membrane resistance even after a period of 30 h, but without UV irradiation steep increase in resistance was reported. TiO₂ nanowire membrane has a strong potential if the membrane possesses adequate mechanical strength.

Zi et al. (2009) synthesized TiO₂ membranes on a porous 316L stainless steel support. The various parameters affecting the microstructure and phase structure of TiO₂ coatings was studied. The aging time for coating the sol was found to be 24 hours. A sintering temperature of 850 °C was used. Thickness of roughly 8 μm and pore sizes of 0.08-0.2 μm was obtained.

In 2009, Li et al. reported self assembly of TNPs on Poly(styrene-alt-maleic anhydride)/poly(vinylidene fluoride) blend ultrafiltration membranes. The presence of carboxylic acid groups on Poly(styrene-alt-maleic anhydride) (SMA) enables the formation of an electrostatic self-assembly of anatase nanoparticles. Greater addition of SMA enhanced the carboxylic acid groups on the membrane, resulting in greater absorption of the TiO₂ nanoparticle. Although no UV irradiation was used in this study, the results are worth noting. The absorption of TiO₂ nanoparticles greatly increased the surface hydrophilicity and the irreversible absorption of foulant could be greatly reduced. The novel membranes showed superior permeability and excellent antifouling property compared to the nascent membrane.

Alem et al. (2009) fabricated mesoporous TiO₂ membrane on porous alumina support via sol-gel method. The permeability and photocatalytic activity were analyzed. It has been reported that the prepared TiO₂ membrane showed immense potential in high-performance water treatment technique due to its ability to degrade pollutants and also the separation of impurities.

Mansourpanah et al. (2009) investigated the self-assembly of nanoparticle on a polyethersulfone/polyimide blend nanofiltration membrane. Diethanolamine was added to the blend membrane to functionalize it with hydroxyl groups. Hydroxyl groups on membrane surface result in excellent adhesion of TiO₂ nanoparticles. The optimum conditions used for self-assembly were similar to that of Rahimpour et al. Increased Diethanolamine content resulted in the uniform assembly of TiO₂nanoparticles. The novel membrane exhibited better fouling resistance and flux recovery.

Alem et al. (2009) synthesized crack-free nanostructured TiO₂ membrane by the sol-gel method. The processing parameters of synthesis of membranes like calcination temperature and time were studied in detail and their effect on the crystalline phase, crystallite size, specific surface area and photocatalysis were examined.

Djafer et al. (2010) developed a simple fabrication method to synthesiz photocatalytically active TiO₂ based ultrafiltration membrane on alumina support using a commercial titania hydrosol. The photocatalytic activity was tested via dye degradation under UV irradiation.

Akbarnezhad et al. (2010) prepared alumina titania ceramic membranes with mesopore and narrow pore size distribution via the sol-gel route. The membrane surface was smooth, homogeneous and crack free. The membrane layer thickness was reported to be 4 μm .

In 2013, You and Wu assembled TiO_2 nanoparticles on polyethersulfone ultrafiltration membrane as reported by Rahimpour et al for treating secondary effluent from the thin film transistor-liquid crystal display manufacturing industry. The self-assembly was obtained by dipping the membranes in TiO_2 nanoparticle suspension for an hour. It was observed that continuous UV irradiation could increase hydrophilicity, constantly destroy organic foulant on the surface and increase the permeate flux. The organic cake formed on the membrane surface lost stability due to subsequent degradation as well as non-adherence to the surface due to increased hydrophilicity. The cake could thus be easily flushed off in a cross flow system. Better self-cleaning property can be obtained by continuous UV irradiation.

Tajer-kajinebaf et al. (2014) synthesized nanostructured photocatalytic SiO_2 - TiO_2 membranes. The methyl orange dye removal capacity of the SiO_2 - TiO_2 membrane was determined to be 63%. Combining separation with photocatalysis, the dye removal was enhanced by 94%.

Doke and Yadav (2014) illustrated the efficiency and novelty of titania membranes synthesized by a polymeric sol-gel technique in the removal of chromium (VI) in surfactant enhanced microfiltration.

Table 2.1 Synthesis of Titanium Dioxide Based Membranes literature summary

Authors	Year	Topic	Observations
Anderson et al.	1988	TiO_2 ceramic membranes via sol-gel method.	Crack free unsupported membranes up to thickness of 120 microns could be obtained.
Chang et al.	1994	Thermal stability of titania membranes was investigated.	Above 450 $^{\circ}\text{C}$ titania underwent phase transformation and membrane pore structure changed.

Wu et al.	2000	Impact of sol concentration and calcination temperature on TiO ₂ tubular membranes	Tubular titania/alumina composite membranes were successfully synthesized by the colloidal route. Thickness of about 1.5 mm was obtained.
Benfer et al.	2001	Titania nanofiltration membranes by polymeric sol gel route	Nanofiltration membranes were synthesized from ultrafiltration membranes by pouring polymeric sols into tubular supports
Ho et al.	2003	A novel type of TFC membrane using TiO ₂ nanoparticles	TFC membrane was developed for application in reverse osmosis. It showed resistance against the microbial fouling.
Kim et al.	2003	TNPs self-assembled on a TFC membrane	The self-assembly of TNP was formed by coordinate and hydrogen bonds with COOH groups of the polymer. These novel membranes showed enhanced photo bactericidal effect.
Bosc and Guizard	2005	Mesoporous anatase coatings for membrane separation coupled with photocatalysis	Coatings exhibited a higher photo-activity than coatings prepared by sol-gel technique
Ding et al.	2006	Novel method to fabricate titania ultrafiltration membranes via dip coating	The thickness of coating was found to vary with the square root of dipping time. Minimum dipping time of 0.5 minutes was needed to obtain a defect free coating.
Bosc et al.	2006	Anatase TiO ₂ membranes with hierarchical porosity	The TiO ₂ coating was synthesized using organic-inorganic hybrid suspensions. This suspension was coated on to porous alumina substrates via dip coating and subjected to heat treatment to eliminate organics.

Madaeni and Ghaemi	2007	Self-cleaning properties of TiO ₂ nanoparticles assembled on a reverse osmosis membrane	Upon UV irradiation, the TiO ₂ coated membranes showed greater flux and fouling resistance than the nascent membrane.
Hong et al.	2008	Complete TiO ₂ membranes for separation and in situ photocatalysis	The membranes were synthesized using an aqueous suspension of TiO ₂ nanoparticles via dip coating method. Anatase coated membranes exhibited good potential for detoxification of industrial effluents
Zhang et al.	2008	TiO ₂ Nanowire membrane	The membrane was flexible and could be shaped as flat sheet or cylinder. The novel membranes showed no elevation in membrane resistance even after a period of 30 h, under UV irradiation.
Li et al.	2009	Self assembly of TNPs on polymer blend ultrafiltration membranes	Carboxylic acid groups on Poly(styrene-alt-maleic anhydride) (SMA) enables electrostatic self-assembly of anatase nanoparticles on the surface of the membrane. TNPs greatly increased the surface hydrophilicity and the irreversible absorption of foulant could be greatly reduced
You and Wu	2013	TiO ₂ nanoparticles assembled on polyethersulfone ultrafiltration membrane	The self-assembly was obtained by dipping the membranes in TiO ₂ nanoparticle suspension for an hour. It was observed that continuous UV irradiation could increase hydrophilicity, constantly destroy organic foulant.

Tajer-kajinebaf et al.	2014	Nanostructured SiO ₂ -TiO ₂ mesoporous membranes	The methyl orange dye removal capacity of the SiO ₂ -TiO ₂ membrane was determined to be 63%. Combining separation with photocatalysis, the dye removal was enhanced by 94%.
Doke and Yadav	2014	Titania membranes for removal of chromium (VI)	Membranes were synthesized via polymeric sol-gel technique. It was observed that ions can also be removed by TiO ₂ membranes via appropriate synthesis processes.

2.2 HIERARCHICAL ASSEMBLY OF PHOTOCATALYST ON POLYMER MEMBRANES

An assembly of TiO₂ nanomaterials on top of polymeric support membranes has been developed and reported in literature. These Hierarchical membranes have shown to have better prospects for being developed into membrane reactors. Initially, a well-dispersed suspension of the nanomaterial in water is prepared. This suspension is filtered through a membrane of suitable pore size. When the filtration medium is pressurized from the top the water gets filtered and the nanomaterial gets compressed and coated over the membrane. One of the significant reports on hierarchical membranes using TiO₂ nanomaterials is by Bai et al (2010). They successfully synthesized a hierarchically multifunctional TiO₂ nano-thorn sphere membrane on top of a cellulose acetate membrane (diameter 47 mm, pore size 0.20 μm). The nanothorn sphere is a nanoarchitecture which is an amalgam of micro and nanostructures. Basically it is a micro size sphere with numerous nano sized thorn like projections on its periphery. This membrane was compared with a similar membrane synthesized using commercial TiO₂ P25 powder. The water permeation and dye removal of methyl blue and humic acid by the membrane were far superior when compared to commercial P25 coated membrane.

In 2011, Bergamasco et al. reported the synthesis of TiO₂ coated cellulose acetate membrane via reactive magnetron sputtering. These novel membranes were used in gravity driven filtration without using any external pressure source. The sputtered membranes showed better turbidity and chlorine removal. Antifouling traits of the membrane were improved due to increase in surface hydrophilicity. Although photocatalytic studies were not conducted, the prospect of sputtering as an efficient way to develop TiO₂ coated membranes is vindicated.

Liu et al (2011) studied hierarchical CuO/ZnO membranes. They were found to be active under both UV and visible spectra. A special nanostructure with CuO nanoparticles was grown on ZnO nanorods was used as the functional layer on commercial glass fiber membrane. The membranes showed improved photodegradation antibacterial activity. Enhanced light utilization rate and enlarged specific surface area resulted in the superior performance of the membranes.

Bai et al (2012) synthesized a hierarchical membrane using N-doped nut-like ZnO nanomaterial. The photocatalyst was uniformly assembled on a polymer base membrane via pressurized filtration technique. The novel member exhibited high permeates flux and good photocatalytic activity during dye degradation experiments. Also, water disinfection capability was demonstrated by antibacterial studies using E-Coli. The superior photocatalytic activity was achieved due to the greater specific surface area of the ZnO nanomaterial functional layer on the membrane surface.

Bai et al (2012) developed multifunctional membrane by using forest like hierarchically structured TiO₂/ZnO nanomaterial synthesized via electro-spinning as the functional layer on a base membrane. These membranes showed multifunctional properties, like high photocatalytic activity, elevated flux, and good antibacterial activity. The membrane functional layer was synthesized by the pressurized filtration technique.

Liu et al (2013) synthesized a multifunctional and hierarchically-nanostructured membrane using TiO₂ nanorods. The membrane showed good performance simultaneous degradation and filtration of impurities. The novel membrane exhibited good flexibility, better flux, enhanced photocatalytic activity with little fouling.

Liu et al (2013) also developed a hierarchical ZnO nanoflake Structured Multifunctional membrane. The membrane exhibited good dye degradation

capabilities and better permeate flux under visible light. Also, membranes showed better antibacterial properties. This multifunctional membrane proved to be an endearing strategy to combine the advantages of membrane separation and photocatalytic oxidation to simultaneously mitigate the membrane fouling under visible light irradiation and promote reuse of the photocatalyst.

A detailed study on hierarchical membranes was done by Gao et al in 2013, using graphene oxide-TiO₂ (GO-TiO₂) microsphere composite. The procedure followed for forming the hierarchical structure was similar to that of Bai et al but the substrate membrane used had a greater pore size (0.45 μm). The improved photocatalytic effect of GO-TiO₂ composites due to the electron acceptor capacity of GO is well established. But in this case, GO sheets also enhance the mechanical stability of the membrane by acting as a binder and interlinked individual microspheres. Similarly, P25 and TiO₂ microsphere membranes were synthesized and compared. During pure water flux study, all membranes showed reduced flux compared to nascent CA membrane, due to the additional coating resistance. Least reduction in flux was observed in graphene oxide-TiO₂ microsphere hierarchical membrane. When a comparative study was made by varying the catalyst loading on top of the membrane, it was observed that an increased loading declined the flux due to increased resistance of a thicker coating.

In 2014, Gao et al again reported TiO₂-GO on a polysulfone membrane. The assembly of TiO₂-GO was achieved in two stages; first membrane was soaked in TiO₂ nanoparticle suspension, then in GO suspension. The TiO₂ nanoparticles interacted with the polar oxygen in the polymer and form an assembly. Later the addition of GO, the polar oxygen in GO surface interacted with the TiO₂ nanoparticles and got deposited on top. The stable TiO₂-GO loading was found to be 62 μg/cm². The novel membranes showed a sharp increase in surface hydrophilicity. The membrane showed rapid flux increase under UV light when compared to a gradual increase in sunlight, due to photo induced hydrophilicity and self-cleaning property. The membrane also exhibited greater photodegradation towards methylene blue under UV light. The membrane exhibited moderate performance even under sunlight

Bai et al (2015) developed novel hierarchical membrane by electro-spinning SrTiO₃/TiO₂ hetero architectures on a CA base polymer membrane. These membranes

showed superior water filtration and concurrent photocatalytic activity. The enhanced photodegradation ability and good permeate flux were due to the high photocatalytic activity of heterojunction SrTiO₃/TiO₂ nanofiber architectures porous layer enabling faster passage of permeate. This work showed much potential for synthesizing hierarchical membranes via electrospinning of photocatalyst on to the membrane surface.

Bai et al (2015) developed a multi-functional CNT/ZnO/TiO₂. The use of CNTs helped in providing a strong backbone for the functional layer thus improving the mechanical properties; also the coupling of TiO₂ and ZnO enhanced the photocatalytic activity. The membranes showed good dye degradation traits with high flux. The use of carbon based material like CNT provided mechanical strength and good photoactivity.

Table 2.2 Hierarchical assembly of photocatalyst on polymer membranes literature summary

Authors	Year	Topic	Observations
Bai et al	2010	Hierarchically multifunctional TiO ₂ nano-thorn sphere membrane	TiO ₂ nano-thorn sphere membrane on top of a cellulose acetate membrane was synthesized. The water permeation and dye removal rates of TiO ₂ nano-thorn membrane were far superior when compared to commercial P25 coated membrane
Liu et al	2011	Hierarchical CuO/ZnO membranes	CuO nanoparticles were grown on ZnO nanorods were used as the functional layer on glass fiber membrane. The membranes showed good photodegradation and antibacterial properties.

Bai et al	2012	Hierarchical membrane using N-doped nut-like ZnO nanostructured material	The novel member exhibited high permeates flux and good photocatalytic activity during dye degradation experiments. Also, water disinfection capability was demonstrated by antibacterial studies using E-Coli.
Bai et al	2012	Multifunctional membrane by using forest like hierarchically structured TiO ₂ /ZnO nanomaterials	The nanomaterial was synthesized via electro-spinning. These membranes showed multifunctional properties, like high photocatalytic activity, elevated flux, and good antibacterial activity.
Liu et al	2013	Hierarchically-nanostructured membrane using TiO ₂ nanorods	The membrane showed good performance in simultaneous filtration and photocatalysis.
Liu et al	2013	Hierarchical ZnO nanoflake Structured Multifunctional membrane	The membrane exhibited good dye degradation capabilities and better permeate flux under visible light. Also, membranes showed antibacterial properties.
Gao et al	2013	Graphene oxide-TiO ₂ (GO-TiO ₂) microsphere composite membrane	The good photocatalytic effect of GO-TiO ₂ composites due to the electron acceptor capacity of GO. GO sheets also enhance the mechanical stability of the membrane by acting as a binder and interlink individual microspheres.

Gao et al	2014	TiO ₂ -GO on polysulfone membrane	The assembly of TiO ₂ -GO was achieved in two stages; first membrane was soaked in TiO ₂ nanoparticle suspension, then in GO suspension. The membranes showed a sharp increase in surface hydrophilicity, rapid flux increase under UV light and self-cleaning property. The membrane also exhibited greater photodegradation. Membranes were active even under sunlight.
Bai et al	2015	Multi-functional CNT/ZnO/TiO ₂ membrane	The use of CNTs helped in providing a strong backbone for the functional layer thus improving the mechanical properties; also the coupling of TiO ₂ and ZnO enhanced the photocatalytic activity.

2.3 ENHANCED PHOTOCATALYTIC ACTIVITY OF TITANIUM DIOXIDE NANOMATERIALS

Zhang et al. (2000) investigated the impact of calcination on photocatalytic activity of TiO₂ nanopowders. The nano-TiO₂ in the anatase, rutile, and both phases were synthesized from TiCl₄ as a precursor. They found that calcination above 400 °C could improve photocatalytic activity but calcination above 600 °C is detrimental.

Li et al. (2005) carried out studies on SiO₂-TiO₂ nanoparticles by hydrothermal process. The SiO₂-TiO₂ nanoparticles exhibited superior photocatalytic activity, with higher SiO₂ content. SiO₂ imparts improved thermal stability; the photocatalytic activity was retained even after calcination at 1273 K.

Gude et al. (2008) reported the photodegradation of methylene blue (MB) on surface modified SiO₂ and SiO₂-TiO₂. Adsorption study of MB on photocatalyst indicates that adsorption is effected by surface alteration functional groups on the surface. The modified SiO₂-TiO₂ showed excellent photodegradation of methylene blue

Ren et al. (2009) synthesized titania-silica composites with mean pore sizes of 3.2 nm. The composite was synthesized using wollastonite and titanium sulfate as precursor. The synthesized porous titania-silica composites had well-crystallized anatase content and exhibited efficient photocatalysis.

Chen et al. (2014) worked on the synthesis of ultrathin anatase TiO₂ nanosheets dominated by 100% high-energy (001) facets using tetra butyltitanate (TBT) and HF as precursors. The synthesized TiO₂ nanosheets showed good photocatalytic activity in the degradation of rhodamine B which was better than Degussa P25. Which is due (001) facets and the efficient inhibition of recombination rates charge carriers.

Sowmya and Meenakshi (2014) investigated UV assisted reduction of nitrate using Ag-TiO₂ composite photocatalyst using oxalic acid as a hole scavenger. The Ag-TiO₂ composite was synthesized by photo deposition technique. The Ag-TiO₂ composite exhibited superior photocatalytic activity than nascent TiO₂.

Gu et al. (2014) synthesized photocatalytic graphene doped TiO₂ nanocomposites via a hydrothermal method using GO and TiO₂ in water. It was found that the good photocatalytic activity is due to the smaller particle size, enhancement in adsorption of pollutants and charge carrier lifetime.

Duo et al. (2015) synthesized rutile TiO₂/BiOCl composites via a low temperature hydrolysis method. The good photocatalytic activity of the rutile TiO₂/BiOCl composites is associated with the hetero junctions between BiOCl and rutile TiO₂, which can broaden the light absorption range.

Table 2.3 Enhanced photocatalytic activity of titanium dioxide nanomaterials literature summary

Authors	Year	Topic	Observations
Zhang et al.	2000	Impact of calcination on the photocatalytic activity of Titania nanopowders	They found that calcination above 400 °C could improve photocatalytic activity but calcination above 600 °C resulted in lowering of photocatalytic activity.

Li et al.	2005	Synthesis of silica-modified titanium dioxide nanoparticles by hydrothermal method	The SiO ₂ -TiO ₂ nanoparticles exhibited superior photocatalytic activity. Nanoparticles was retained even after calcination at 1273 K.
Ren et al.	2009	Titania-silica composites synthesized using wollastonite and titanium sulfate	High specific surface area, large pore volume, and narrow size distribution particles were obtained. The synthesized porous titania-silica composites had well-crystallized anatase content and exhibited efficient photocatalysis.
Chen et al.	2014	Ultrathin anatase TiO ₂ nanosheets dominated by 100% high-energy (001) facets	The synthesized TiO ₂ nanosheets showed excellent photocatalytic activity in the degradation of organic dye, which was better than that of the commercially available Degussa P25.
Sowmya and Meenakshi	2014	UV assisted reduction of nitrate using Ag-TiO ₂ composite photocatalyst	The Ag-TiO ₂ composite was prepared by photo deposition method. The Ag-TiO ₂ composite exhibited superior photocatalytic activity than nascent TiO ₂
Gu et al.	2014	Photocatalytic graphene doped TiO ₂ nanocomposites via a facile hydrothermal method	It was found that the good photocatalytic activity is due to the smaller particle size, enhancement in adsorption of pollutants and charge carrier lifetime.
Duo et al.	2015	Rutile TiO ₂ /BiOCl composites by a facile low temperature hydrolysis method	The good photocatalytic activity of the rutile TiO ₂ /BiOCl composites is associated with the hetero junctions between BiOCl and rutile TiO ₂ , which can broaden the light absorption range.

2.4 POLYMER NANOCOMPOSITE MEMBRANES

Yan et al. (2005) studied the impact of Al_2O_3 nanoparticle addition in polyvinylidene fluoride (PVDF) ultrafiltration membrane. They observed that the membrane surface morphology was altered and the surface roughness increased. The permeate flux of the modified membrane was increased due to increase in the surface hydrophilicity and the efficient filtration area due to the addition of inorganic Al_2O_3 nanoparticles. The improved hydrophilicity of the nanocomposite membrane also improved the antifouling property.

The effect of addition of TiO_2 nanoparticles and their size on the performance of PVDF membrane was analyzed. The results showed that nanosize affected the performance and structure of the nanocomposite membranes. Smaller nanoparticles could enhance the antifouling property of the membrane profoundly. Experiments also indicated that smaller TiO_2 nanoparticles had a strong effect on the crystallization of PVDF during phase inversion (Cao et al. 2006).

Choi et al. (2006) fabricated multi walled carbon nanotube (MWCNT) polymer blend membrane with PSF. They reported that MWCNT acts as a good modifier for the development of functional microporous PSF membranes. The hydrophilicity of the membrane surface, the pore size and porosity could be controlled based on additive content. By using the appropriate amount of MWCNTs, it was feasible to improve the flux and the solute rejection simultaneously.

Taurozzi et al (2008) investigated the effect of silver incorporation on the performance of polysulfone/silver nanocomposite membranes with various porosities. They observed the inbuilt antibacterial property owing to the gradual discharge of ionic silver by the nanocomposite which can be effectual in mitigating intrapore biofouling in membranes. Such nanocomposites can be used as future materials for developing macroporous membrane spacers to hinder the biofilm formation on downstream membrane surfaces.

PVDF/ SiO_2 nanocomposite hollow fiber ultrafiltration membranes were synthesized by sol-gel technique. The mechanical properties and thermal stability of composite membrane were improved. The presence of silica, improved the membrane hydrophilicity thus enhancing the permeability and antifouling properties (Yu et al. 2009).

Razmjou et al. (2011) investigated the effect of mechanical and chemical modification of TiO₂ nanoparticles on the surface chemistry, structure and fouling properties of Polyethersulfone (PES) UF membranes. The additions of modified nanoparticles in membranes exhibited a considerable enhancement in fouling behavior and permeate flux recovery.

Han et al. (2011) studied the performance of PVDF composite hollow fiber ultrafiltration membrane incorporated with various nanoparticles. The nanocomposite membranes showed higher permeate flux, better thermal and mechanical properties. However, the rejection of Bovine serum albumin (BSA) changed discordantly with different nanoparticles.

Antifouling enhancement of PVDF microfiltration membranes by adding Mg(OH)₂ nanoparticles was reported by Dong et al. 2011. Improved hydrophilicity was due to the addition of Mg(OH)₂ nanoparticle has contributed in an increase in permeability of the membrane. The supremacy of the PVDF/Mg(OH)₂ membrane in filtering E.coli solution was noteworthy, since resistances with respect to time decreased considerably. The composite membrane could be efficient in mitigating flux losses due to biofilm formation.

Rahimpour et al. (2011) studied the antifouling and bactericidal properties of TiO₂ incorporated nanocomposite PVDF/ sulfonated polyethersulfone (SPES) membranes. They observed a considerable increase in surface hydrophilicity of TiO₂ incorporated membranes. And also a pore size reduced with the addition of TiO₂ in the membrane cast solution occurred. The permeate flux of pure water and BSA solution of TiO₂ entrapped PVDF/SPES membranes were low compared to the nascent PVDF/SPES membrane. However, the antifouling property and long term flux stability were greatly improved.

Functionalized carbon nanotubes as an additive to improve the surface properties and performance of PES membrane was reported by Rahimpour et al. (2011). The hydrophilicity of membranes increased significantly with the addition of functionalized MWCNTs. By the addition of appropriate amounts of functionalized MWCNTs, the flux could be increased. The antifouling performance of nanocomposite membranes was also enhanced.

Hamid et al. (2011) carried out morphological analysis and performance study of polysulfone/titanium dioxide ultrafiltration membrane for humic acid removal. It was observed that membranes with TiO₂ exhibited a higher hydrophilicity compared to the nascent PSF membranes. The improvement in hydrophilicity played a key role in reducing various resistances, mainly those due to concentration polarization, cake layer formation, and adsorption.

A novel cellulose acetate nanocomposite membrane using TiO₂ nanoparticles was synthesized and analyzed by Abedini et al. (2011). Nanocomposite membranes had improved thermal stability than the pristine CA membrane. Increasing the amount of TiO₂ nanoparticles in the casting solution leads to greater membrane porosity. Permeate flux of the nanocomposite membranes was improved owing to the addition of TiO₂.

Richards et al. (2012) reviewed polysulfone membranes modified with various nanoparticles for application in water treatment. In their review, they noted that TiO₂/PSF and Ag/PSF nanocomposite membranes are the most investigated membranes. Ag/PSF membranes have shown to possess antimicrobial properties to reduce biofilm formation. The membrane characteristics were greatly enhanced by the addition of TiO₂, Al₂O₃ and ZrO₂ nanoparticles and nano silica. Tensile strength and hydrophilicity were also enhanced.

Performance and adsorption capabilities of TiO₂ nanoparticle incorporated PVDF hybrid membranes were studied. The content of TiO₂ had a significant effect on the performances of the hybrid membranes, and improved hydrophilicity and permeability. Enhanced antifouling properties were also observed for the hybrid membranes (Zhang et al. 2012).

Ahn et al. (2012) reviewed the fabrication and desalination applications of Carbon nanotube based membranes. They noted that membranes based on carbon nanotubes (CNT) are a promising technology for water purification applications. These membranes show high water flux and lower biofouling potential. CNT based membranes are free from various problems faced in case of conventional membrane separation process which also require a greater energy and maintenance.

Properties of ultrafiltration membranes composed of polysulfone and poly(1-vinyl pyrrolidone) grafted silica nanoparticles (PVP-g-silica) were reported by Song and

Kim (2013). The flux at 1 wt% additive was significantly more than that of pure PSF. The hydrophilicity of the membrane improved. The membranes exhibited enhanced fouling resistance.

Li et al. (2013) studied the effects of silver nanoparticles on PVDF membrane. Membrane flux and antibacterial tests were conducted to characterize the antifouling properties of the membrane. Flux recovery ratio (FRR) increased by about 40 % after the addition of silver nanoparticles on the membrane surface, revealing that the antifouling performance of PVDF membrane was enhanced by the addition of silver nanoparticles. Concurrently the antibacterial tests confirmed that PVDF membrane showed greater anti-biofouling activity because of silver nanoparticles.

Performance of TiO₂ nanotube added PSF/chitosan (CS) membranes were studied. The pure water flux of membranes was many times more than that of pure PSF UF membranes. The BSA rejection studies revealed the improved antifouling performance of membranes due to more hydrophilicity of TiO₂ nanotube additive. Highest fouling resistance ratio of 76% was obtained. The BSA rejection values for all nanocomposite membranes remained more or less same (Kumar et al. 2013).

Table 2.4 Polymer nanocomposite membranes literature summary

Authors	Year	Topic	Observations
Cao et al.	2006	TiO ₂ nanoparticles addition in PVDF membrane	Smaller nanoparticles can enhance the antifouling traits profoundly.
Razmjou et al.	2011	TiO ₂ nanoparticles in Polyethersulfone (PES) UF membranes	The additions of modified nanoparticles in membranes exhibited a considerable enhancement in fouling behavior and permeate flux recovery.
Rahimpour et al.	2011	TiO ₂ incorporated nanocomposite PVDF/sulfonated polyethersulfone (SPES) membranes.	They observed a considerable increase of hydrophilicity of membranes. And also pore size reduced with the greater addition in the membrane cast solution occurred.

Hamid et al.	2011	Performance study of PSF/TiO ₂ UF membrane	It was observed that membranes with TiO ₂ showed more hydrophilicity than nascent PSF membranes. The improvement in hydrophilicity played a key role in reducing various resistances.
Abedini et al.	2011	TiO ₂ nanoparticles/cellulose acetate nanocomposite membrane	Increasing the amount of TiO ₂ nanoparticles in the casting solution leads to greater membrane porosity and increase in permeate flux.
Zhang et al.	2012	TiO ₂ nanoparticle incorporated PVDF hybrid membranes	The content of TiO ₂ had a significant effect on the performances of the hybrid membranes, and improved hydrophilicity and permeability. Enhanced antifouling properties were also observed.
Kumar et al.	2013	TiO ₂ nanotube incorporated Polysulfone/chitosan membranes	The flux of nanotube membranes was much more than that of nascent PSF. The BSA rejection experiments revealed the good antifouling performance of membranes due to the hydrophilicity of TiO ₂ nanotube additive.

PREAMBLE FOR THE FOLLOWING CHAPTERS

The following chapter (chapter 3 to chapter 9) discusses about the synthesis and characterization of TiO₂ based nanomaterials and their applications in either membrane-based water purification or photocatalyst based water treatment.

Chapter 3: This chapter discusses about the synthesis and characterization of TiO₂ nanostructures, TiO₂ nanofibers (TNF) and TiO₂ nanosheets (TNS).

Chapter 4: This chapter discusses about the synthesis and characterization of TiO₂ nanofibers incorporated PSF ultrafiltration membranes.

Chapter 5: This chapter discusses about the synthesis and characterization of silver doped TiO₂ nanofibers and its application in photocatalytic hierarchical membranes.

Chapter 6: This chapter discusses about the synthesis and characterization of TiO₂ nanosheets incorporated PSF ultrafiltration membrane for dye rejection.

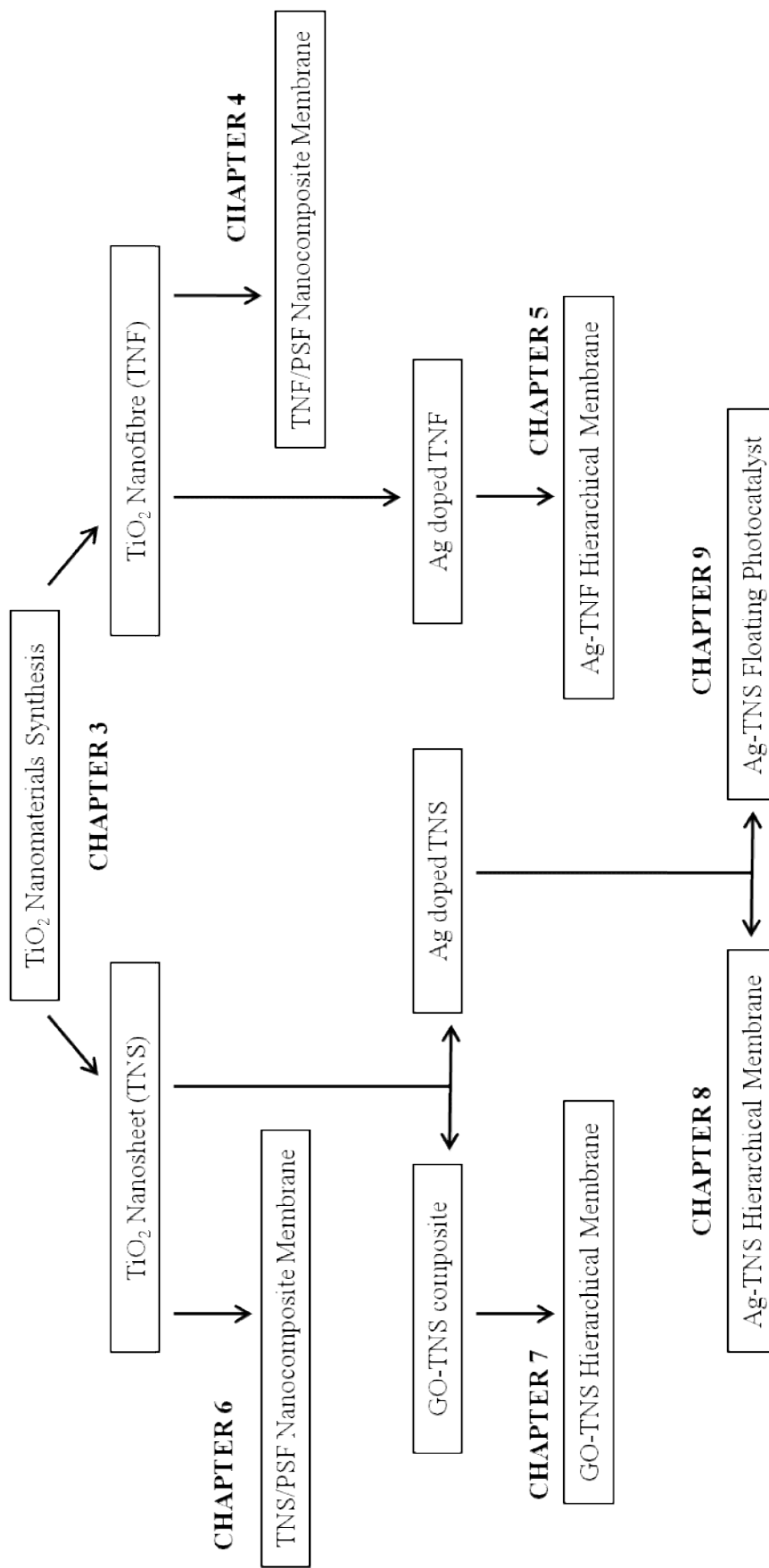
Chapter 7: This chapter discusses about the synthesis and characterization of graphene oxide (GO) modified TiO₂ nanosheets and its application in photocatalytic hierarchical membranes.

Chapter 8: This chapter discusses about the synthesis and characterization of Silver doped TiO₂ nanosheets and its application in photocatalytic hierarchical membranes.

Chapter 9: This chapter discusses about the synthesis and characterization of silver doped TiO₂ nanosheets/Polysulfone composite based floating photocatalyst for solar water treatment.

A scheme of research work is provided below for better understanding of the interrelation between various chapters.

SCHEME OF RESEARCHWORK



CHAPTER 3

SYNTHESIS OF TiO₂ NANOSTRUCTURES

3.1 INTRODUCTION

In this chapter synthesis and characterization of TiO₂ nanostructures are discussed. TiO₂ nanostructures namely, nanofibers and nanosheets were synthesized and characterized. These nanomaterials were then used in various applications for water treatment in the form of nanocomposite membranes and photocatalytic hierarchical membranes. Further modifications and applications of these TiO₂ nanostructures will be discussed in detail in the subsequent chapters.

3.2 SYNTHESIS OF TNF

3.2.1 Materials

Titanium (IV) oxide (TiO₂) nano powder (particle size 21 nm) was purchased from Sigma-Aldrich Co, Bangalore, India. Ethanol, sodium hydroxide (NaOH), hydrochloric acid (HCl, 37%) and ammonium hydroxide were purchased from Merck, India Ltd. All the chemicals were used without further purification.

3.2.2 Hydrothermal synthesis of TNF

In brief, 2.5 g of TiO₂ nano powder was added to 300 mL of 12 M NaOH aqueous solution and stirred for 30 minutes. After stirring, the suspension was poured into a Teflon lined stainless steel autoclave. The autoclave was placed in a hot air oven for 3 days at 170 °C. The product after hydrothermal treatment was cleansed thoroughly with distilled water and then with dilute HCl (pH-2) till the pH of the solution became 7. The nanofiber suspension was again washed with distilled water to remove any NaCl content. Thus, obtained nanofibers were dried in a hot air oven for 24 h at 60 °C and calcined at 500 °C for 2 hours in a muffle furnace.

3.3 SYNTHESIS OF TNS

3.3.1 Materials

Tetra butyl titanate (TBT) 98% was purchased from Sigma-Aldrich Co, Bangalore, India. Hydrofluoric acid (40%) was purchased from Nice chemicals, Kochi.

3.3.2 Hydrothermal synthesis of TNS

10 mL of TBT was added drop wise into a hydrothermal autoclave containing 3 mL of Hydrofluoric acid with stirring. The hydrothermal autoclave was kept at 200 °C for 24 h in a hot air oven. After 24 hours, the autoclave was allowed to cool down to ambient temperature. Sample obtained were centrifuged, washed multiple times with distilled and ethanol. Residue obtained was dried at 50 °C for 12 hours.

3.4 CHARACTERIZATION OF TiO₂ NANOSTRUCTURES

The morphology of the TiO₂ nanofibers were analyzed using scanning electron microscope (SEM, Jeol JSM-6380LA). All samples were sputtered with gold before analysis. TEM, JEOL JEM-2100 was used for analyzing the TiO₂ nanosheets. For TEM analysis, a very small quantity of sample was dispersed in ethanol and loaded on a carbon coated copper grid. The specific surface area of the nanostructures and commercial TNP (Sigma-Aldrich) was compared using Brunauer–Emmett–Teller (BET) analysis. UV-Visible spectrometer (Hitachi, U-2900) was used to estimate dye concentration

3.4.1 Photocatalytic activity

The photocatalytic activity was assessed via congo red dye degradation under optimum conditions as reported by Muhammad (2015). The dye concentration of 15 ppm, catalyst loading of 25 mg and neutral pH was used for analysis. To 100 mL dye solution 25 mg of catalyst was added and dispersed via stirring. The solution was continuously aerated via air injector. The solution was irradiated by two UV Lamp (18 W). 2 mL sample was collected at 30 min interval and centrifuged to separate the powder catalyst. The samples were then subjected to UV-Visible spectroscopy for estimating dye concentration. The schematic of the experimental setup of the photocatalytic reactor is shown in Fig. 3.1.

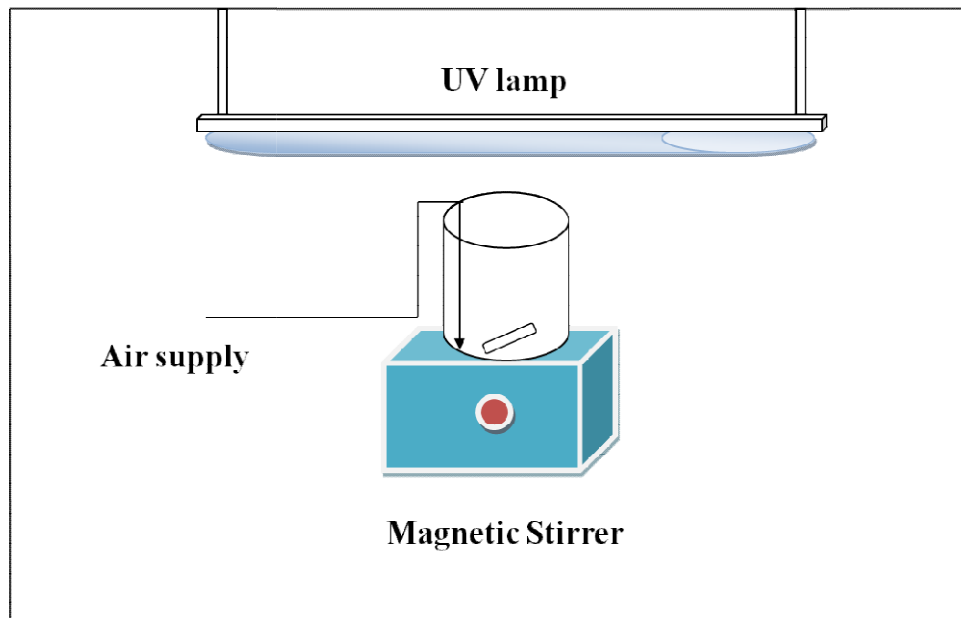


Fig. 3.1 The schematic of the experimental setup of the photocatalytic reactor

The experimental setup consisted of a magnetic stirrer over which the test sample containing the required quantity of dye solution and photocatalyst was loaded in a beaker and stirred using a magnetic pellet. Above the beaker UV lamps were provided for adequate UV irradiation for the reaction mixture. The reaction mixture was continuously aerated via air injector line. The whole setup was placed inside a closed sheet metal chamber to prevent leakage of UV rays.

3.5 RESULTS AND DISCUSSION

The nanofibers synthesized by hydrothermal method were characterized using SEM (Fig. 3.2). As seen from the SEM image, TiO_2 nanofibers with diameters of around 100 nm and length of 3-4 μm were obtained.

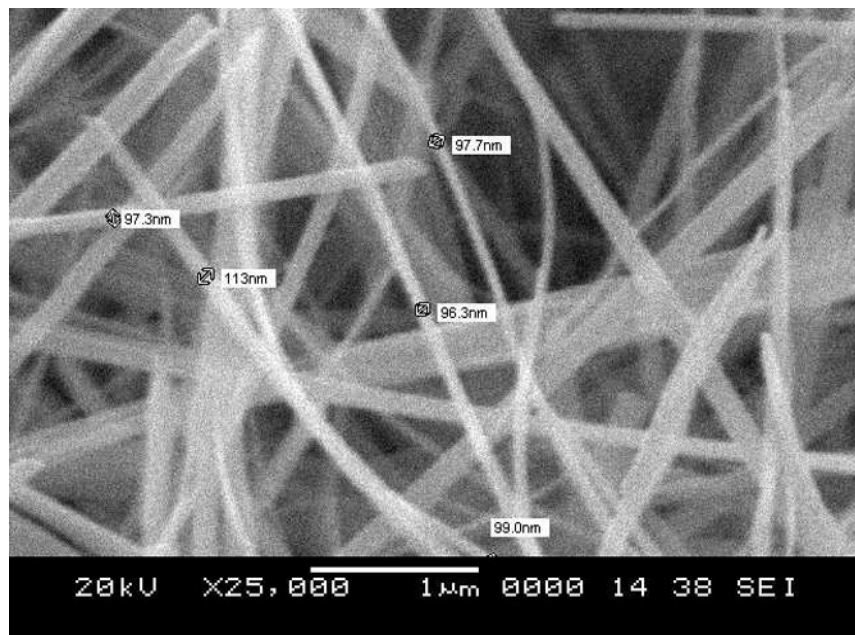


Fig. 3.2 SEM image of TNFs

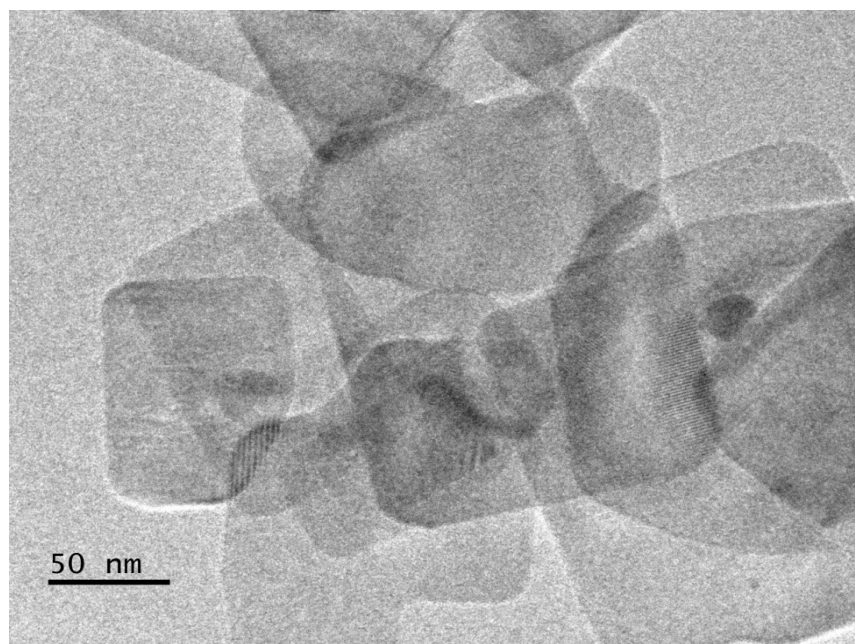


Fig. 3.3 TEM image of TNS

TEM image of synthesized TiO_2 nanosheets is shown in Fig. 3.3. In the figure individual flake like rectangular nanosheets can be observed. The thin sheet structure of the TiO_2 nanosheets can be seen in the TEM image. Thickness of TNS could not be estimated since no vertically aligned sheets could be observed but by the

translucence under electronbeam, indicating that they have a thickness of only a few nanometers (Chen et al. 2014).

Table 3.1 BET Surface area analysis of various TiO₂ nanostructures

Nanomaterial	TNP	TNF	TNS
Specific Surface area (m ² /g)	54.31	38.45	60.48

The BET analysis of TiO₂ nanostructures (Table 3.1) revealed that TiO₂ nanosheets had a greater specific surface area when compared to the synthesized commercial TNP. But TNF showed least comparatively less specific surface area due to the higher diameter (close to 100 nm). Were as nanoparticles were of diameter 21 nm and nanosheets had a very low thickness of the order of a few nanometers. As the diameter or thickness of the nanostructure decreases greater specific surface area is achieved for a material.

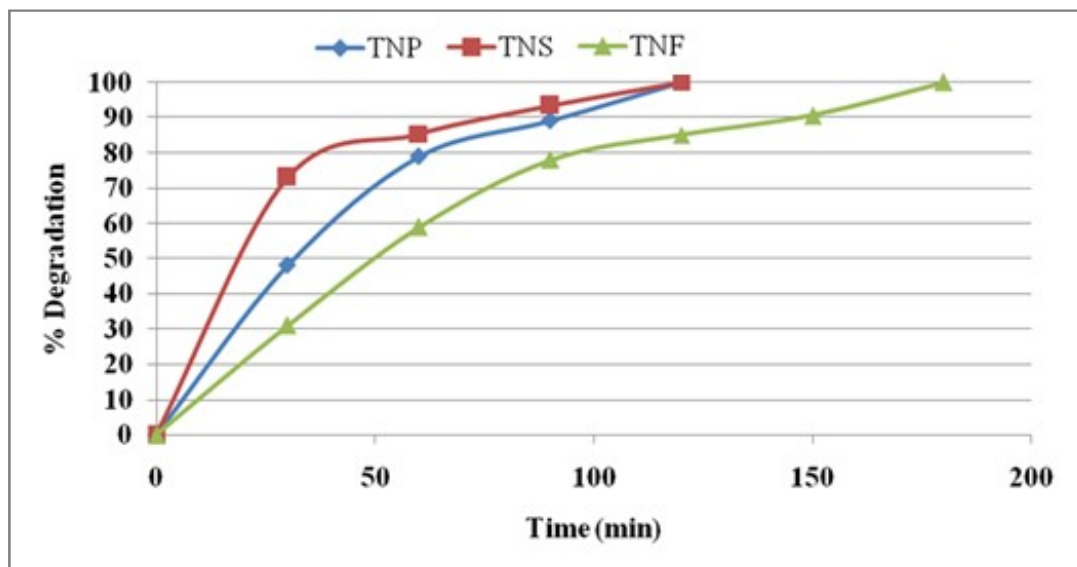


Fig 3.4 Photocatalytic dye degradation studies of various TiO₂ nanostructures

Photocatalytic degradation studies are shown in Fig. 3.4. As observed from the figure, the degradation increased as time progressed for all the photocatalysts. All the three degradation processes reached 100 % degradation but the time taken to achieve the same varied. TNP and TNS reached complete degradation in a shorter period of time, whereas TNF took more time. Among TNS and TNP, initial degradation was more

rapid for TNS. It was observed that TNS and TNP showed comparable performance in degrading the Congo red dye. But TNF showed poor performance, which could be due to the low specific-surface area of TNF. It is evident that the synthesized TNS has a better photocatalytic activity than TNF.

CHAPTER 4

TiO₂ NANOFIBER/POLYSULFONE (TNF/PSF) NANOCOMPOSITE ULTRA-FILTRATION MEMBRANE

Abstract

Titanium dioxide nanofibers were synthesized via alkaline hydrothermal method using TiO₂ nanopowder. These nanofibers were used to make composite polysulfone ultrafiltration membranes along with polyethylene glycol as pore forming agent. The obtained samples were characterized using scanning electron microscope, X-ray diffraction, and attenuated total reflectance infrared spectroscopy. Contact angle measurements were used to estimate hydrophilicity of the membrane. Performance of the membrane was analyzed using pure water flux studies and antifouling studies with bovine serum albumin as the standard protein for rejection. The composite membranes exhibited better performance in both permeability and antifouling property.

4.1 INTRODUCTION

Polysulfone (PSF) is a widely used polymeric material for ultrafiltration membranes due to its good chemical stability and mechanical properties. The performance of a membrane depends on its wettability in water-based filtration processes. Polysulfone is hydrophobic in nature and this result in poor flux and high fouling. The hydrophobic nature of the membrane can be changed by using anyone of the following methods; chemical surface treatment, blending with other polymers and hydrophilic additives. Polyethylene glycol (PEG) has been reported as an excellent additive to enhance permeation by improving the porosity of the membrane (Ma et al. 2011). PEG is also used in the membrane to improve the dispersion of other additives (Dong et al. 2012). But higher concentration of PEG results in poor rejection and mechanical behavior (Kim et al. 1998). Researchers have achieved enhanced performance by blending various nanoparticles in PSF membranes (Zhang et al. 2012).

TiO₂ nanoparticles have been reported as a performance enhancement additive in PSF membranes (Yang et al. 2007). But, it has been observed that property enhancement happens only up to 2 wt.% addition of TiO₂. Beyond 2 wt.% addition, the membrane loses its properties due to particle agglomeration. Also rheological properties of casting solution changes beyond 2 wt.% of TiO₂ and a drastic increase in viscosity was observed. Titanium dioxide nanofibers (TNF) are one of the morphological forms of titanium dioxide nanoparticles and it has an advantage over the other forms due to its higher aspect ratio. TNF being in fiber form can serve as a better reinforcement in composites due to greater interface interaction (He et al. 2013). Based on the literature survey incorporation of titanium dioxide nanofibers in PSF was not reported. Thus in this study, TNF was used as additives in PSF casting solutions to cast nanocomposite membranes with different compositions. Membranes were characterized using SEM, X-Ray diffraction (XRD), and Attenuated Total Reflectance Infra Red Spectroscopy (ATR-IR). Contact angle measurements were made to evaluate membrane hydrophilicity. The performance of these membranes were evaluated using pure water flux (PWF) and antifouling studies using bovine serum albumin (BSA) as a standard protein for rejection.

4.2 MATERIALS AND METHODS

4.2.1 Materials

Polysulfone (molecular weight 35,000 Da) and Bradford reagent was purchased from Sigma-Aldrich Co, Bangalore, India. 1-Methyl-2-pyrrolidone (NMP), Polyethylene Glycol (PEG) 600 and ethanol were purchased from Nice chemicals, Kochi. All the chemicals were used without further purification.

4.2.2 Preparation of TNF incorporated PSF membranes

For the preparation of 1 wt.% membrane, Polysulfone (20 wt.%), NMP (75 wt.%) and Poly Ethylene Glycol (5 wt.%) were taken and kept for stirring at 60 °C over a period of 4 h for the complete dissolution of PSF. 1wt.% of TNF (with respect to the weight of polymer solution) was added to the polymer solution at the same temperature and again stirred for 30 min.

Table 4.1 Blend compositions of Membranes

Membranes	Polymer solution			TNF (wt.% of polymer solution)
	PSF (wt.%)	PEG (wt.%)	NMP (wt.%)	
M-0	20	5	75	0
M-1	20	5	75	1
M-3	20	5	75	3
M-5	20	5	75	5
M-10	20	5	75	10

The resultant cast solution was poured on to a glass plate and spread using a glass rod. It was then submerged in distilled water (Nair et al. 2013). During phase inversion the NMP (solvent) diffuses out in to the coagulation media and the water (non-solvent) diffuses in to the membrane. The out diffusion of the solvent results in the rapid solidification or precipitation of the membrane polymer. The mutual exchange of NMP and water in the membrane results in generation of pores. Similar procedures were used for the remaining membranes (Table 4.1).

4.3 CHARACTERIZATION

4.3.1. ATR-IR analysis

ATR-IR spectra were obtained via Jasco4200 IR Spectrometer in the range of 4000-650 cm^{-1} . The spectral analysis of TNF and composite membranes was conducted.

4.3.2. XRD analysis

X ray diffractograms were obtained using Rigaku Miniflux 6000, X-ray Diffractometer. The diffractograms were obtained at $0.06^\circ/\text{s}$ in the 2θ range $10-60^\circ$.

4.3.3. SEM analysis

Jeol JSM-6380LA, SEM was used to acquire SEM images. The membrane pieces were cryogenically fractured using liquid N_2 before taking cross sectional images. All samples were sputtered with gold before scanning.

4.3.4. Contact angle measurement

FTA-200 Dynamic contact angle analyzer was employed to estimate the contact angle of membranes via sessile droplet method.

4.3.5. Permeation properties

Sterlitech HP4750 stirred dead end filtration cell with exposed membrane area of 14.6 cm² was employed to study the permeation characteristics of the membranes. Membranes were kept immersed in water for one day before carrying out flux study. Variation of (PWF) with time was studied. Permeate was collected after 20 min of contact to 0.2 MPa transmembrane pressure. Permeate sample was collected at 5 minutes interval. The PWF (J_w) was calculated using the following relation:

$$J_w = \frac{Q}{\Delta t A} \quad (1)$$

Where J_w is expressed in Lm²h⁻¹ and Q is the volume of permeate collected in Δt (h) time period for a area A (m²).

4.3.6. Antifouling characteristics

The antifouling characteristics were analyzed as per literature (Zhao et al. 2011). PWF of the membrane J_{w1} (L/m²h) was obtained at 0.2 MPa TMP. The antifouling property of the membrane was studied using BSA as standard protein for rejection. 0.8g/L of an aqueous solution of BSA was made and used for rejection study for 90 minutes. Later the membrane was cleansed with distilled water for 20 minutes and PWF J_{w2} is determined once again. The antifouling capacity was estimated in terms of flux recovery ratio (FRR) using the following equation:

$$FRR(\%) = \frac{J_{w2}}{J_{w1}} \times 100 \quad (2)$$

In order to determine the rejection capacity of the membrane, feed and permeate solution samples were collected and Bradford reagent was added. Samples were left idle for 10 minutes before analyzing using UV-Spectrometer. The % BSA protein rejection was determined using the below equation:

$$\%R = \left(1 - \frac{C_p}{C_f}\right) \times 100 \quad (3)$$

4.4 RESULTS AND DISCUSSION

4.4.1. Membrane characterization

4.4.1.1. ATR-IR analysis

The ATR-IR spectrum of TNF is shown in Fig. 4.1 (a). The peak at 894.8cm⁻¹ corresponds to the longitudinal optical mode of anatase phase of TiO₂. The presence

of polymeric Ti-O chains in the nanofibers can be identified by lowering of transmittance beyond 650 cm^{-1} (Reza et al. 2013). The broad peak appeared around 3375 cm^{-1} corresponds to O-H vibrations of Ti-OH groups due to physisorbed water content. ATR-IR spectra of M-0, M-10, and TNF are compared in Fig. 4.1. The characteristic peaks of PSF at 1297.86 cm^{-1} (S=O asymmetric stretch), 1240 cm^{-1} (C-O-C stretch), 1152.26 cm^{-1} (S=O symmetric stretch) can be seen in the composite membrane (Kumar et al. 2013). Apart from the PSF peaks, a notable peak that appears in M-0 is the broad peak around 3400 cm^{-1} which is due to the incorporation of PEG. The peaks in the TNF spectrum at 3375 cm^{-1} and 650 cm^{-1} are combined with similar M-0 peaks in the region to give lower peaks at 3299 cm^{-1} and 690 cm^{-1} in the M-10 spectrum. The merger of peaks implies a good interaction between TNF and PSF the broad -OH peak around $3300\text{-}3400\text{ cm}^{-1}$ is of great importance as it gives an idea of interactions with in the composite and also about the dispersion of the additive. The significant diminution in -OH peak of M-10 when compared to pure TNF indicates the lowered polarizability of hydroxyl group within the polymer. When the filler is polar and the polymer is nonpolar then the filler-filler interaction is much stronger than polymer-filler interaction. Higher concentrations of filler thus result in agglomeration and non-uniform dispersion (George et al. 2014). In the present work, the inclusion of hydrophilic PEG which has hydroxyl groups greatly helps in better dispersion of TNF, even at higher concentrations.

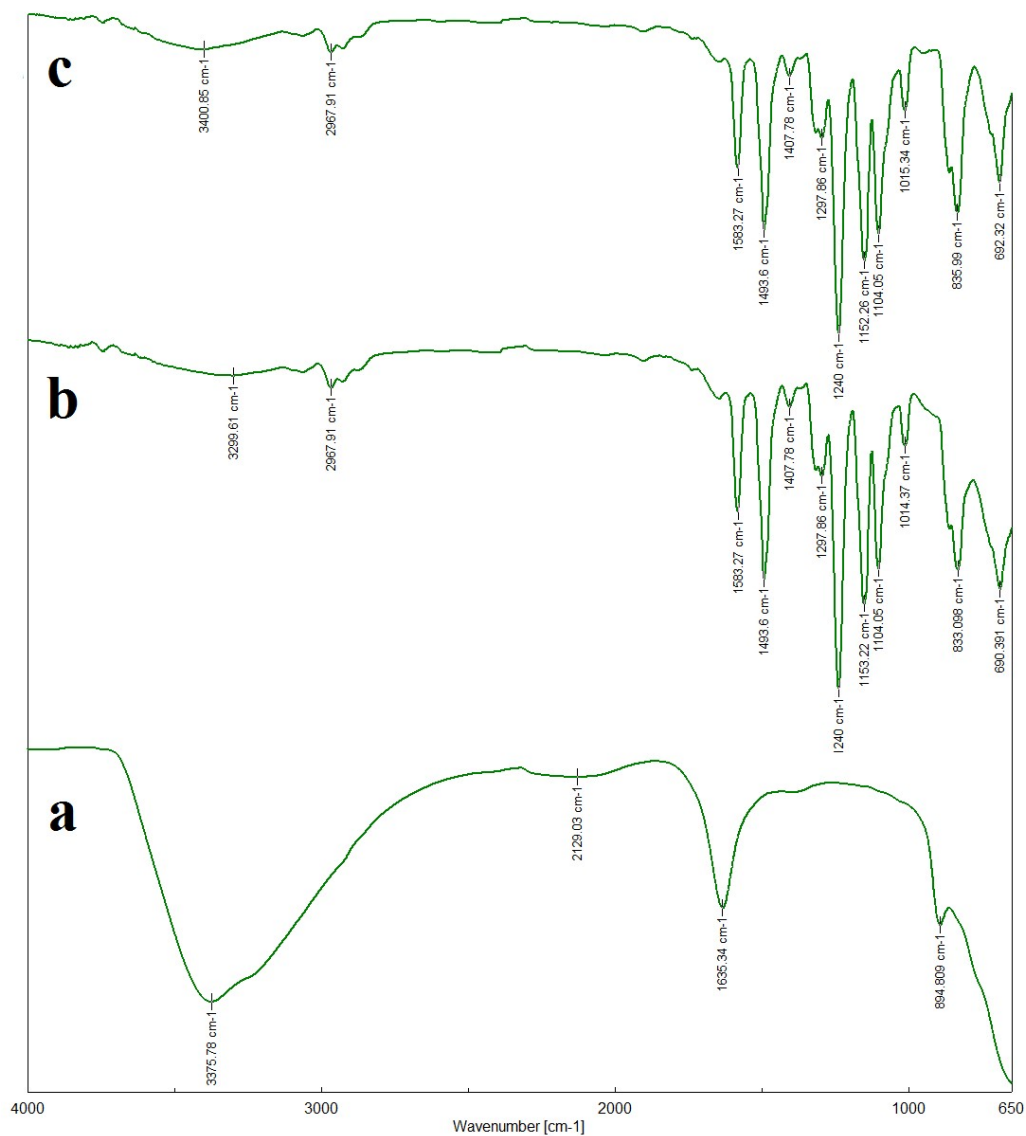


Fig. 4.1 ATR-IR spectra. (a) TNF; (b) M-0; (c) M-10.

4.4.1.2. XRD analysis

The XRD pattern of TNF, M-0, and M-10 are compared in Fig. 4.2. The characteristic peaks at 25.4°, 38.5°, 48° and 53.8° in the powder diffraction pattern of TNF indicate the presence of anatase phase (Zaleska et al. 2008). XRD of M-0 shows no peak indicates the absence of crystalline phase, affirmative in case of an amorphous polymer. Anatase characteristic peaks around 25.4°, 38.5°, 48° and 53.8° in the powder diffraction pattern can be seen in the M-10 membrane at a lower

intensity. The small shift in peaks indicates effective incorporation and good interaction between filler and matrix (Yang et al. 2007).

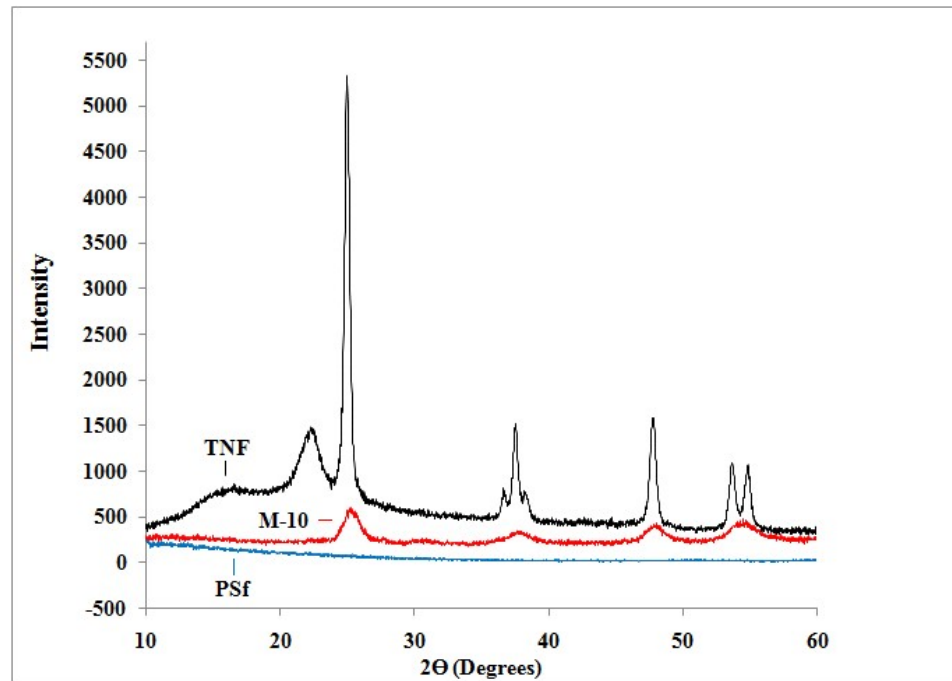


Fig. 4.2 XRD patterns of TNF, PSF, and M-10.

4.4.1.3. Morphology of the membrane

SEM analysis of the membranes synthesized having different concentrations of TNF is shown in Fig. 4.3. All the membranes display asymmetric construction, having dense top layer, porous sub layer, and fully developed macro pores layer. It is apparent from SEM images that rise in the addition of TNF caused lowering of finger like projection and lowered their length (Singh et al. 2013). The development of spongy structure in the sub layer was improved with higher additive content. The viscosity of cast solution increases with increasing additive content. This increased viscosity affects the kinetics of phase inversion as it retards the diffusion of solvent and non-solvent. The greater cast solution viscosity, solvent's out-diffusion is favored over nonsolvents in-diffusion into the solution resulting in the formation of membranes with smaller pores. Choi et. al (2006) reported similar trend in case of addition of multi-walled carbon nanotubes (above 4 wt.%) in polysulfone blend membranes. Yang et. al (2007) reported increased rheological hindrance beyond the rheological percolation threshold with increasing concentration of TNP additive

above 2 wt.%. The increased hydrophilicity due to the hydrophilic additive plays an important role in overcoming the increasing rheological hindrance. There are also reports on the addition of TiO₂ nanoparticles at higher concentrations, where it didn't result in reduction of pore size or flux (Zhang et al. 2006). In this context the addition of PEG would play a significant role apart from being a hydrophilic pore former, it also improves the dispersion of the filler and the interaction between TNF and PSF during membrane formation. Dong et. al (2012) reported that low concentration of PEG (5 wt.%) when used during phase inversion resulted in better dispersion of nanoadditives with in the membrane matrix and also increased the porosity. But when PEG is used at higher concentrations, it resulted in the accumulation of nanoadditives inside the membrane pore and caused loss in membrane properties.

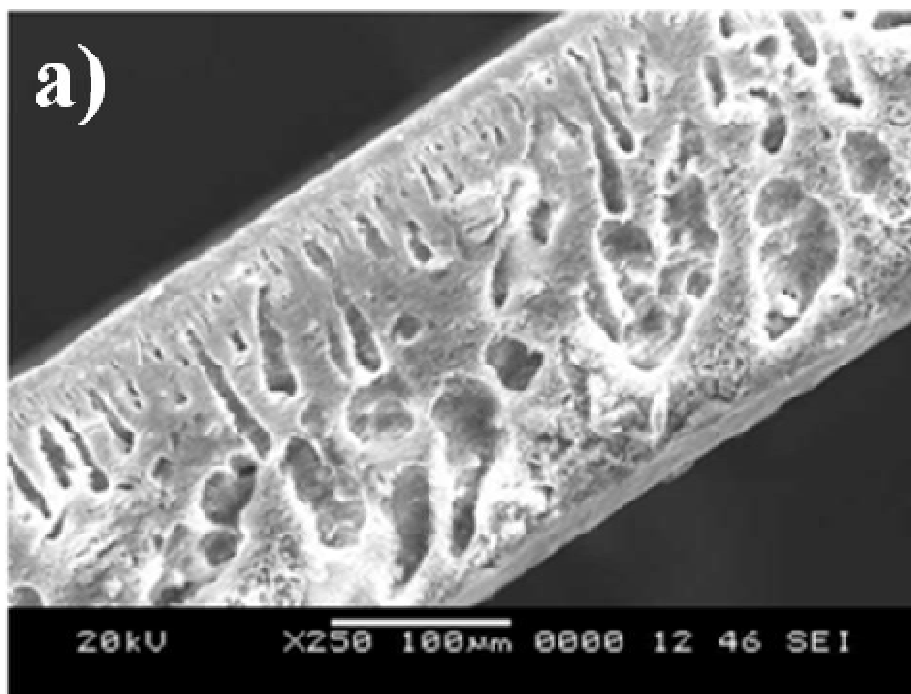


Fig. 4.3 Cross-sectional SEM images of membranes. (a) M-0; (b) M-1; (c) M-3; (d) M-5; (e) M-10.

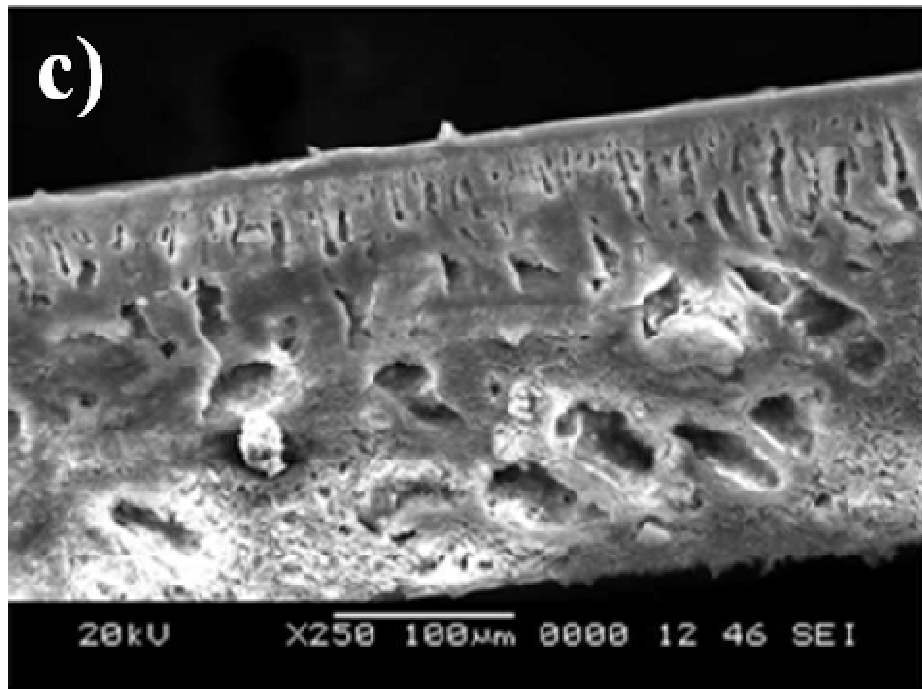
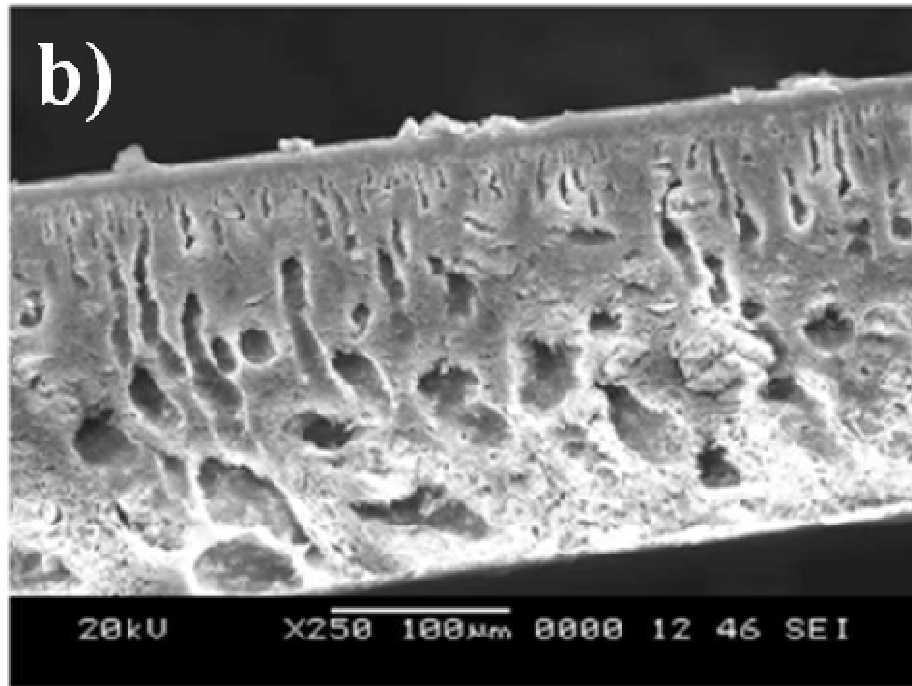


Fig. 4.3 Cross-sectional SEM images of membranes. (a) M-0; (b) M-1; (c) M-3; (d) M-5; (e) M-10.

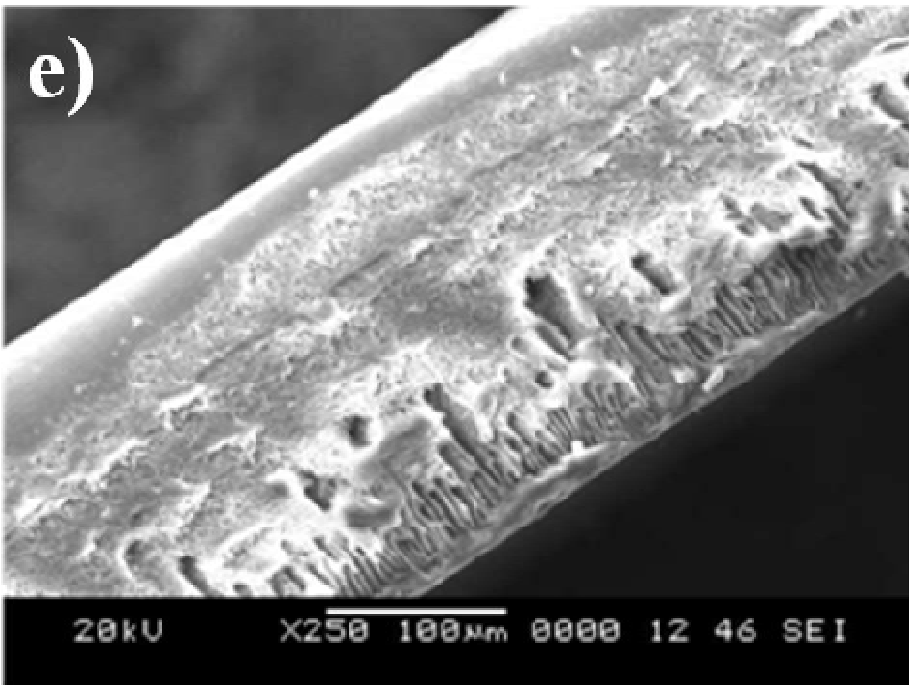
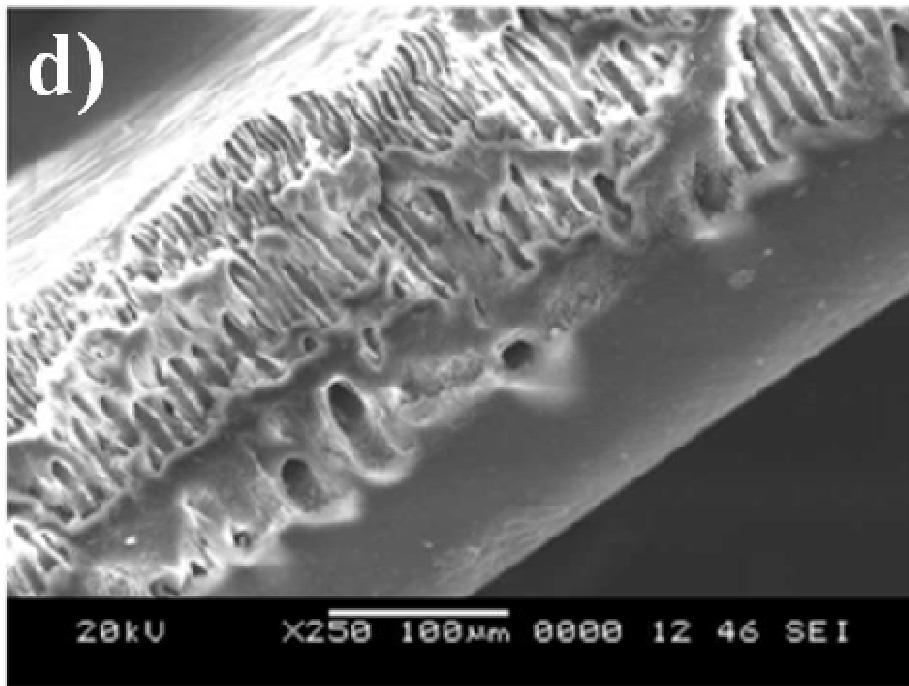


Fig. 4.3 Cross-sectional SEM images of membranes. (a) M-0; (b) M-1; (c) M-3; (d) M-5; (e) M-10.

4.4.1.4. Hydrophilicity of membranes

Hydrophilicity of a membrane is the key factor in determining the flux and antifouling capacity of the membrane. The low hydrophilicity results in adsorption/deposition of organics on the membrane surface (Sotto et al. 2013). When hydrophilic metal oxides like TiO_2 are added, presence of these particles on the membrane surface result in improved membrane hydrophilicity. The extend of hydrophilicity enhanced is thus depended on the availability of particles on the surface and is therefore a function of concentration and dispersion of the particles. So in general, unless there are issues related to rheological hindrance during phase inversion or deposition of particles inside pores, the addition of hydrophilic additive will increase surface wettability and reduce the contact angle. From the analysis (Fig. 4.4), it was observed that the contact angle of TNF blend PSF membranes gradually reduced from 73.88° for 0 wt.% TNF content to 48.88° for the 10 wt.% TNF content. The significant drop in contact angle is an obvious sign of improving the hydrophilicity. It can be concluded that the increase in the hydrophilicity could be due to the hydrophilicity of TNF additive.

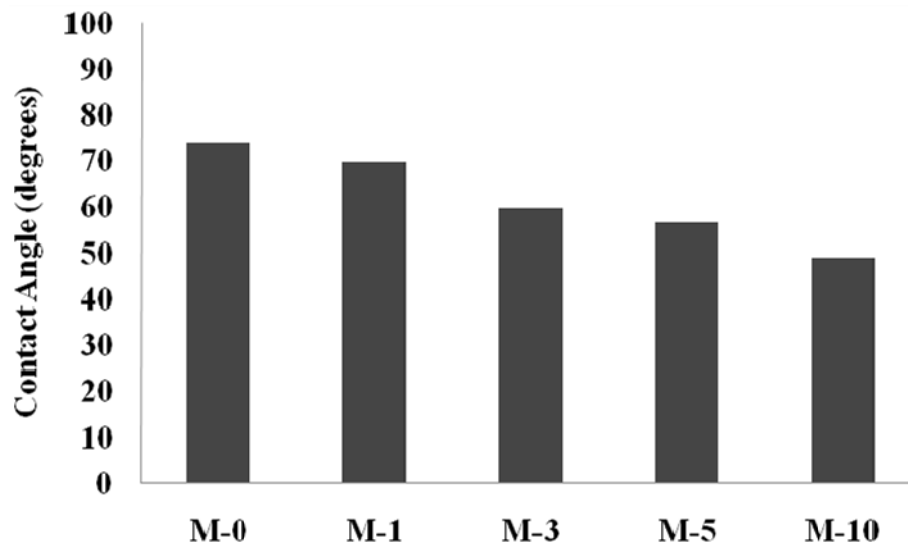


Fig. 4.4 Contact angle of the different membranes.

4.4.1.5. Membrane permeability and antifouling properties

Membrane performance was evaluated in terms of time dependent PWF, BSA rejection and flux recovery after BSA rejection (Teliet al. 2012). Initially, during

PWF, all membranes showed flux decline due to mechanical compaction. Flux study i.e. PWF, flux during BSA rejection and the recovered flux testing was done at 0.2 Mpa TMP and 25 °C for 90 min till the flux reached near steady state condition. The PWF flux of different membranes is compared in Fig. 4.5 (a). The nascent PSF (M-0) membrane showed minimal flux. M-1 membrane showed a slight improvement in pure water flux. At 3 wt.% addition of TNF for M-0, the flux doubled in comparison to nascent PSF membrane. For M-5, the flux further improved and at 10 wt.% addition in case of M-10, flux attained maximum steady state value.

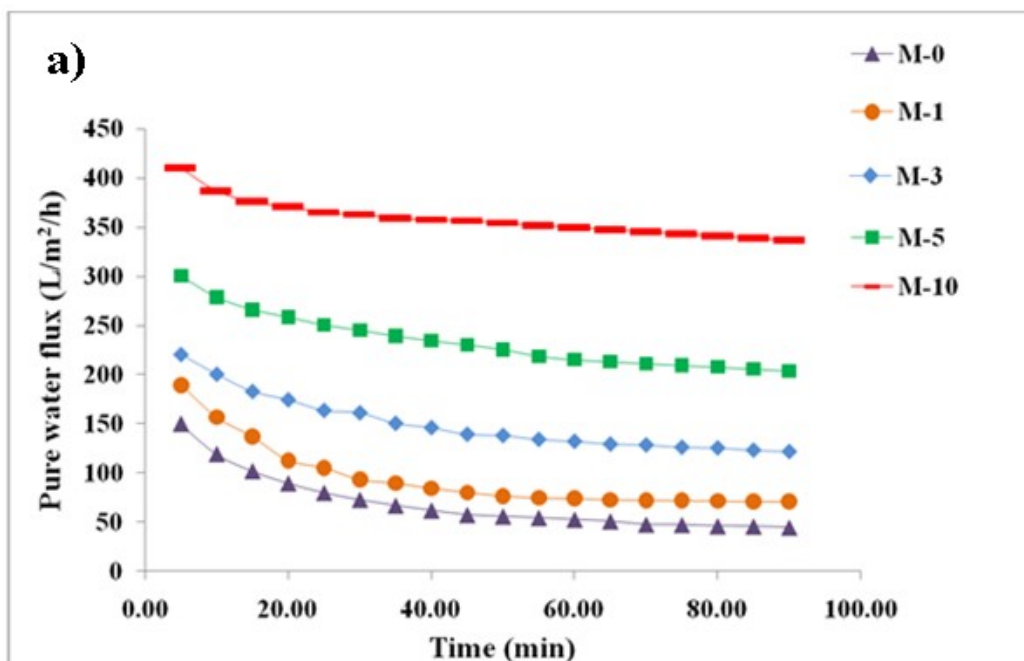


Fig. 4.5 Permeation and antifouling studies of the membranes. (a) PWF; (b) flux during BSA rejection; (c) flux recovery ratio.

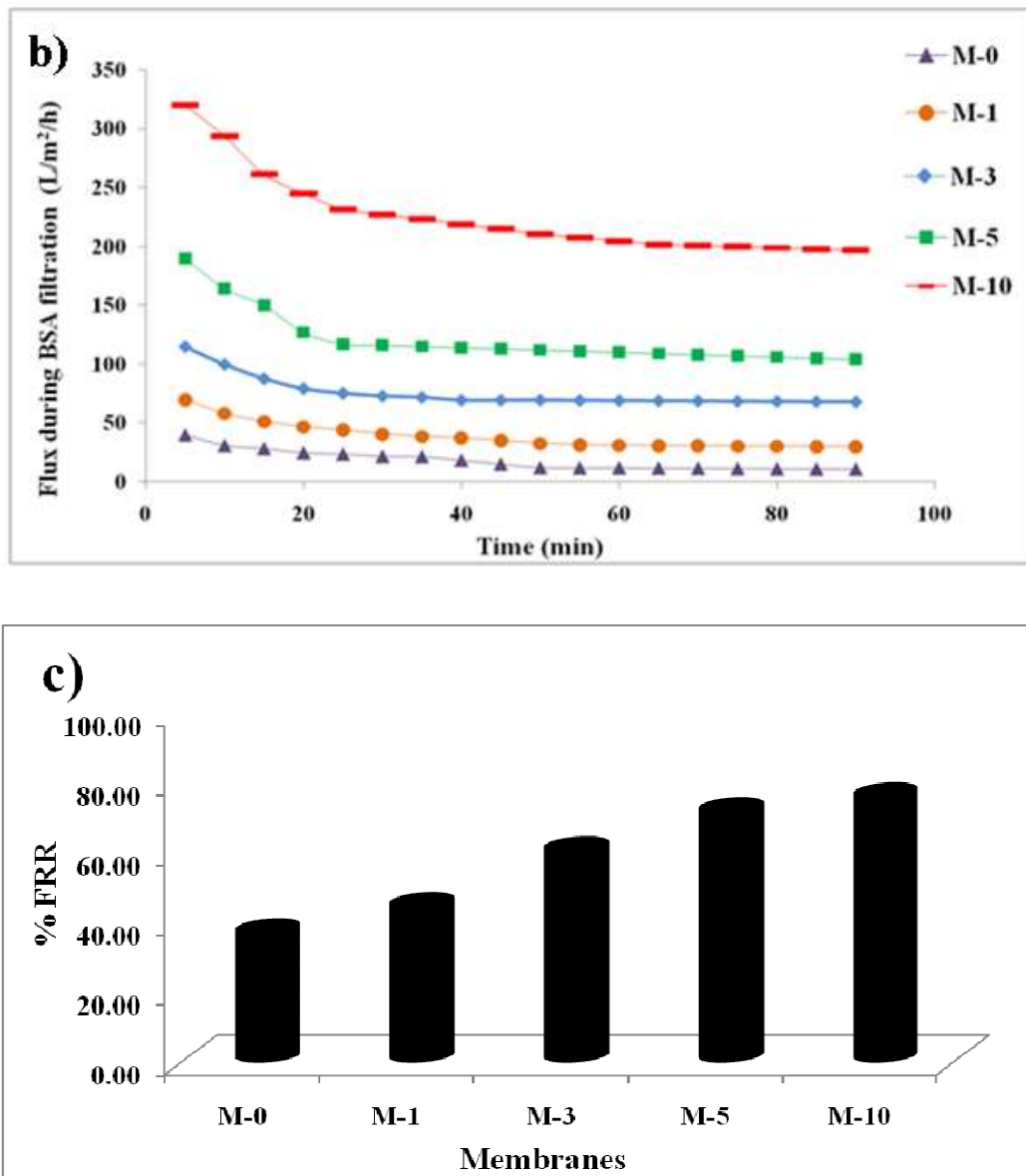


Fig. 4.5 Permeation and antifouling studies of the membranes. (a) PWF; (b) flux during BSA rejection; (c) flux recovery ratio.

As reported by Dong et. al (2012), when the concentration of nanoadditive is increased, permeation enhancement can occur as long as the additive is well dispersed within the polymer and does not agglomerate at the pores. The increasing trend of flux is an indication of better dispersion of TNF in the membrane and it is also an indication of minimal trapping of TNFs in the pores. The enhanced

hydrophilicity of membrane due to the addition of TNF is the key reason for the enhancement of permeability.

Nair et al. 2013, fouling leads to flux reduction and reduces membrane life time. BSA rejection studies simulate the effect of fouling on the membranes. The nascent PSF (M-0) membrane has no hydrophilic TNF and thus gets fouled easily with drastic drop in flux. M-1 and M-3 membranes also showed high flux drop due to fouling. M-5 membrane showed nominal flux drop and maintained moderate flux. M-10 membrane showed best performance with lesser flux drop and high steady state flux. All membranes exhibited similar permeation reduction in BSA rejection; lower flux reduction could be observed with higher TNF content in membrane (Fig. 4.5b). The BSA rejection of M-0, M-1, M-2, M-3 and M-5 membranes were 94%, 92%, 90%, 89% and 86%. After BSA rejection the membranes were cleansed and the pure water flux was determined (Fig. 4.5c). The nascent PSF (M-0) membrane showed least flux recovery due to the hydrophobic nature of PSF. M-1 and M-3 membranes showed 50 % flux recovery due to improved hydrophilicity. M-5 membrane showed a good flux recovery of above 60% and M-10 membrane exhibited better flux recovery of 76%. The hydrophilic TNF on the membrane surface improved the interaction with aqueous medium thus weakening interactions between membrane surface and protein molecules. This enables easy cleaning of foulant from the membrane surface, greatly enhancing the recyclability of the membranes.

4.5 CONCLUSIONS

Titanium oxide nanofibers were successfully synthesized within the size range of 90-100 nm diameters. PSF/TNF composite membranes were successfully synthesized and characterized using SEM, XRD, ATR-IR and contact angle measurements. The performance of membrane was analyzed using pure water flux, FRR, and percentage rejection. The membranes were seen to possess asymmetric structure. Contact angle measurements indicated a clear increase in membrane hydrophilicity with increasing concentration of TNF content. The PSF/TNF composite membranes showed better permeability than nascent PSF membrane. The membrane with 10 wt.% addition of TNF showed the highest value for pure water flux. Lower flux decline was observed

for the composite membranes in BSA rejection. 10 wt.% TNF addition recorded a maximum FRR of 76%.

CHAPTER 5

Ag-TiO₂ NANOFIBER (Ag-TNF)HIERARCHICAL MEMBRANES FOR PHOTOCATALYTIC DEGRADATION OF DYES

Abstract

TiO₂ nanoparticles have been widely studied for photocatalytic degradation of dyes, but their small size makes catalyst recovery difficult. When compared to TiO₂ nanoparticles, nanofibers are larger in size and exhibit good mechanical properties. Doping TiO₂ with suitable modifiers like silver can further boost their performance. In the present work, TiO₂ nanofibers were synthesized using hydrothermal method. The obtained TiO₂ fibers were then doped with silver via photo-deposition method under ultra-violet light irradiation. Scanning electron microscopy, energy dispersive X-ray spectroscopy, Fourier transform infra red spectroscopy and X-ray diffraction were used to characterize the nanofibers. Future, these nanofibers were used to synthesize a hierarchical photocatalytic membrane to enable continuous degradation and filtration. The effects of catalyst loading on permeation and dye removal were studied using rhodamine B. The silver doped TiO₂ nanofiber membranes exhibited good dye removal capabilities.

5.1 INTRODUCTION

Nano-size photocatalyst especially TiO₂ has attracted much attention over a decades. High specific surface area of TiO₂ nanomaterials has increased the photocatalytic activity but the smaller size has also increased the difficulty to recover the photocatalyst from the reaction mixture. Recent research in nanotoxicology infers the toxic nature of TiO₂ nanoparticles (Shi et al. 2013). Upon intravenous exposure, TiO₂ nanoparticles can cause pathological lesions of the liver, spleen, kidneys, and brain. Also, inhalation studies in rats have shown to result in lung tumors. Hence, when such materials are used for water treatment, complete recovery becomes mandatory. Researchers have been working on various methodologies to immobilize photocatalyst to facilitate catalyst recovery, and one such method is immobilizing the photocatalyst on top of a support membrane. Such assembly is called as a

hierarchical membrane which enables simultaneous photocatalytic degradation and membrane filtration (Bai et al. 2015). It is a good alternative to conventional photocatalytic degradation, since it enables continuous operation. For the formation of a good hierarchical membrane, the photocatalyst loaded on the top should form a uniform stable coating. Nanoparticles are least preferred in the synthesis of hierarchical membranes since their geometry doesn't allow stable film formation. Nanothorns, micro spheres and graphene-based composites of TiO_2 have been reported as suitable materials to develop stable hierarchical membranes (Gao et al. 2013).

TiO_2 nanofiber is a one-dimensional nano-form of TiO_2 . The major advantage of nanofiber is that they form an interconnected web like structures when stacked together. Zhang et al (2008) had previously reported a free-standing TNF membrane, but the membrane could only operate at low transmembrane pressures due to its fragile nature. In hierarchical membrane, the base membrane provides additional mechanical support enabling operation at higher pressures. Tang et al (2016) had recently reported an Ag/AgBr/TNF membrane for water purification with special emphasis on the antibacterial properties of the membrane. In the chapter, we discuss the synthesis of Ag- TiO_2 nanofiber hierarchical membrane and its application for dye removal. Rhodamine B dye was used as the model pollutant. Dye removal studies were conducted in presence and absence of UV irradiation to analyze the effect of adsorption and photocatalytic degradation on dye removal.

5.2 MATERIALS AND METHODS

5.2.1 Materials

Rhodamine-B dye was purchased from Sigma-Aldrich Co, Bangalore, India. Cellulose acetate membrane (Dia- 4.7 cm and pore size - 200nm) was obtained from Sartorius stedim biotech, Bangalore, India. Silver nitrate (AgNO_3), ammonium hydroxide and ethanol were procured from Nice chemicals Pvt Ltd, Cochin, India.

5.2.2 Synthesis of Ag-TNF composite

1.5 g of TNF was added to 250 mL of 15 mM AgNO_3 aqueous solution, the pH was made to 7 by adding ammonium hydroxide. The solution was stirred thoroughly and exposed to UV radiation for 4 h. The obtained dark purple product was washed thrice

with water and ethanol and dried in a hot air oven at 60°C. The procedure for Ag doping was adopted from Sowmya & Meenakshi (2015), which was originally used for the synthesis of Ag doped nanoparticles.

5.2.3 Synthesis of Ag-TNF Hierarchical Membrane

Suitable quantities of Ag-TNF as given in Table 5.1 were dispersed in 100 mL of distilled water and loaded into a filtration assembly (Tarsons-50021). Cellulose acetate membrane of diameter 47 mm and pore size 0.2 μm was used as the support membrane. Vacuum was applied using a vacuum pump (Technic-TID-75-S, Pressure 0.379 MPa) connected to the filtration setup. Water passed through the membrane as permeate, leaving behind a layer of Ag-TNF on the membrane surface. In 2010, Bai et. al had reported the synthesis of hierarchical Membrane via above method using TiO_2 nanothorns. Later, the procedure was commonly known as pressurized assembly.

Table 5.1 Photocatalyst loading of various membranes

Membrane	A-50	A-100	A-150	A-200	A-250
Ag-TNF Loading (mg)	50	100	150	200	250

5.3 CHARACTERIZATION

Scanning electron microscope (SEM, Jeol JSM-6380LA) was used to study the morphology of samples; samples were gold sputtered before imaging. EDS was also done using the same SEM. XRD diffractograms of the samples were obtained using X-ray Diffractometer (Rigaku Miniflux 6000). The Fourier transform infra-red spectroscopy (FTIR) of the sample was done using Shimadzu FTIR- 8400S spectrometer. UV-Visible spectrometer (Hitachi, U-2900) was used to estimate rhodamine B (RHB) dye concentration at a wavelength of 553 nm.

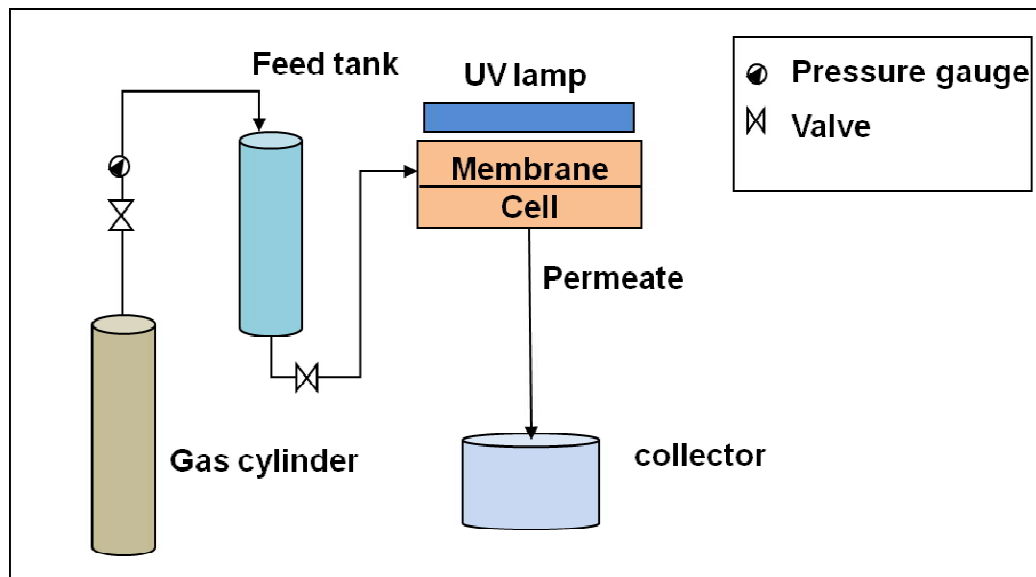


Fig. 5.1 Schematic representation of membrane testing unit

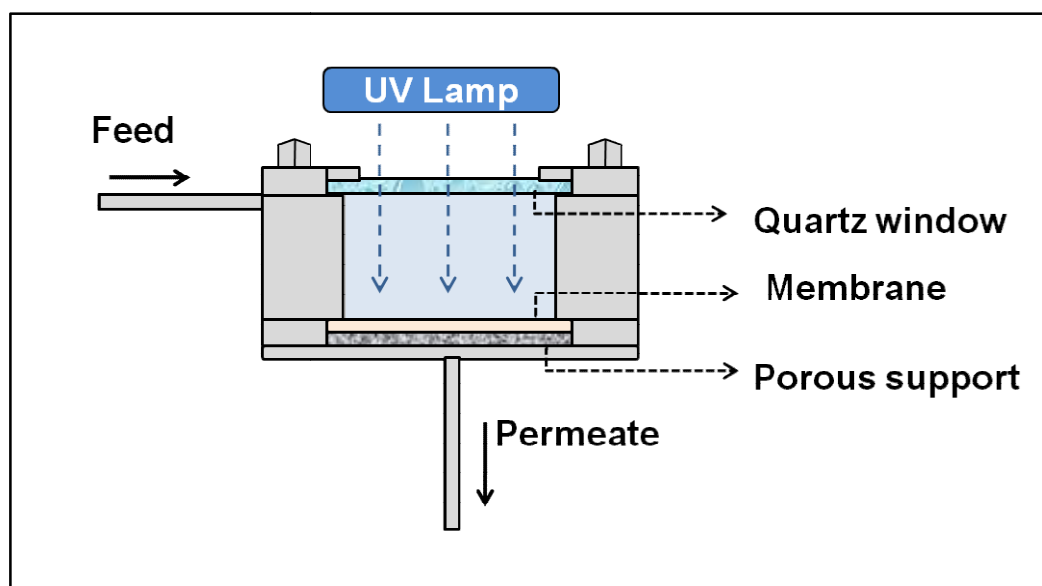


Fig. 5.2 Schematic representation of UV irradiated membrane cell

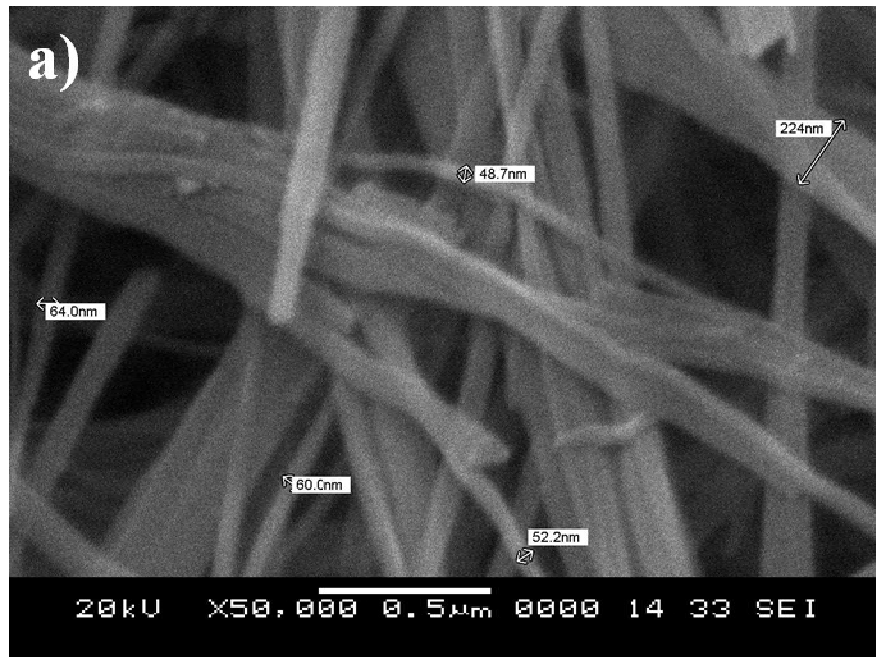
The membrane performances in terms of permeate flux and dye removal was studied using a custom-made dead-end filtration unit (Fig. 5.1) with an effective membrane area of 14.6 cm^2 . The filtration unit consists of an oxygen gas cylinder for pressurizing the feed, a two-liter feed tank and a membrane cell. The membrane cell is equipped with a quartz glass window on top for UV irradiation (Fig. 5.2). The flux studies were conducted at 0.1 MPa transmembrane pressure. 15 mgL^{-1} RHB dye

solution in distilled water was used for the dye removal studies. The dye removal (%R) was determined using the following equation:

$$\%R = \left(1 - \frac{C_p}{C_f}\right) \times 100 \quad (1)$$

5.3 RESULTS AND DISCUSSION

SEM images (Fig. 5.3a) reveals that the synthesized nanofibers have diameters under 100 nm and length of few micrometers. The surface image of Ag-TNF membrane's (Fig. 5.3b) clearly shows the nanofiber assembly on the base membrane. XRD peaks of TNF at 25.5°, 38.06°, 48.22° and 55.3° correspond to anatase phase of TiO₂ (Fig. 5.4). In the XRD pattern of Ag-TiO₂ composite, apart from TNF peaks, two new peaks have emerged at 38° and 46.4° which correspond to metallic silver (Sowmya & Meenakshi, 2015). The new peak at 32.6° indicates the presence of AgO (Masuda et al. 2009). The FTIR spectrum of TNF and Ag-TNF are compared in Fig. 5.5. The characteristic broad peak of TiO₂ between 800-400 cm⁻¹ is seen in both the spectrum. The bands corresponding to the -OH group on TiO₂ at 3400 cm⁻¹ and 1410 cm⁻¹ are also observed. The peak at 1384 cm⁻¹ indicates the presence of residual nitrates after the photo-deposition reaction. All the peaks of TiO₂ are retained in Ag-TiO₂ spectra. The EDS spectra of Ag-TNS membrane (Fig. 5.6) confirms the presence of 2.57 atomic % of silver.



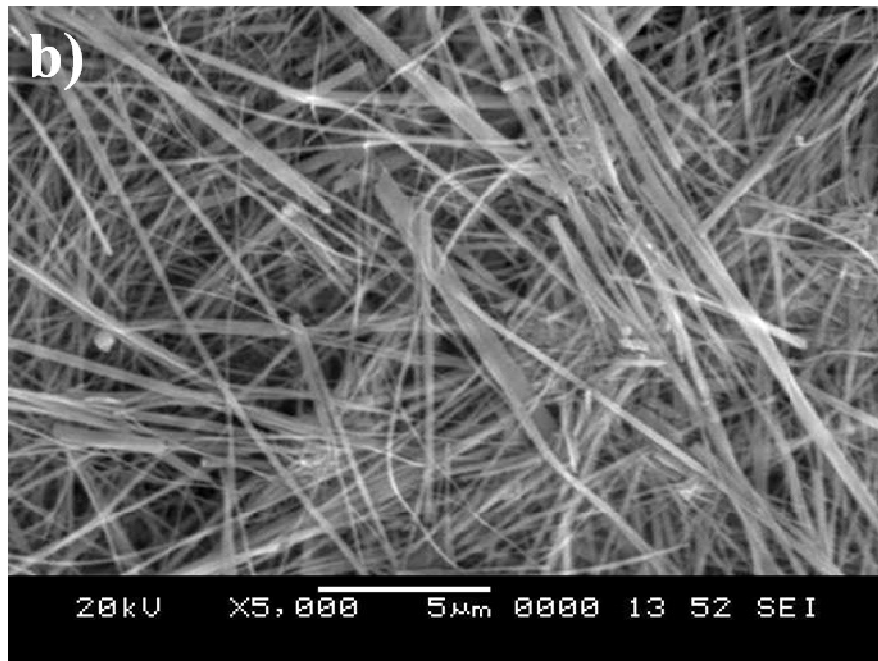


Fig. 5.3 SEM images of a) Ag-TNF and b) Ag-TNF HM

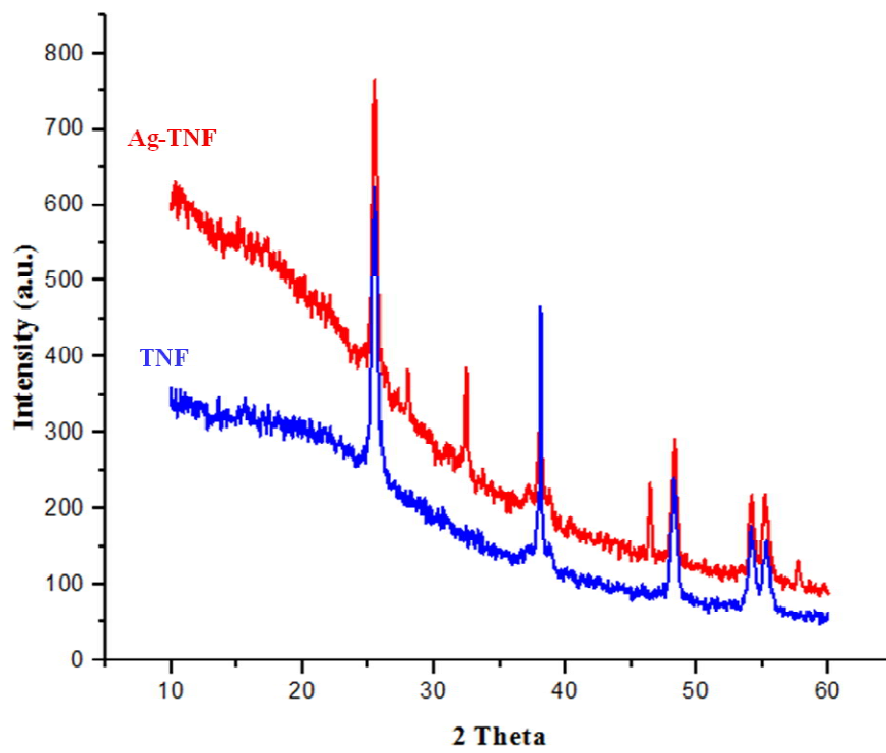


Fig. 5.4 XRD of TNF and Ag-TNF

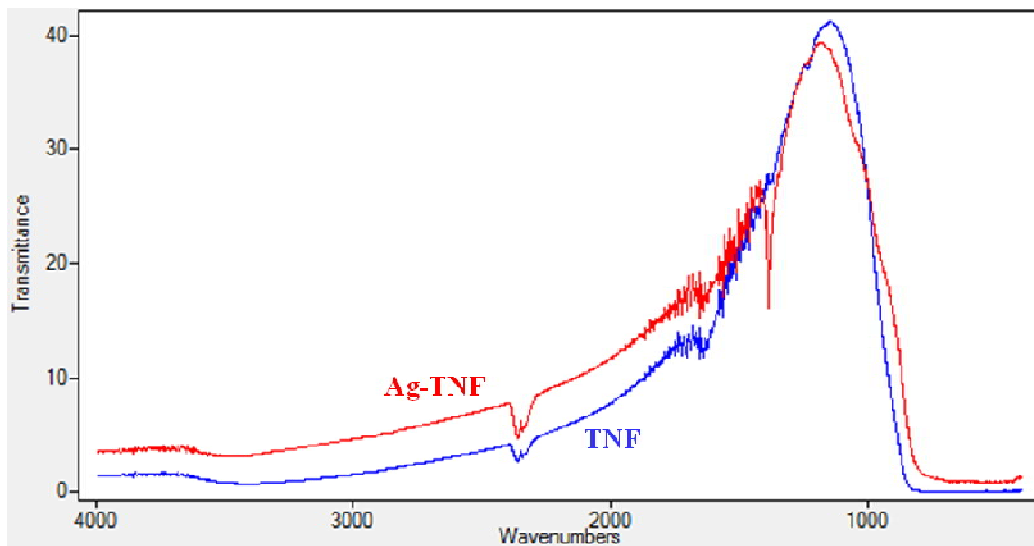


Fig. 5.5 FTIR spectrum of TNF and Ag-TNF

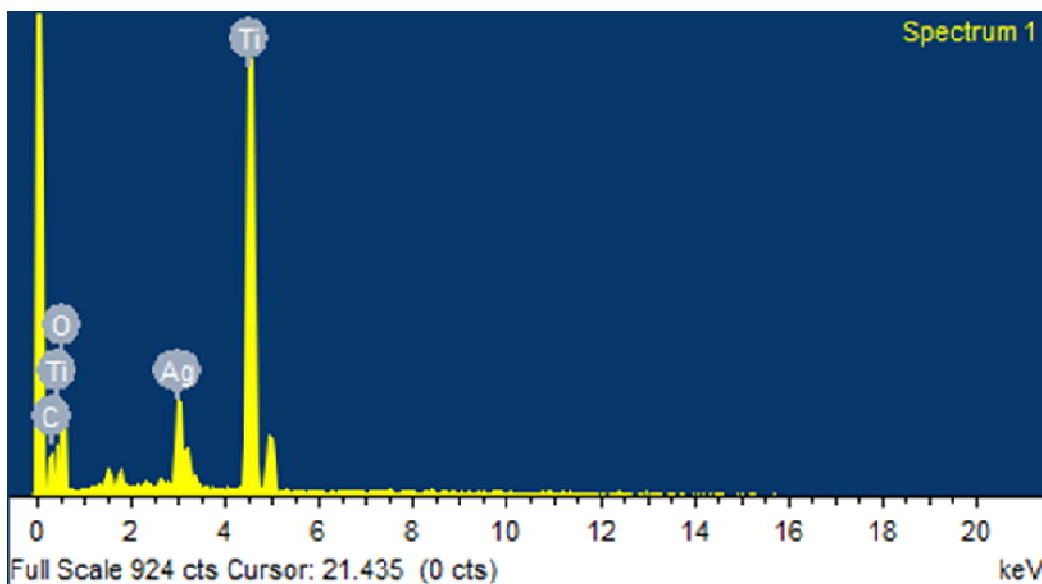


Fig. 5.6 EDS spectra of Ag-TNF

A significant decrease in membrane permeates flux is observed with increasing Ag-TNF loading in the membrane (Fig. 5.7). The addition of Ag-TNF layers on top of membrane surface creates additional resistance to flow (Diparezaet al. 2008). The decline in flux was drastic at lower catalyst loading due to pore blockage by TNF. As the TNF layer builds up, due to the very high porosity of the nanofiber network, lesser

resistance is offered, hence the flux drop becomes gradual. The decrease in flux provides greater contact time between the photocatalyst and the dye and enables better interaction. Dye removal studies reveal that the dye removal capacity of the membranes increased with greater TNF loading (Fig. 5.8). In absence of UV radiation, the Ag-TNS is capable of adsorbing the RHB dye via surface hydroxyl groups of TiO_2 . In presence of UV light electrons and holes are formed on TiO_2 , these charge carriers react with the aqueous medium to form hydroxyl radicals ($\bullet\text{OH}$) (Kordouli et al. 2015). These hydroxyl radicals react with the dye and degrade it to simpler molecules. On addition of silver to TiO_2 , electrons get transferred to silver thereby improving the charge separation efficiency and decreasing the recombination rate. Thus Ag-TNS acquires better photocatalytic activity. Nearly complete dye removal was obtained in case of 250 mg Ag-TNF loaded membrane under UV irradiation. The dye removal studies in absence of UV irradiation measure the dye adsorption capability of the Ag-TNS (Fig. 5.9). Ag-TNS exhibited good dye adsorption traits. Obviously, with increased adsorbent concentration, dye removal in absence of UV also increased. But unlike photocatalytic degradation, adsorption of dye leads to exhaustion of the photocatalyst. The reuse cycle studies of Ag-TNS membranes for dye removal invariably establish the same (Fig. 5.8).

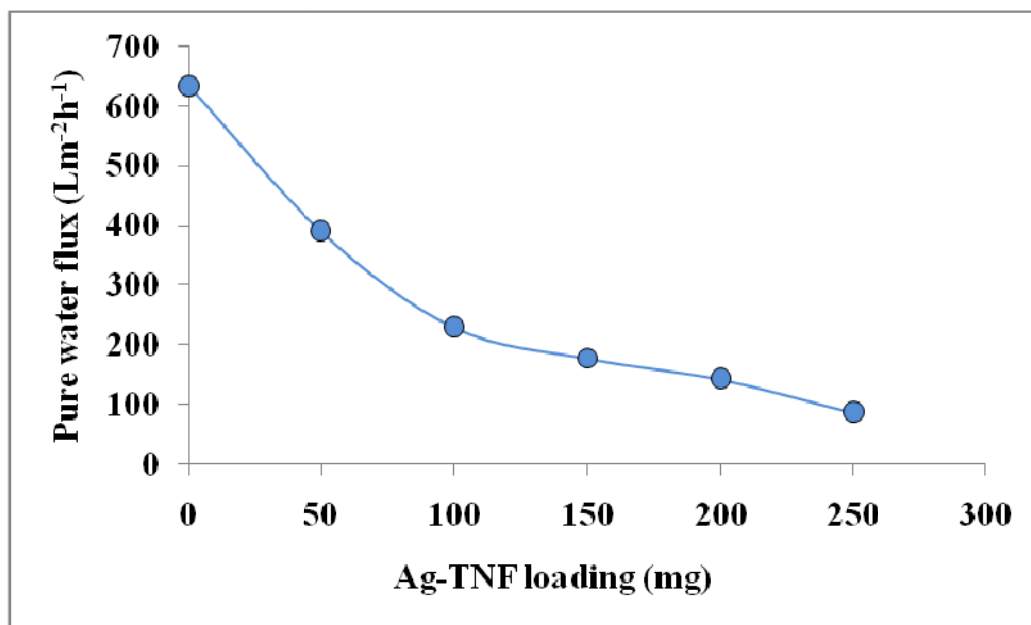


Fig. 5.7 Flux of various membranes

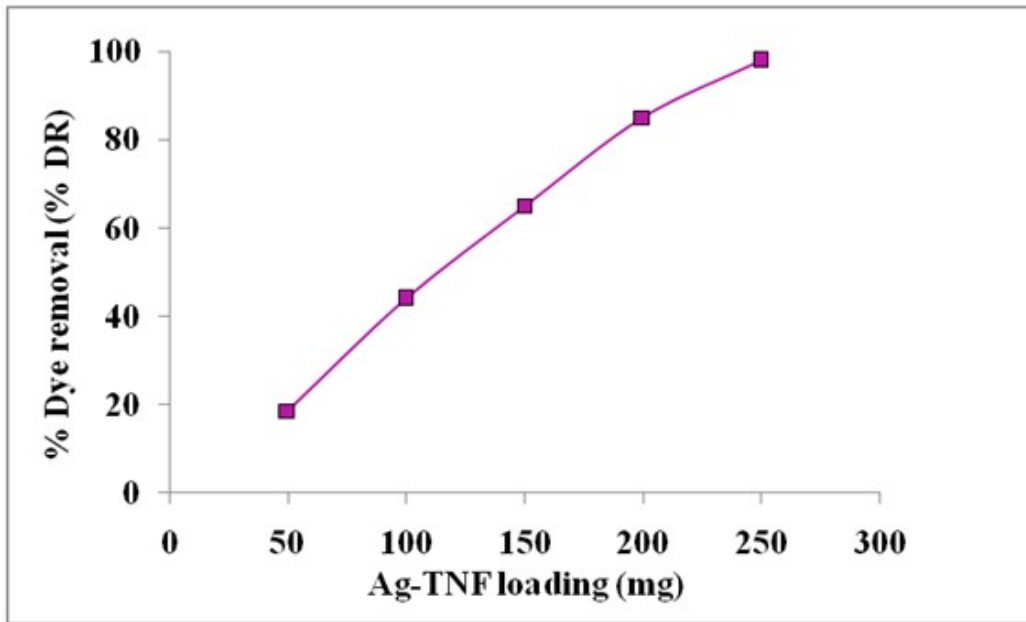


Fig. 5.8 Dye removal (DR) in presence of UV radiation by various membranes

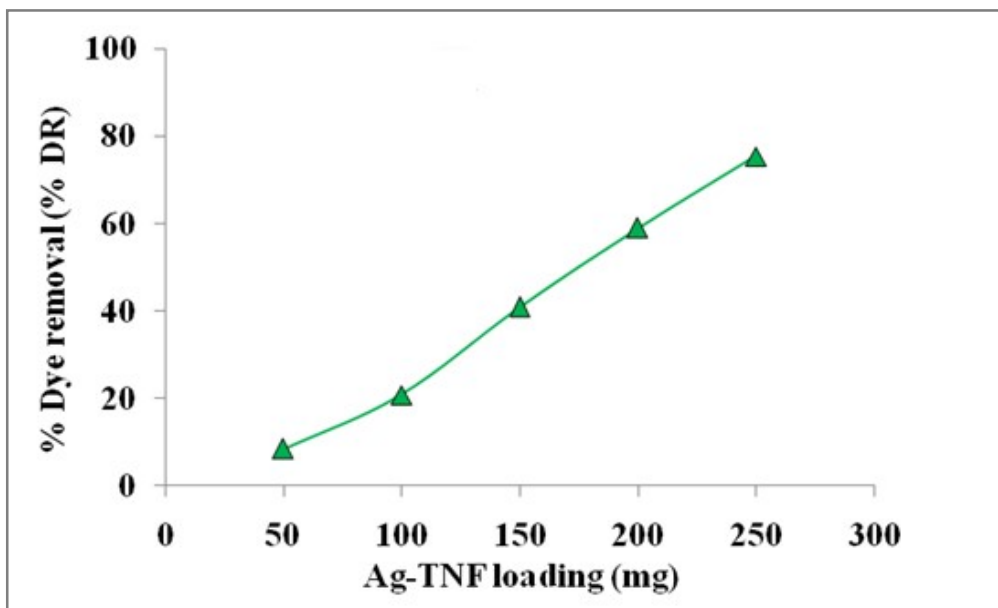


Fig. 5.8 Dye removal (DR) in absence of UV radiation by various membranes

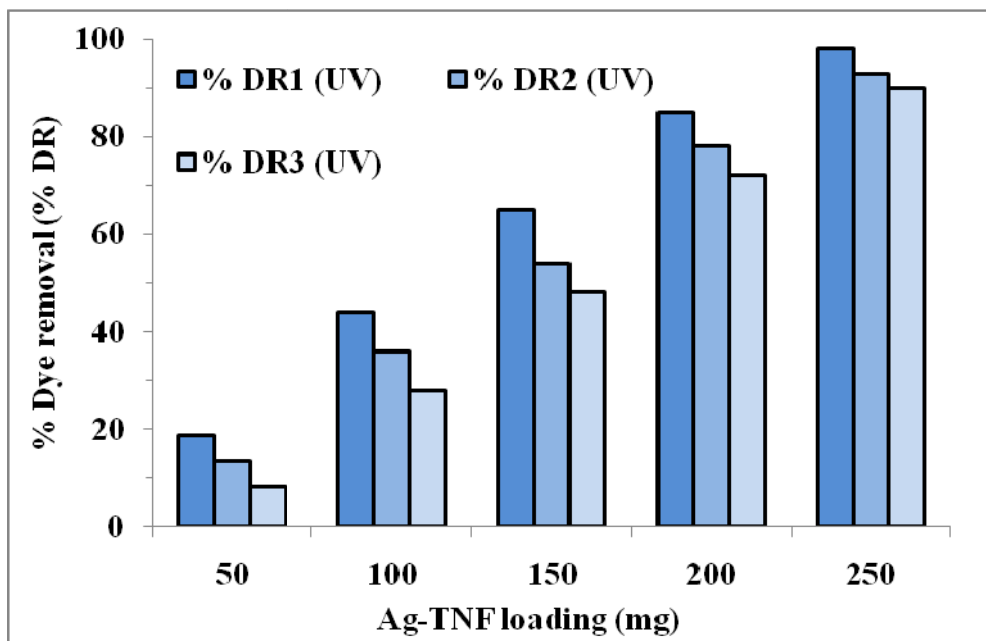


Fig. 5.10 Reuse cycles of the in presence of UV radiation membranes

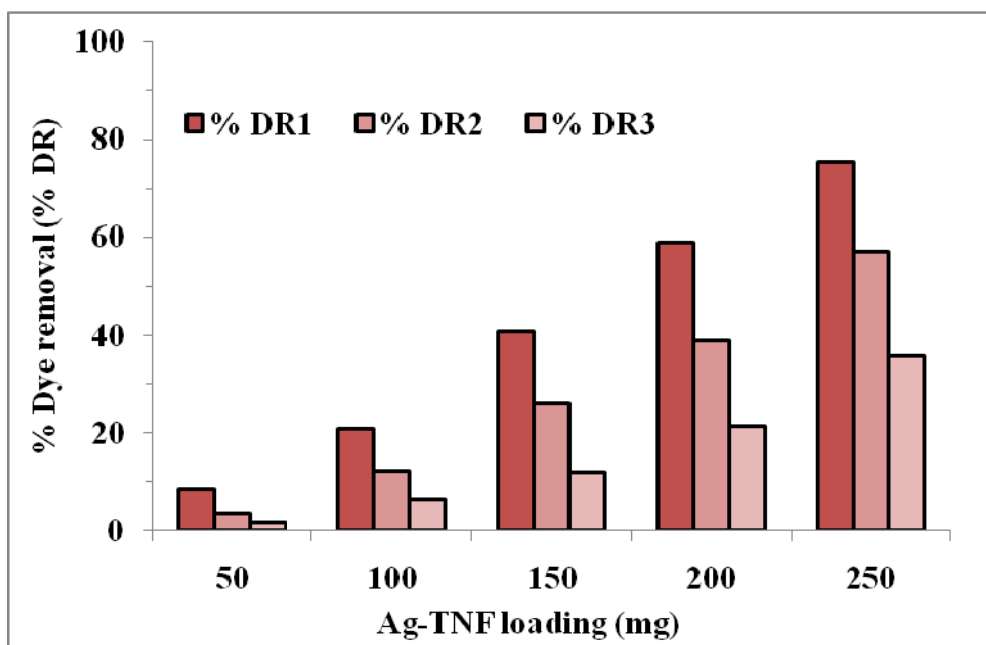


Fig. 5.11 Reuse cycles of the in absence of UV radiation membranes

Under UV irradiation the membranes are able to exhibit better dye removal efficiency on repeated use (Fig. 5.10). The dye removal efficiency increased with higher Ag-

TNS loading since lower flux provides greater time for photocatalytic degradation reaction (Bai et al. 2012). In case of dye removal in absence of UV, the reuse cycles clearly indicate a drastic drop in dye removal efficiency due to catalyst exhaustion (Fig. 5.11). The best performance was observed for 250 mg loaded membrane wherein under UV irradiation the dye removal in the third reuse cycle still remained above 90.1%, dropping only by 9.9 %. Where as in absence of UV, dye removal dropped by 52 % in the third reuse cycle. The photocatalyst reuse studies clearly suggest that Ag-TNS membranes, especially at higher catalyst loading exhibit superior photocatalytic dye degradation capabilities and hence can deliver reliable performance.

5.4 Conclusion

TiO₂ nanofibers synthesized consisted of anatase phase which exhibits good photocatalytic activity. Silver doped nanofibers were synthesized as confirmed from XRD and EDS. The Ag-TNF hierarchical photocatalytic membranes were synthesized with various catalyst loadings. The Ag-TNF membranes showed higher flux drop with increasing catalyst loading but the lower flow rate provided greater contact time for photodegradation. Although Ag-TNF can adsorb the RHB dye, the dye removal due to adsorption declined drastically with reuse of the photocatalyst. The performance of Ag-TNF membranes to remove the dye under UV irradiation increased with higher photocatalyst loading. Complete degradation of rhodamine B dye was obtained in case of 250 mg Ag-TNF loaded membrane. 250 mg Ag-TNF loaded membrane could maintain dye removal efficiency up to 90.01 % in the third reuse cycle indicating consistent performance and reusability.

CHAPTER 6

TiO₂ NANOSHEET INCORPORATED POLYSULFONE (TNS/PSF) NANOCOMPOSITE ULTRAFILTRATION MEMBRANES FOR DYE REMOVAL

Abstract

Incorporation of nanomaterials in polymeric membranes is an effective means to improve membrane performance. In the present work, a novel additive TiO₂ nanosheet was incorporated in polysulfone membrane. TiO₂ nanosheets were synthesized by hydrothermal method and blended with polysulfone. The membranes performance was evaluated via pure water flux, bovine serum albumin rejection and antifouling studies. Further the membranes were subjected to dye rejection application using Congo red and Rhodamine-B dyes. The membranes were characterized using scanning electron microscopy; X-ray diffraction and contact angle measurement. The nanocomposite membranes exhibited superior permeation, antifouling and dye rejection traits.

6.1. INTRODUCTION

In case of PSF membrane, titanium dioxide nanomaterials have been widely reported as nano additives (Mahlambi et al. 2014). So far, the addition of TiO₂ nanoparticles, nanotubes have been reported in the literature and it is observed that incorporation of TiO₂ nanoparticles and nanotubes at a higher concentration in PSF, reduces membrane performance due to delayed demixing because of a rheological hindrance (Hamid et al. 2011, Kumar et al. 2013). Whereas in our previous work (Chapter 4) the addition of TiO₂ nanofibers in PSF membranes, at higher additive content the membrane properties improved significantly. It is a well-established fact that the morphology of nano additive significantly affects the membrane modification and performance (Vatanpour et al. 2012). TiO₂ nanosheets are yet another nanostructure of TiO₂ that has attracted much attention recently (Zou et al. 2014). Nanosheets are 2D nano structures with a thickness of few nanometers. Such nanostructures are important due to their high surface energy and high specific surface area (Yang et al.

2011, Chen et al. 2014). In this chapter, we discuss the addition of titanium dioxide nanosheets (TNS) as a novel additive in PSF membranes. To the best of our knowledge, TNS as a polymer membrane additive has not been reported before. TNS is incorporated as an additive in PSF membrane casting solution to prepare nanocomposite membranes. The performance of the membrane was evaluated in terms of pure water flux, BSA rejection, and flux recovery. The membranes were used for dye rejection application using Congo red and Rhodamine-B dyes as a model pollutant.

6.2 MATERIALS AND METHODS

6.2.1 Materials

Rhodamine-B dye and Bradford reagent were purchased from Sigma-Aldrich Co, Bangalore, India. Congo red dye powder was purchased from Nice chemicals, Kochi. 1-methyl-2-pyrrolidone (NMP), Bovine serum albumin (BSA) and polyethylene glycol (PEG, $M_w \sim 600$ Da) were purchased from Merck specialties private ltd., West Mumbai.

6.2.2 Preparation of TNS incorporated PSF membranes

For the synthesis of S-1 membrane, PSF (20 wt%) and NMP (80 wt%) were mixed and stirred at 60 °C over a period of 4 h for complete dissolution of PSF to obtain a homogeneous solution. 1.0wt% (with respect to polymer solution) of TiO_2 nanosheets (with respect to the weight of polymer solution) was added to the solution. The resultant cast solution was poured on to a glass plate and spread using a glass rod. It was then submerged in distilled water (Nair et al. 2013). During phase inversion the NMP (solvent) diffuses out in to the coagulation media and the water (non-solvent) diffuses in to the membrane. The out diffusion of the solvent results in the rapid solidification or precipitation of the membrane polymer. The mutual exchange of NMP and water in the membrane results in generation of pores. Similar procedures were used for the remaining membranes (Table 6.1).

Table 6.1: Blending compositions of Membranes

Membranes	Polymer solution (PS)		TiO ₂ (wt% of PS)
	PSF (wt%)	NMP (wt%)	
S-0	20	80	0
S-1	20	80	1
S-3	20	80	3
S-5	20	80	5
S-7	20	80	7
S-10	20	80	10
S-12	20	80	12
S-15	20	80	15

6.3 CHARACTERIZATION

6.3.1 XRD analysis

X-ray diffraction analysis was done using goniometer (JEOL Dx-GE-2P, Japan), X-ray diffractometer equipped with monochromatized high-intensity Cu K α radiation ($\lambda=1.54058\text{\AA}$). The diffractograms were obtained at $0.16^\circ/\text{s}$ in the 2θ range of $10-70^\circ$. Accelerating voltage was set to 30 kV and a current of 20 mA. XRD was used to find the crystallinity of nanosheets, as well as the TNS, incorporated PSF membranes.

6.3.2 SEM analysis

Morphology of synthesized TiO₂ nanosheets and membrane samples were analyzed using SEM (JSM-6380LA). The samples were frozen in liquid nitrogen and fractured before gold sputtering.

6.3.3 TEM analysis

The morphology of synthesized TNS was analyzed by Transmission electron microscopy (TEM, JEOL, JEM 2100). The TEM sample was prepared by dispersing the TNS sample in ethanol and then depositing a drop of these diluted dispersions on a TEM grid.

6.3.4 Contact angle measurement

FTA-200 Dynamic contact angle analyzer was used to estimate the contact angle of membranes using sessile droplet method. To avoid error, three measurements were made at different locations and the average is reported.

6.3.5 Permeation properties

Sterlitech HP4750 stirred dead end filtration cell with an effective membrane area of 14.6 cm² was used to study the performance of the membranes. Membranes were kept immersed in distilled water for 24 h before carrying out flux study. The permeate collection was initiated after 20 min of exposure to 0.4 MPa transmembrane pressure (TMP) at 25 °C. The flux study was conducted for a time period of 90 minutes to enable the flux to reach near steady state condition. The pure water flux (J_w) was determined by means of the following relation:

$$J_w = \frac{Q}{\Delta t A} \quad (1)$$

Where J_w is expressed in L/m²h and Q is the amount of water collected for Δt (h) time duration using a membrane area of A (m²).

6.3.6 Antifouling properties

The antifouling property of the membrane was studied as per the procedure reported in the literature. In Brief, initial pure water flux of the membrane J_{w1} (L/m²h) was obtained at 0.4 MPa transmembrane pressure for 90 min. The antifouling property of the membrane was studied using BSA as standard protein for rejection. 0.8g/L of an aqueous solution of BSA passed through the membrane for 60 minutes. Later membrane was washed with distilled water for 20 minutes and PWF J_{w2} (L/m²h) was determined once again. The membranes antifouling capacity was estimated in terms of FRR using the following equation:

$$FRR(\%) = \frac{J_{w2}}{J_{w1}} \times 100(2)$$

In order to determine the rejection capacity of the membrane, feed and permeate solution samples were collected and treated with Bradford reagent. The blue color solution is formed when adding Bradford reagent. Samples were kept at room temperature for 10 minutes before analyzing using UV-Spectrometer. The

absorption peak of BSA is found to be 595 nm. The % BSA rejection of the membrane was determined using the below equation:

$$\%R = \left(1 - \frac{C_p}{C_f}\right) \times 100(3)$$

6.3.7 Dye rejection study

Congo red and Rhodamine-B dye (50 ppm) was prepared and at 0.4 MPa trans-membrane pressure to study the dye rejection. The permeate collected was subjected to UV-Vis spectroscopy to estimate residual dye concentration at a wavelength of 498 nm and 553 nm respectively. Percentage rejection values of dye were calculated using equation 3, where C_p (mg/L) and C_f (mg/L) are the dye.

6.4 RESULTS AND DISCUSSION

6.4.1 Membrane characterization

6.4.1.1 XRD analysis

XRD patterns of S-0, S-10, and TNS are compared in figure 6.1. The major XRD peaks of TNS at 25.2°, 37.72°, 47.98° and 54.98° can be indexed to anatase phase. The major anatase peaks observed in TNS samples are also observed in S-10 membrane, which shows that TNS was incorporated into membranes effectively. S-0 pattern does not give any characteristic sharp peaks which indicate amorphous polysulfone, without any crystalline phase (Yang et al. 2007).

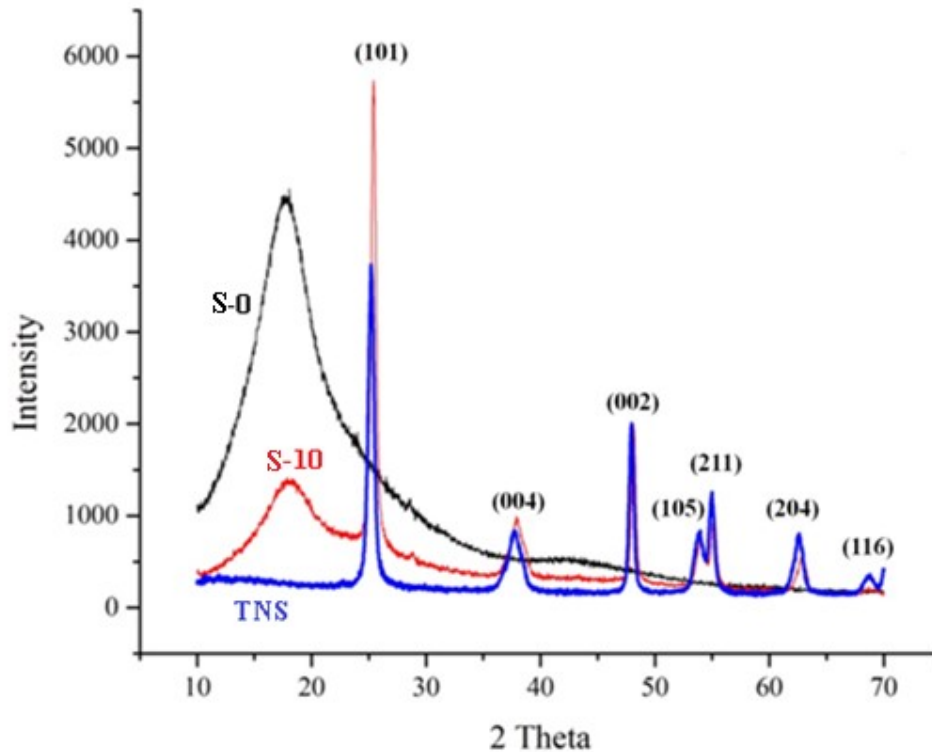


Fig. 6.1 XRD patterns of S-0, S-10, and TNS.

6.4.1.2 Morphology of the membranes

Cross-section of the membranes synthesized with different concentrations of TNS was analyzed using SEM and is shown in figure. 6.2. All the membranes have typical asymmetric structure with finger like macro voids in macro pore region, less porous sub layer formation and a top layer with less pore density (Ganesh et al. 2012). As the TNS concentration increased from 1 wt% to 5 wt%, the presence of micro passages in the top layer and macro voids in macro pore region have decreased rapidly. With the addition of particulates, the viscosity of the casting solution increases, this delays demixing process thereby retarding rapid exchange of solvent and non-solvent (Gupta et al. 2015). Delayed demixing results in lesser pore formation in the membrane. From 7 wt% TNS addition onwards porous sub layer formation becomes significant and was predominant in 12 and 15 wt%. In S-12 and S-15 membranes, porous sub layer and macro voids regions merged. Also, the macro voids and spongy sub layer increased significantly in case of S-12 and S-15 when compared to other membranes.

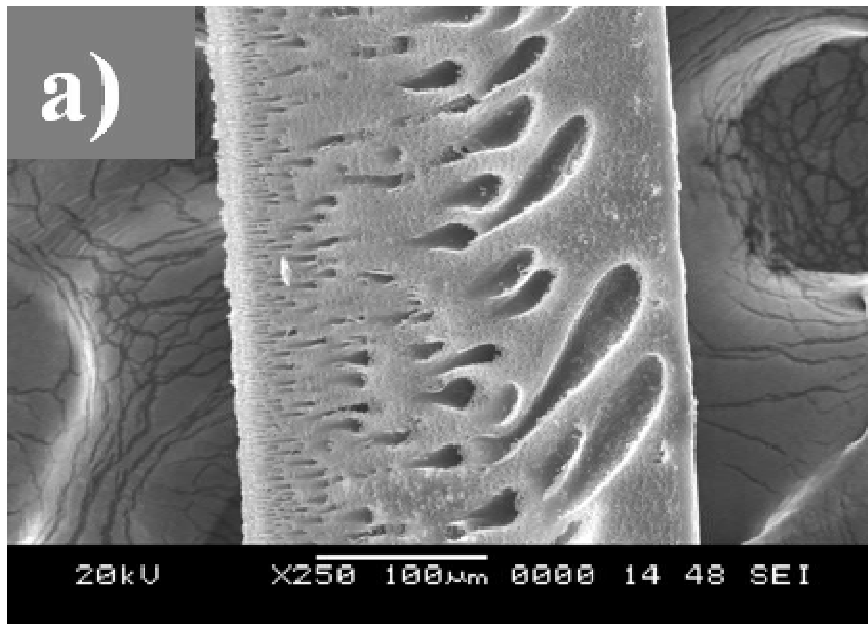
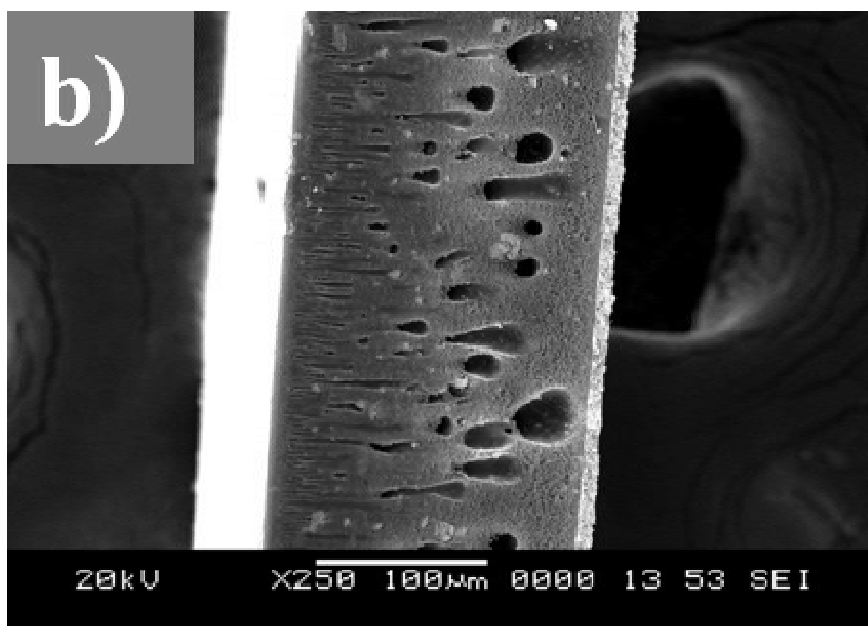


Fig. 6.2 SEM images of the membranes. a) S-0, b) S-1, c) S-3, d) S-5, e) S-7, f) S-10, g) S-12, and h) S-15.



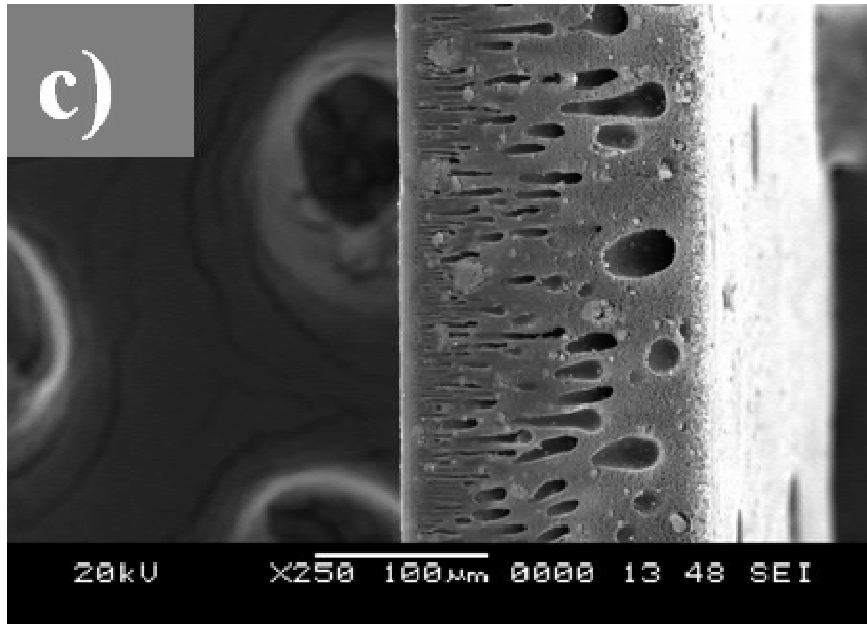
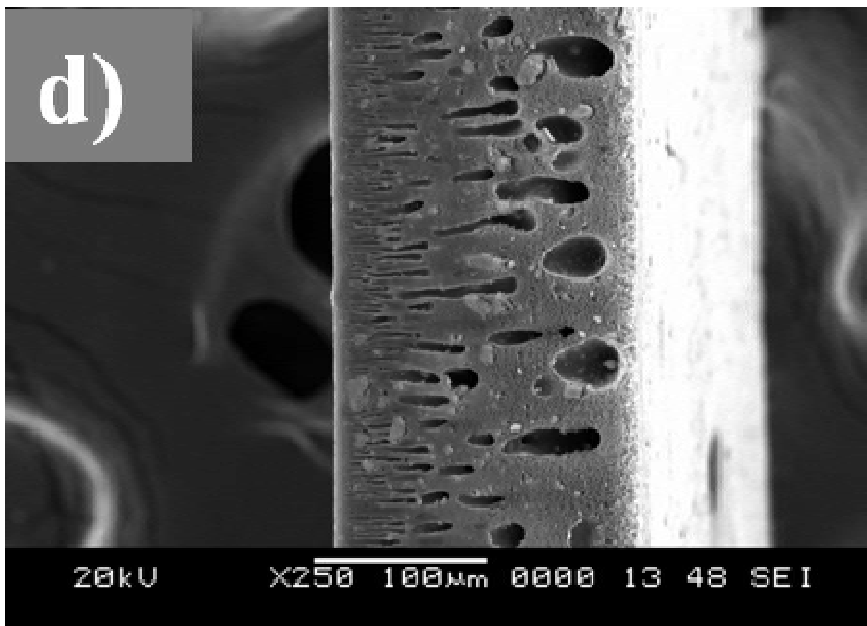


Fig. 6.2 SEM images of the membranes. a) S-0, b) S-1, c) S-3, d) S-5, e) S-7, f) S-10, g) S-12, and h) S-15.



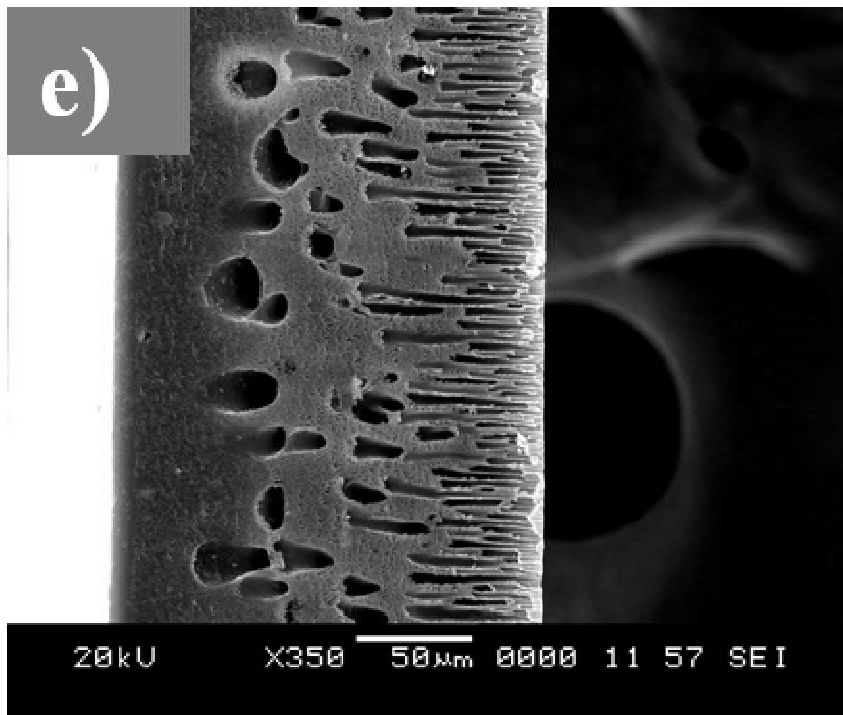
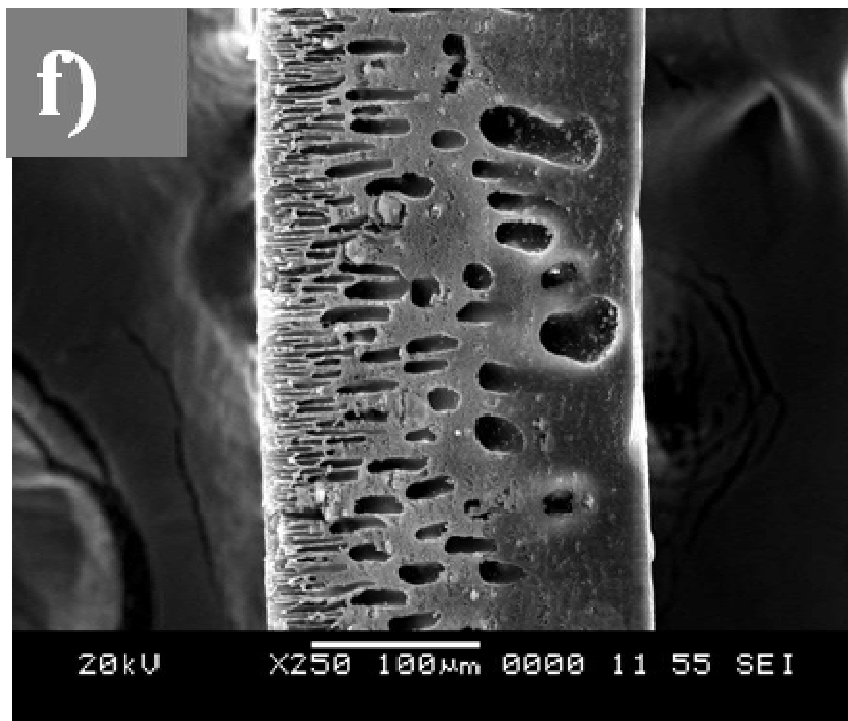


Fig. 6.2 SEM images of the membranes. a) S-0, b) S-1, c) S-3, d) S-5, e) S-7, f) S-10, g) S-12, and h) S-15.



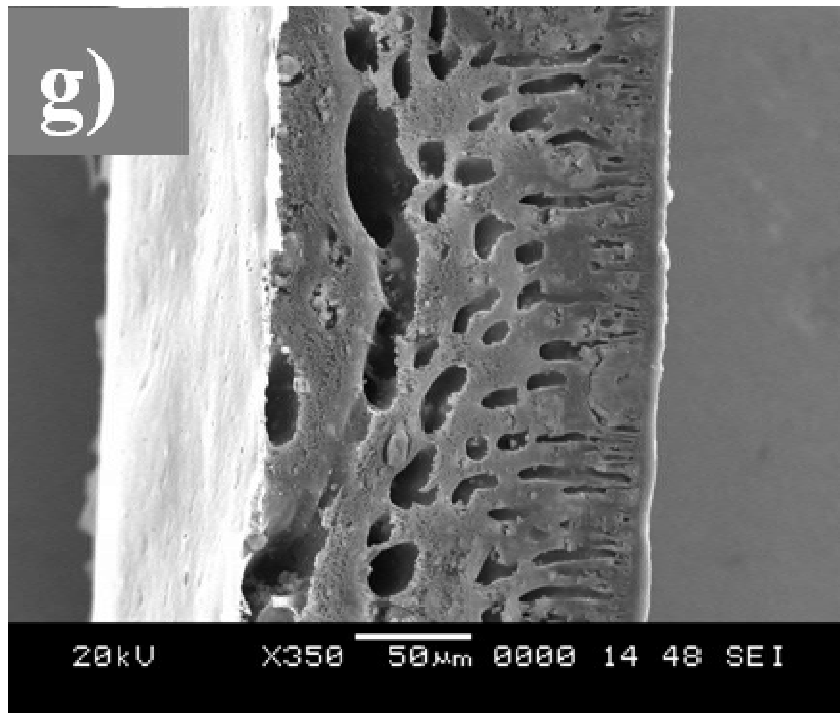
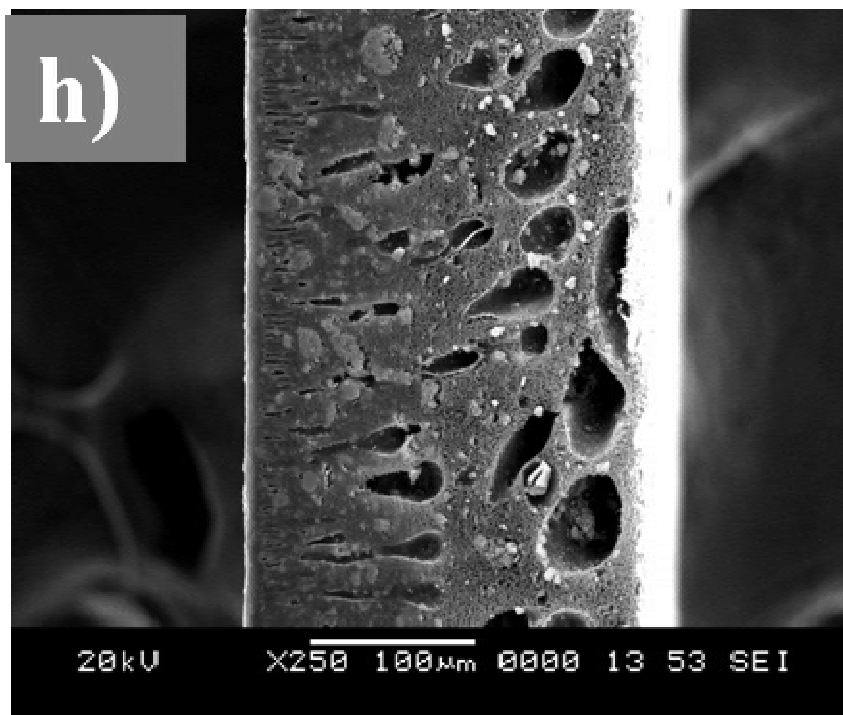


Fig. 6.2 SEM images of the membranes. a) S-0, b) S-1, c) S-3, d) S-5, e) S-7, f) S-10, g) S-12, and h) S-15.



With increase in hydrophilic TNS addition affinity towards water is increased. This favors the in-diffusion of nonsolvent into the membrane. This can help in overcoming the viscosity barrier and results in greater porosity (Kumar et al. 2013). This is evident from the pore formation in porous sub layer and macro void region for membranes having above 7 wt% TNS content. Better water affinity of the membrane due to greater hydrophilic additive can thus enhance phase inversion and produce membranes with slightly higher pore size. From the SEM images, it appears that up to 5 wt% of TNS addition the porosity has decreased. The addition of TNS and subsequent hydrophilicity enhancement could not significantly enhance the kinetics of phase inversion up to 5wt%. For 7 wt% and above, the appreciable increase of macro void and pore indicates that the phase inversion rate was improved due to the addition of hydrophilic TNS (Ahmad et al. 2013).

6.4.1.3 Hydrophilicity of membranes

If the hydrophilicity is high, the affinity between water and membrane surface is more, which is a desirable criterion for achieving high flux and antifouling property.

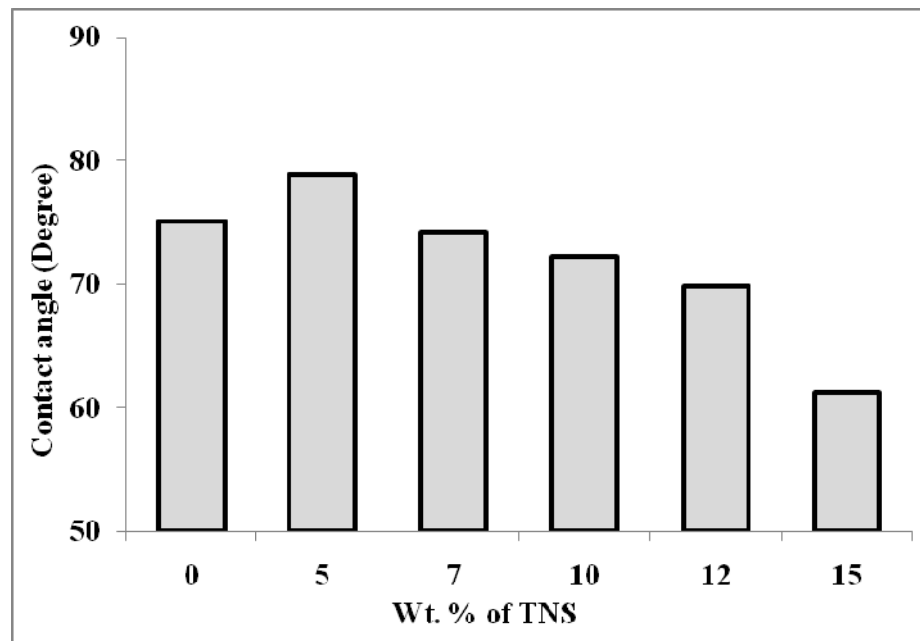


Fig. 6.3 Contact angle measurement of membranes

Due to high surface tension on the hydrophilic membrane surface, water filmformation takes place instead of droplets and thereby reduces the contact angle.

Fig. 6.3 shows contact angle measurement of the synthesized membranes. The increased addition of hydrophilic TNS, contact angle of membranes decreased from 75.04° for nascent PSF to 61.25° for S-15 membrane. S-5 membrane showed higher contact angle compared to S-0 membrane, indicating lower hydrophilicity or lower pore size. The increase in hydrophilicity of the membranes above 7 wt% TNS content is due to the presence of hydrophilic TNS (Dong et al. 2012).

6.4.1.4 Membrane permeability and antifouling properties

Since PEG was not used as pore former in this study the membrane fluxes were much less when compared to the results observed in Chapter 4. For nascent PSF membrane, a low steady state flux was observed. The PWF is shown in Fig. 6.4. For 1 wt% addition of TNS, the flux dropped to a much lower value, which can be explained by reports of Yang et. al (2007) on addition of TNP in PSF. The viscosity of cast solution increases with increasing additive content. This increased viscosity affects the kinetics of phase inversion as it retards the diffusion of solvent and non-solvent. The higher the solution viscosity, solvent's out diffusion from the cast solution is favored over nonsolvent diffusion into the solution resulting in the formation of membranes with smaller pores. Increased rheological hindrance beyond the rheological percolation threshold with increasing concentration of TNP above 2 wt% was observed. Choi et. al (2006) also reported such trend in case of addition of MWCNTs in polysulfone. The increased hydrophilicity due to the hydrophilic TNS additive will help in overcoming the increasing rheological hindrance. This can be observed in case of 3 wt% addition of TNS as flux although low is improved in comparison to 1 wt% addition of TNS. Flux showed further improvement at 5 wt% addition although the flux values remained lower when compared to nascent PSF membrane.

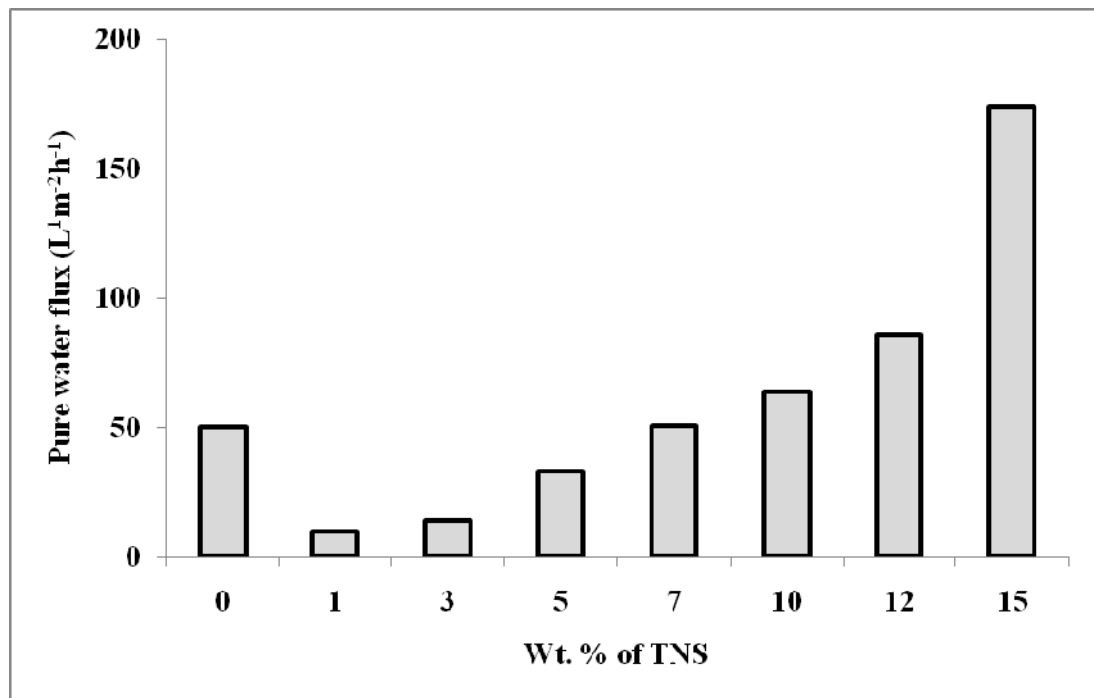


Fig. 6.4 PWF of membranes.

It was thus observed that the increase in TNS concentration has resulted in lower PWF in case of S-1, S-3 and S-5 membranes. The decrease in flux is due to low porosity compared to S-0 membrane as seen from the SEM images (Fig 6.2).

The low pore size is due to increase in viscosity of casting solution (acts as a frictional barrier) which affects the mutual diffusivities of solvent and nonsolvent during phase inversion forming a closed structure with lesser pore volume relatively. S-1 and S-3 are therefore not considered for further study because of their poor flux. The decreasing flux for S-5 membrane can also be assumed from the lower contact angle resulting due to lower porosity. The increasing PWF trend starts from 7 wt% TNS, which can be attributed to increase in hydrophilic nature of membranes which starts to overcome the rheological hindrance and improves the porosity of the membrane at greater TNS addition. Further increase in flux is observed for S-10 and S-12 membranes due to improved hydrophilicity. S-15 exhibited three times higher flux than nascent PSF because of high hydrophilicity and increase in sponginess of the membrane.

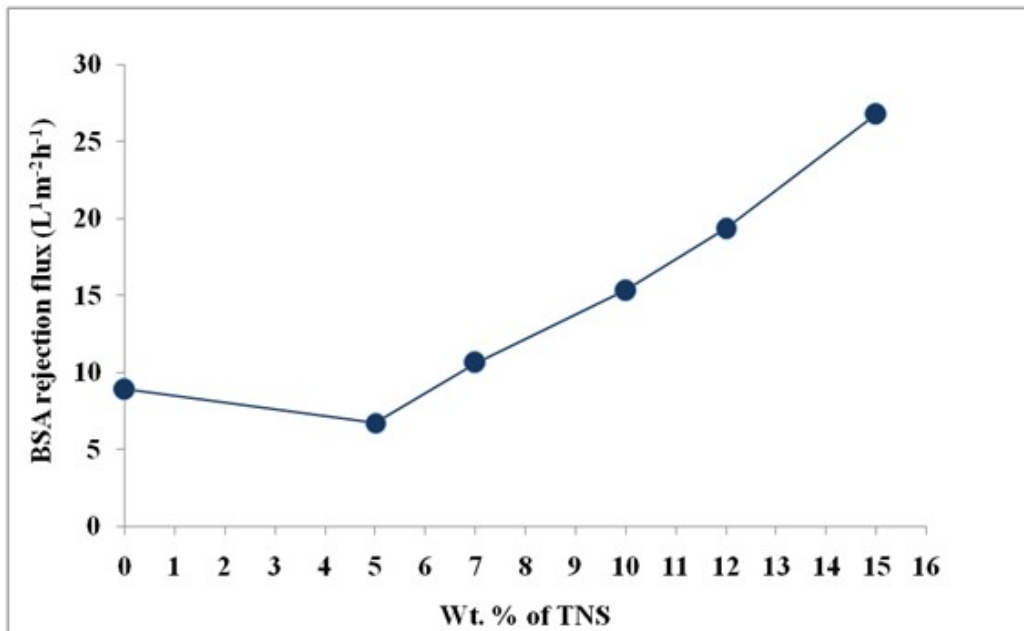


Fig. 6.5 BSA rejection flux of membranes.

BSA rejection was carried out to estimate the antifouling properties. Fouling reduces the rejection flux due to deposition of rejected BSA protein and subsequent cake formation. The BSA rejection fluxes are shown in Fig. 6.5. Due to the natural hydrophobicity, nascent PSF membrane showed heavy fouling and very low flux during BSA rejection. S-5 membrane also showed low flux due to lower pore size and lower hydrophilicity. S-7 and S-10 membranes showed higher permeate fluxes due to improved hydrophilicity. S-12 and S-15 membranes showed higher steady state fluxes due to high concentration of hydrophilic TNS. The BSA rejection flux thus drastically decreased when compared to PWF, but the rejection flux improved comparatively at higher TNS content.

The BSA rejection values of the membranes are shown in Fig. 6.6. The maximum rejection of 96.45% was obtained for S-5 membrane due to low porosity compared to S-0 membrane. With the addition of TNS, the rejection values decreased slightly and S-15 gave the lowest rejection and the highest flux. But all membrane could maintain BSA rejection above 90%.

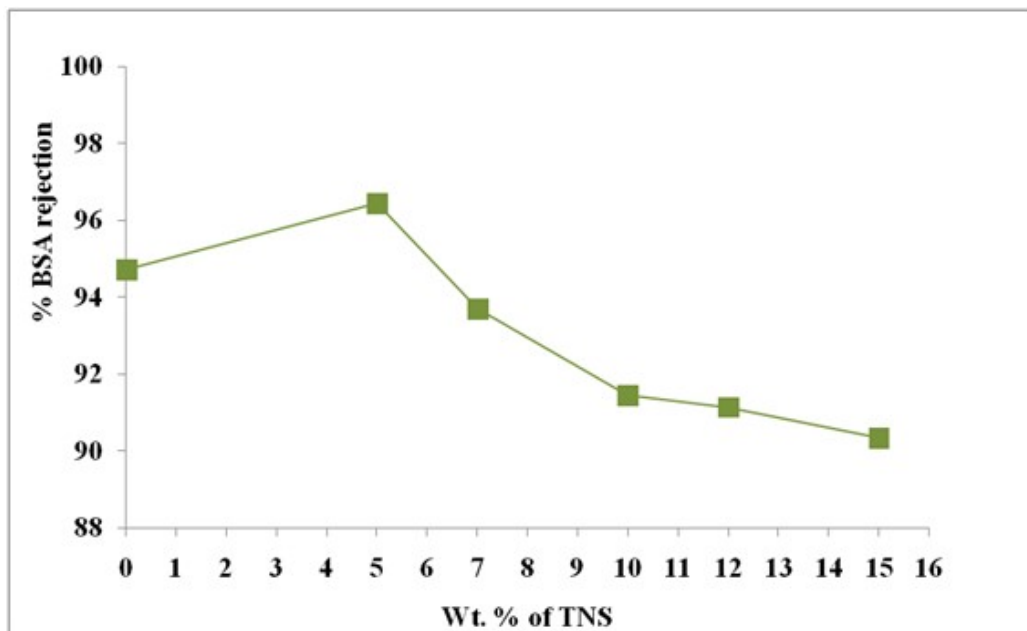


Fig. 6.6 BSA rejection by the membranes.

FRR value indicates the reusability and wash ability of the membrane. For nascent PSF due to hydrophobic nature the membrane surface is easily susceptible to protein adhesion hence the wash ability is reduced resulting in low flux recovery. The FRR value increased compared to S-0 membrane with the increase in TNS concentration (Fig. 6.7). For S-7 and S-10 the flux recovery improved since hydrophilicity of the membrane increased. The increasing trend was observed till S-12 membrane and later it decreased for S-15 membrane. The maximum FRR value was observed for S-12 membrane. The interaction with the aqueous medium was enhanced with the presence of hydrophilic TNS on membrane surface there by weakening the interactions between protein molecules and membrane surface (Arthanareeswaran et al. 2010). Because of weaker interactions, the foulant can be easily cleaned from the membrane surface and thus increase the life of the membrane. However, the decrease in FRR value for S-15 membrane indicates irreversible fouling. The protein molecules penetrated into membrane pores instead of superficial deposition on the membrane, thereby reducing the flux recovery.

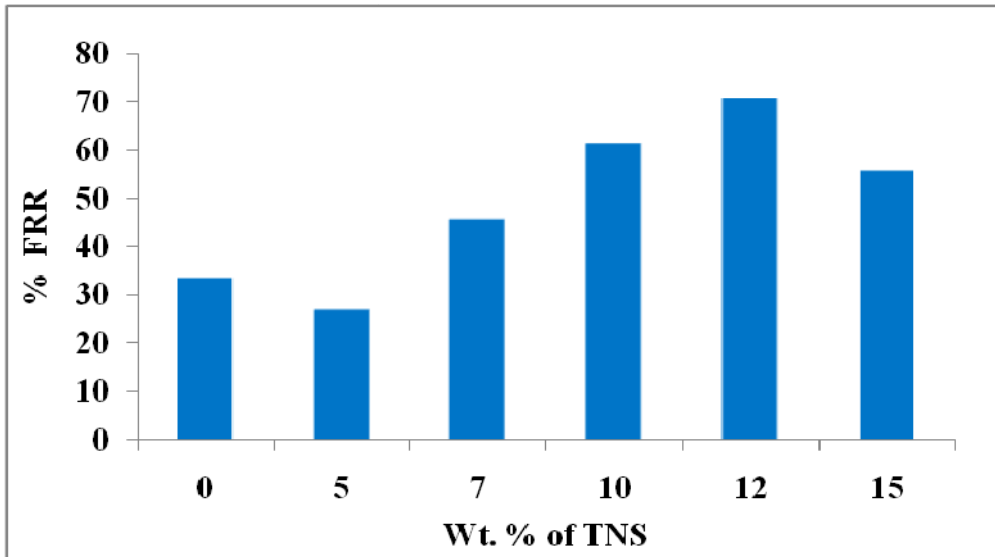


Fig.6.7 Percentage FRR of membranes.

6.4.1.5 Dye rejection

The Congo red dye rejection flux of the membranes is shown in Fig. 6.8. All TNS incorporated membranes showed better Congo red dye rejection (above 90%) than nascent PSF (Fig. 6.9). Although S-5 showed high dye rejection, the permeate flux obtained was comparatively lower. S-12 and S-15 membranes exhibited good dye rejection along with permeate fluxes of 5 to 6 times higher than S-0.

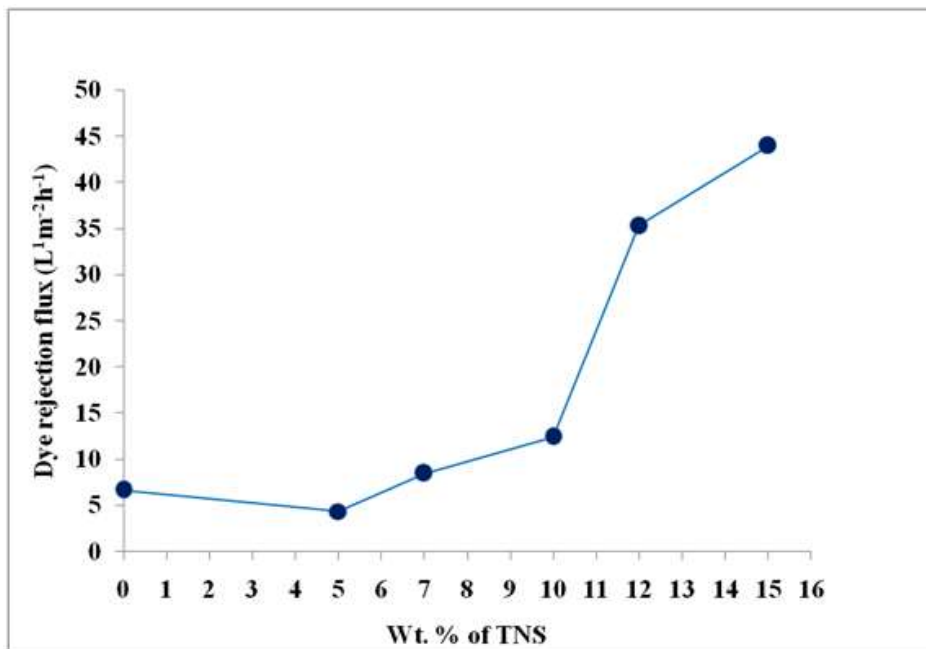


Fig. 6.8 Congo red dye rejection flux of membranes.

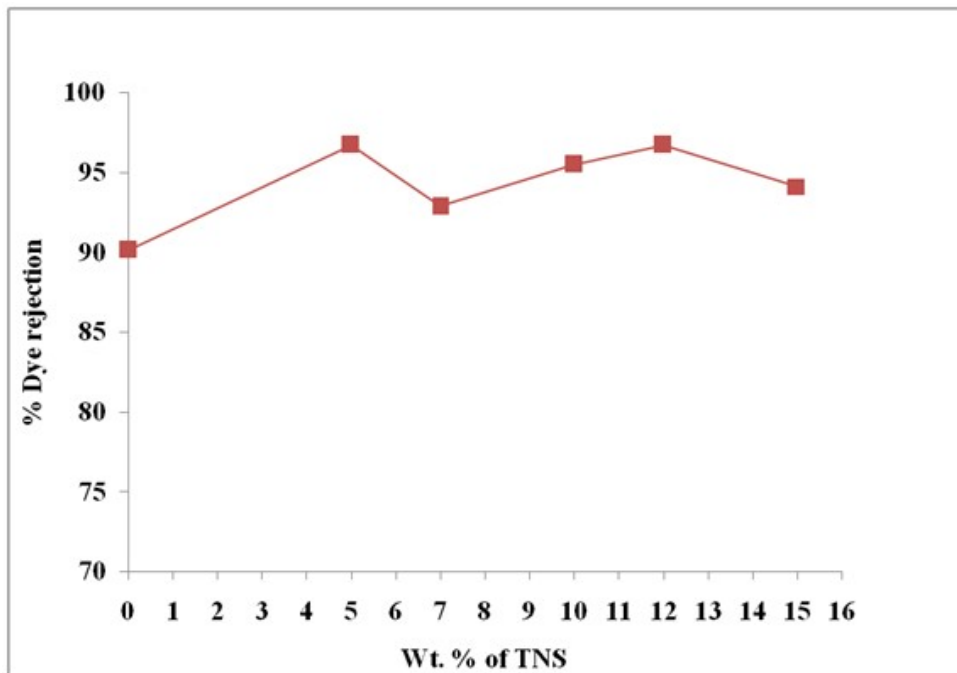


Fig. 6.9 Congo red dye rejection by the membranes.

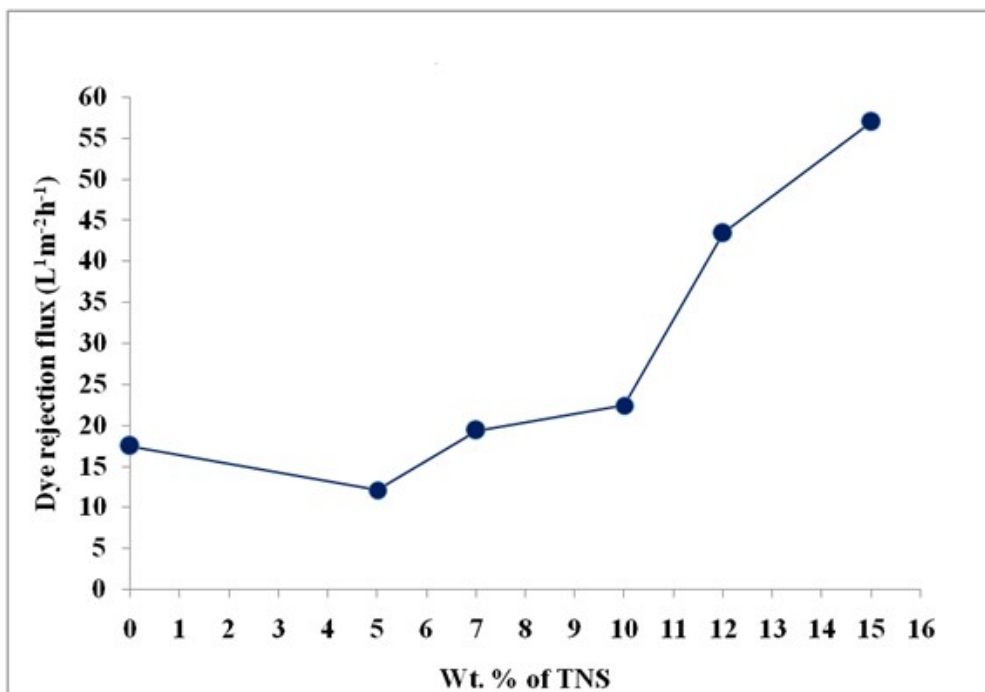


Fig. 6.10 Rhodamine B dye rejection flux of membranes.

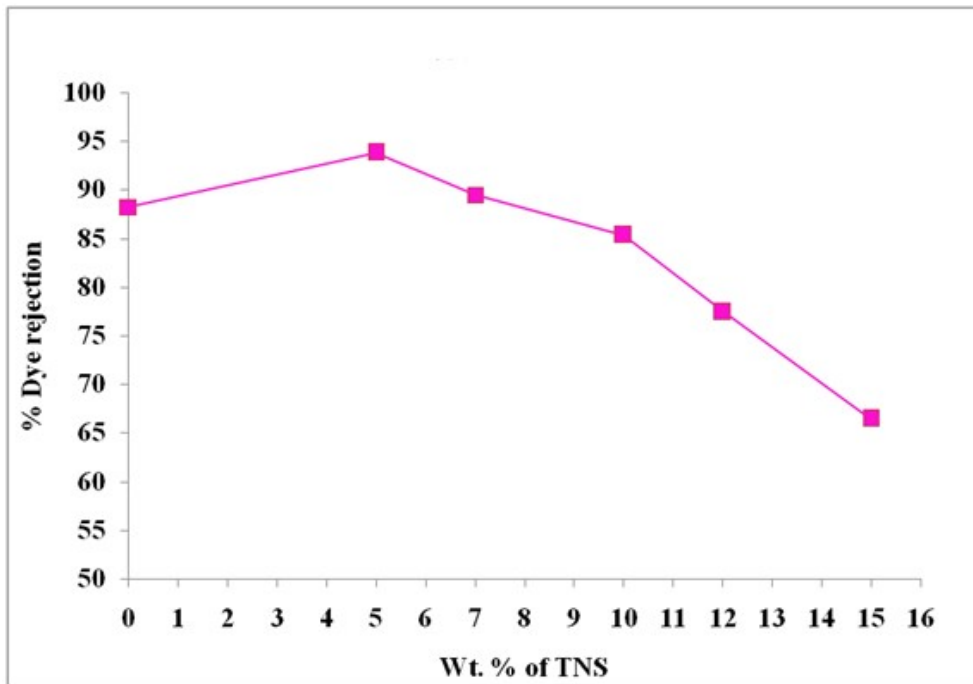


Fig. 6.11 Rhodamine-B dye rejection by the membranes.

Also a slightly decreasing trend in dye rejection was observed from S-5 to S-7 but Congo red dye adsorption capability of TNS increased the rejection at higher TNS content in membranes (Amin et al. 2015, Kordouli et al. 2015).

Rhodamine-B dye rejection trends are shown in Fig. 6.10. All membranes showed better permeate flux and lower rejection for Rhodamine-B when compared to Congo red owing to the comparatively smaller size of Rhodamine-B molecules. Similar to Congo red rejection study, S-5 membrane exhibited better rejection but permeate flux was low. The permeate flux improved gradually from S-7 to S-10 and the drastic increase was observed for S-12 and S-15. The drastic hike in permeate flux of S-12 and S-15 was associated with a heavy drop in dye rejection capacity, S-15 showed a minimum dye rejection of 66.4% (Fig. 6.11). S-7 and S-10 membranes exhibited better performance with dye rejections above 85% and better permeate flux.

6.5 CONCLUSION

TiO₂ Nanosheets were successfully synthesized and effectively incorporated into polysulfone membrane. The performance of the membranes showed a declining trend

at a lower additive concentration up to 5 wt%, but at higher concentrations, property enhancement was significant. Three times increase in pure water flux when compared to nascent polysulfone was observed for S-15 membrane. A maximum of 70.3 % flux recovery was obtained for S-12 membrane, owing to the drastic increase in membrane hydrophilicity due to TNS addition. Better Congo red dye rejection flux was also obtained with higher TNS content. Best results for Congo red rejection were obtained for S-12 and S-15 membranes with dye rejection of above 94% and 5 to 6 times increase in permeate flux. In case of Rhodamine-B rejection, the smaller size of the dye resulted in higher permeate flux accompanied by a decrease in dye rejection. S-7 and S-10 membranes were found optimal for Rhodamine-B rejection, with dye rejections above 85% and comparatively higher permeate fluxes. In summary, TNS could effectively enhance the overall performance of the membrane. Good dye rejection characteristics of the TNS incorporated membranes indicate potential application in a membrane assisted photocatalysis.

CHAPTER 7

TiO₂ NANOSHEET-GRAPHENE OXIDE (TNS-GO) PHOTOCATALYTIC HIERARCHICAL MEMBRANE FOR WATER PURIFICATION

Abstract

A hierarchical membrane with layer of photocatalyst coated on top of the membrane surface has emerged as a better alternate for immobilization of photocatalyst. Studies have revealed that nanoparticles are not pliable for synthesis of hierarchical membranes due to their smaller size and low stability after deposition. TiO₂ nanosheets serve as better alternate due their thin structure which enables table layer formation. Integrating the nanosheets with modifiers like graphene oxide can further enhance the photocatalytic activity. The sheet structure of graphene oxide enhances stable film formation and also acts as support for interconnecting TiO₂ nanosheets. In this work, TiO₂ nanosheets are modified with graphene oxide and used to develop a hierarchical membrane by depositing a catalyst coating on a support membrane. The hierarchical membrane performance was studied using Congo red dye as model pollutant and the effect of catalyst loading on the permeate flux and dye removal were analyzed.

7.1. INTRODUCTION

Hierarchical membranes as discussed in chapter 5 are good alternate to immobilize photocatalyst and also obtain better photocatalyst exposure. Various TiO₂ structures like nanoparticles, nanowires, nanofibers, nano thorns and microspheres have been reported in the synthesis of hierarchical membranes (Bai et al. 2010). TiO₂ nanosheets (TNS) are 2D nanostructures with nanoscale thickness. The thin sheet structure enables stable layer formation on deposition. These nanostructures are difficult to synthesize with effective size control. Hydrothermal methods have been recently used to produce good anatase nanosheets (Chen et al. 2014). As seen in chapter 3, TNS showed better photocatalytic activity than TNF. Photocatalytic activity can be further enhanced by modifying the material with suitable dopants or forming composites

with modifiers. To the best of our knowledge, there have been no reports on the application of TiO₂ nanosheet in hierarchical membranes. Graphene oxide (GO) is a widely studied modifier to enhance the photocatalytic activity of TiO₂(Gao et al. 2014). When employed in hierarchical membranes, GO has also shown to impart better mechanical stability to photocatalyst layer (Gao et al. 2013). In this chapter, the synthesis of TNS-GO hierarchical membrane for simultaneous water filtration and photodegradation is discussed.

7.2 MATERIALS AND METHODS

7.2.1 Materials

Graphene oxide sheets were purchased from Sigma-Aldrich Co, Bangalore, India. Congo red dye was procured from Nice Chemicals, Cochin, India. Cellulose acetate membrane (Dia - 47 mm and pore size - 200 nm) was obtained from Sartorius stedim biotech, Bangalore, India.

7.2.2 Synthesis of TNS-GO

GO (20 mg) was dispersed in 100 mL distilled water under constant stirring. The dispersion was sonicated for 30 min to enable exfoliation of the GO sheets. A dispersion of TNS (100 mg) was prepared in 100 ml water with constant stirring. Both the dispersions were mixed and stirred vigorously for 2 h. The obtained product was dried at 60°C in a hot air oven (Gao et al. 2013).

7.2.3 Synthesis of photocatalyst coated hierarchical membrane

Hierarchical membranes were synthesized using cellulose acetate base membrane (Sartorius Stedim Biotech, Dia - 47 mm and pore size - 200nm). The base membrane was positioned properly in a filtration assembly. A varying amount of TNS-GO photocatalyst as given in Table 8.1 were dispersed in 100 mL of distilled water and loaded into the filtration cell. During high-pressurefiltration, the photocatalyst got evenly coated on the surface of the base membrane.

Table 7.1 Photocatalyst loading of various membranes

Membrane	G-50	G-100	G-200	G-300	G-400
Ag-TNF Loading (mg)	50	100	200	300	400

7.2.4 Characterization

Synthesized samples were observed under field emission scanning electron microscope (FESEM, Zeiss Sigma) and scanning electron microscope (SEM, Jeol JSM-6380LA). All samples were sputtered with gold before analysis. Further Transmission electron microscope (TEM, JEOL JEM-2100) was used to analyze the TNS samples. X-ray Diffractometer (Rigaku Miniflux 6000) equipped with monochromatized high-intensity Cu K α radiation ($\lambda = 1.54178 \text{ \AA}$) was used to analyze the crystalline nature of the samples. UV-Visible spectrometer (Hitachi, U-2900) was used to estimate congo red dye concentration at a wavelength of 498 nm.

7.2.5 Performance study of the membranes

The permeation properties of the membranes were studied using a lab scale dead end filtration cell as described in chapter 5. The cell consists of a Quartz glass window on the top to enable UV irradiation. The active area of the membrane cell was 14.6 cm². The membrane cell was connected to a feed tank which was pressurized using an oxygen cylinder. The flux studies were carried out at a transmembrane pressure of 0.2 MPa.

Permeate flux (J) was calculated using the following equation:

$$J = Q/(\Delta t A) \quad (1)$$

Where J is the flux expressed in Lm⁻²h⁻¹ and Q (L) is the amount of water collected for Δt (h) time duration using a membrane of area A (m²).

Dye removal studies were carried out using the same dead end filtration cell. 50 mg L⁻¹ of Congo red dye solution was prepared in distilled water and 100 mL dye solution was used for each dye removal study. Dye removal studies were done in the presence and absence of UV radiation to evaluate the effects of adsorption and photocatalytic degradation. Permeate obtained after dye removal study was subjected to UV-Vis spectroscopy to estimate residual dye concentration.

7.3 RESULTS AND DISCUSSION

7.3.1 Characterization of TNS

FESEM image of TNS is shown in Fig. 7.1; from the figure individual square flakes of TiO_2 nanosheets can be observed. Magnified image (Fig. 7.1 b) of TNS reveals the sheet structure of the TiO_2 nanosheets.

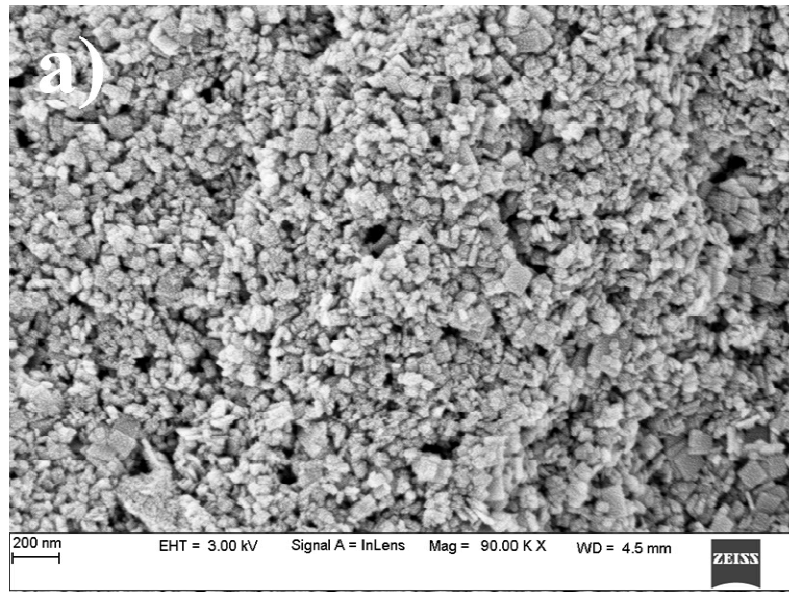


Fig. 7.1 a) FESEM image of TNS

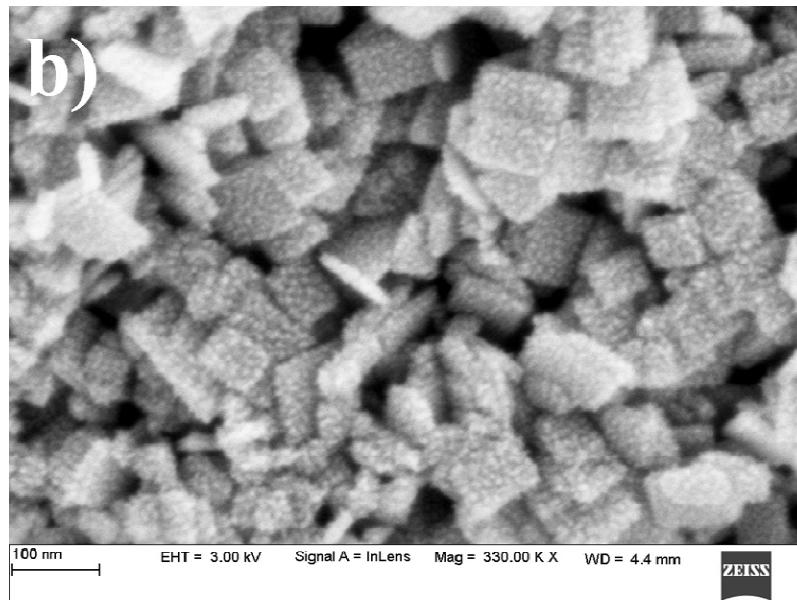


Fig. 7.1 b) Magnified image FESEM image of TNS

X-ray diffraction patterns of TNS are shown in Fig. 7.2. The major XRD peaks were observed at 25.8°, 37.6°, 48.6° and 55.4° which correspond to anatase phase of TiO₂ (JCPDS No. 21-1272) (Masuda et al. 2009). In general, anatase phase of TiO₂ is preferable for superior photocatalytic activity. Hence TNS can serve as a good photocatalyst for the synthesis of the hierarchical membrane.

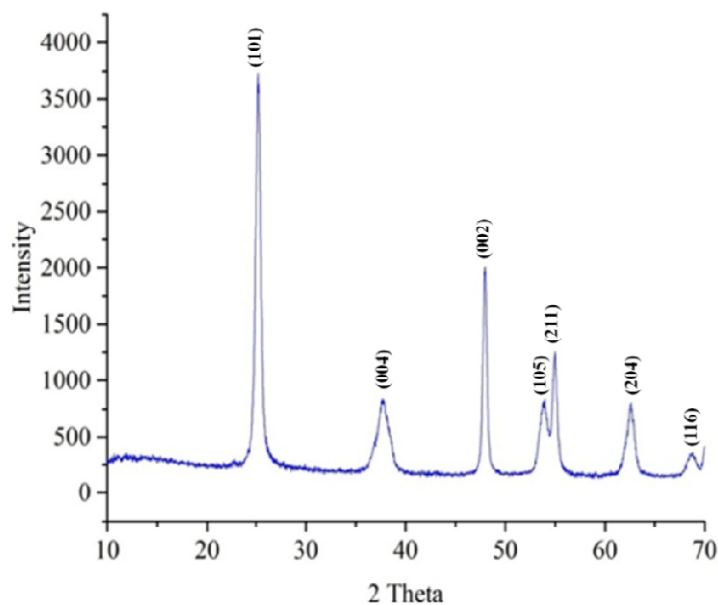


Fig. 7.2 XRD pattern of TNS

7.3.2 Characterization of TNS-GO hierarchical membrane

The hierarchical membrane was synthesized by depositing TNS-GO on the polymer membrane. Fig. 7.2 (a) shows the FESEM image of TNS-GO and the presence of TNS on the GO sheet can be observed from the figure. In the cross sectional image of the hierarchical membrane Fig. 7.3 (b), the porous cellulose acetate support membrane can be seen completely coated with TNS-GO. TNS-GO has formed a uniform stable coating over the membrane surface. The strength of the coating was verified by repeated washing of the coated membrane with water and it was observed that TNS-GO was intact on the membrane surface.

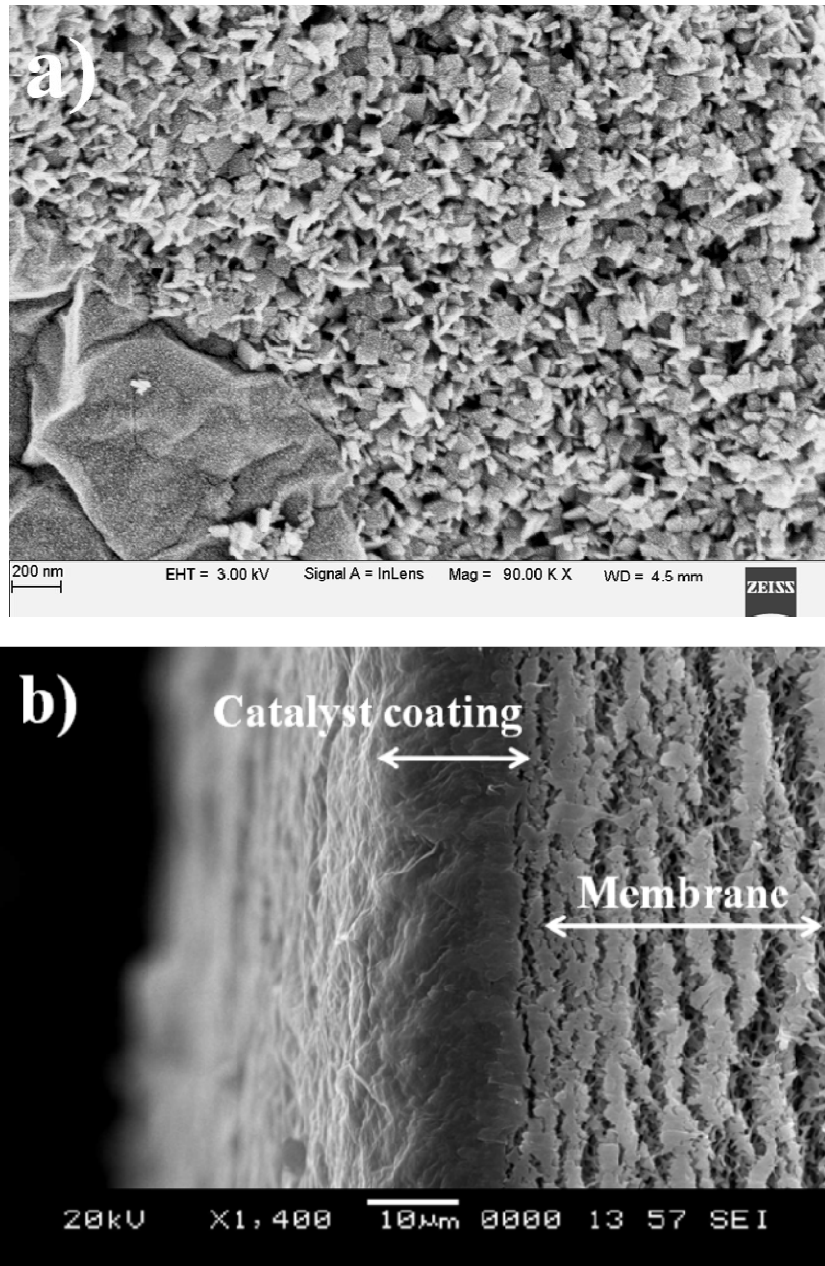


Fig. 7.3 a) FESEM image of TNS-GO b) SEM image of G-100 membrane cross section

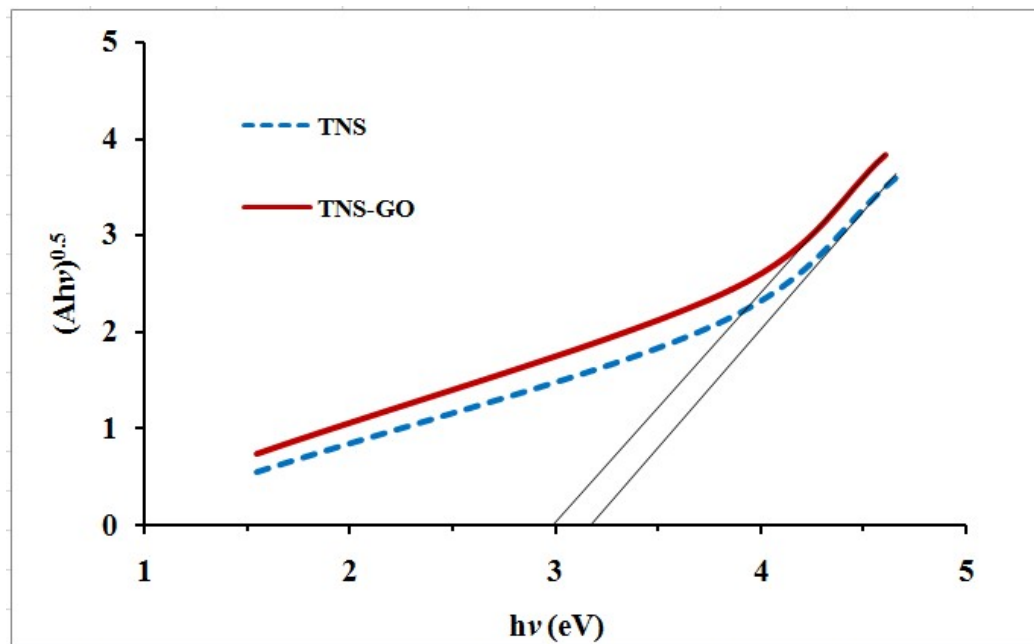


Fig. 7.4 Tauc plots for band gap estimation of photocatalysts

Energy band gap estimation of the TNS-GO was carried out by analyzing the UV-Vis spectral absorption peaks as reported in the literature (Uddabdrao et al. 2016). The Tauc plots indicate the reduction of EG from 3.2 eV to 2.98 eV on adding GO to TNS (Fig. 7.4).

7.3.3 Performance study of TNS-GO membranes

The flux of various membranes is given in Fig 7.5. Theoretically, the addition of TNS-GO on the membrane surface blocks the surface pores and results in permeate flux reduction (Dipareza et al. 2008). A gradual reduction in PWF has been observed as TNS-GO loading was gradually increased, but the dye removal gradually increased (Fig. 7.6). In a hierarchal membrane, lower flux enhances the interaction between the dye and the catalyst and improves the dye removal. But very low flux will unnecessarily prolong the filtration process. Hence in a hierarchal membrane, there is always a tradeoff between the permeate flux and dye removal.

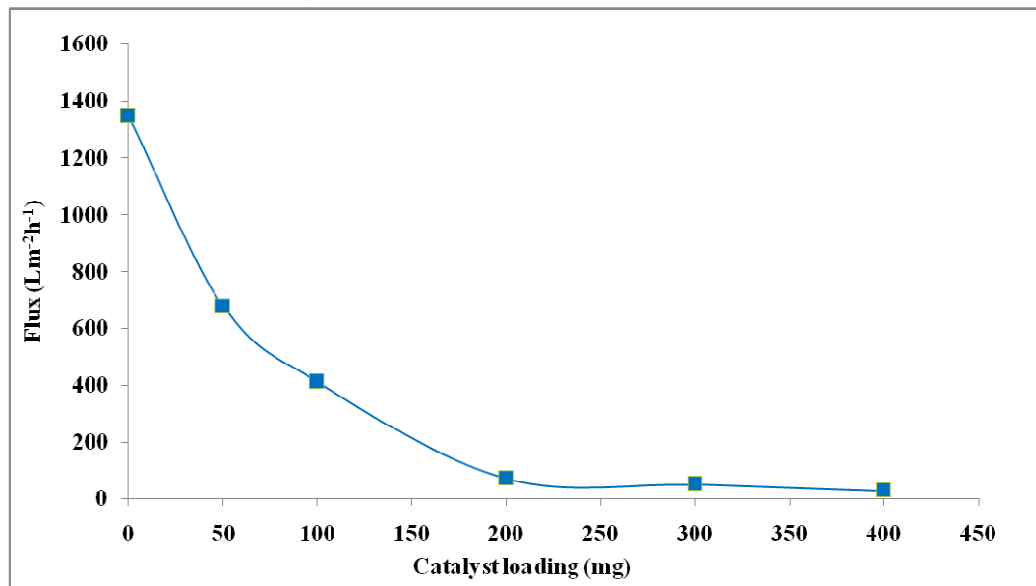


Fig.7.5 Flux of various membranes

As the TNS-GO loading increases, there is an appreciable increase in dye removal, complete dye removal was obtained in case of G-400 with the lowest flux of 29.3 Lm⁻²h⁻¹. The TNS-GO can remove the dye in two ways, either by adsorption or by photocatalytic degradation (Bai et al. 2015). The presence of reactive oxygen atoms, carboxyl, and hydroxyl groups enable GO to interact effectively with Congo red resulting in good adsorption (Debnath et al. 2014). In aqueous media, the surface hydroxyl groups of TiO₂ facilitate the adsorption of Congo red dye (Kordouli et al. 2015). Up on UV irradiation, the contact between TNS and GO enables e⁻ transfer from TNS to GO. Electron transfer improves photocatalytic activity by lowering the charge recombination rate. The electrons and holes generated during UV irradiation react with O₂ and H₂O in the media to form •OH which enable photodegradation of the dye. Hence, the top portion of the catalyst coating which receives radiation will involve in photodegradation. The remaining underneath portion will adsorb the dye. Dye adsorption is undesirable since it adversely affects catalyst reusability. The thickness of the membrane should be such that it photodegrades the maximum amount of dye and still offers minimal flux drop.

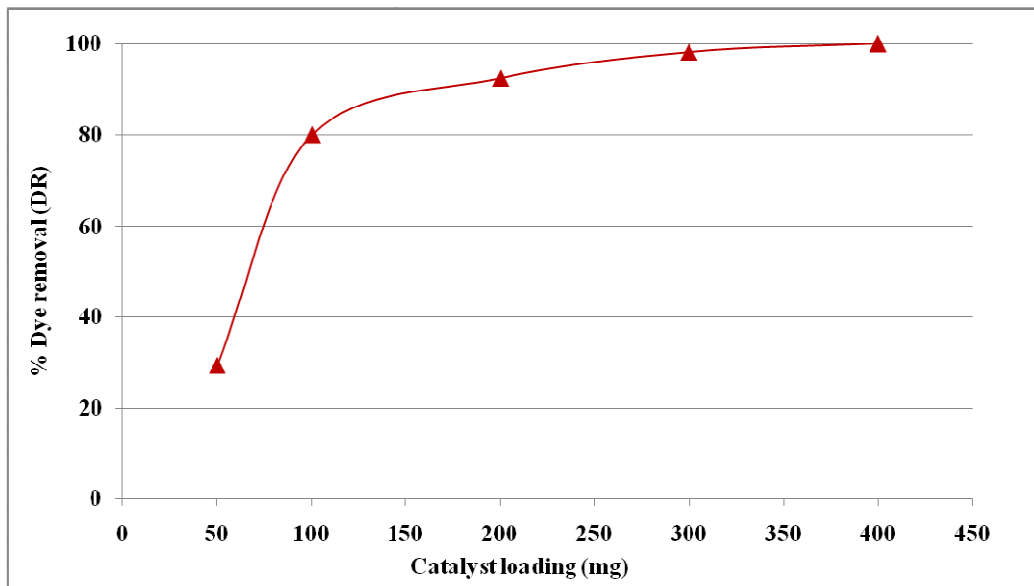


Fig.7.6 Dye removal (DR) of various membranes in presence of UV radiation

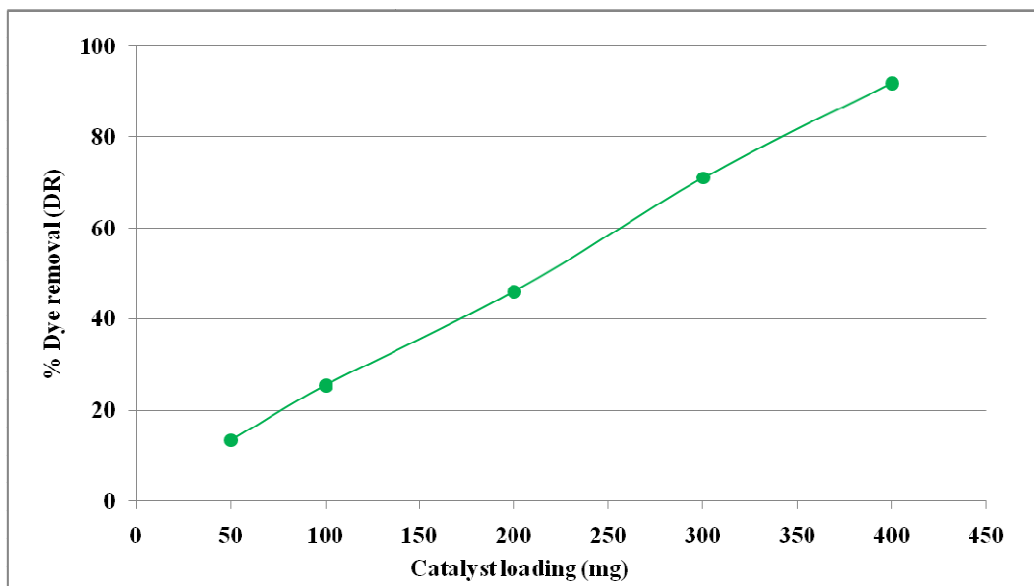


Fig.7.7 Dye removal (DR) of various membranes in absence of UV radiation

UV radiation can't penetrate into the entire thickness of the catalyst coating. The dye removal study done in the absence of UV irradiation evaluates the effect of adsorption (Fig. 7.7). It is observed that amount of dye absorbed is directly proportional to the catalyst loading. Beyond 100 mg of catalyst loading, adsorption played a significant role. In case of G-400, which had given 100% dye removal under

UV irradiation, is capable of removing 94.5% of the dye just by adsorption. It is evident that beyond G-100, increased loading didn't improve photodegradation. The membrane surface area which is exposed to UV radiation is constant and does not further increase with catalyst loading. By comparing the difference between the dye removed in presence and absence of UV light, it is evident that G-100 membrane could achieve maximum photodegradation of dye. Also when compared to higher catalyst loaded membranes, G-100 exhibited superior permeate flux. The G-100 membrane is thus more efficient and reusable.

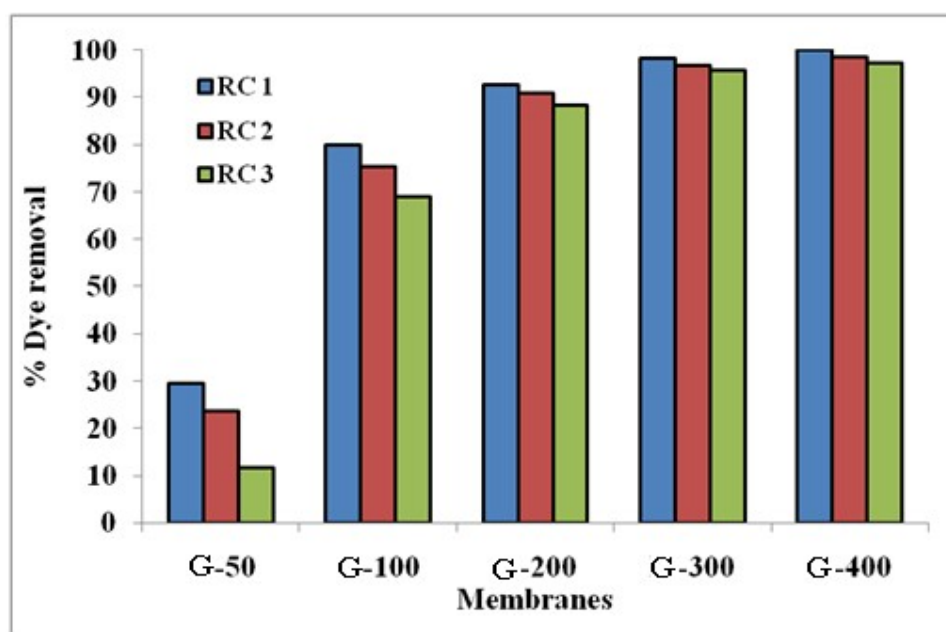


Fig.7.6 Reuse cycles (RC) of the membrane for Dye removal

The membrane reuse cycles were carried out and the results are shown in Fig. 7.8. It is observed that except G-50 membrane all other membranes showed consistent dye removal traits. The adsorption phenomenon weakens with continuous reuse of the photocatalyst. At higher catalyst loading the lower flux provides sufficient residence time for efficient dye degradation via photocatalysis.

7.4. CONCLUSIONS

TNS-GO coated hierarchical membranes were successfully synthesized for simultaneous water filtration and photocatalytic degradation. At higher catalyst

loading the permeate flux dropped heavily due to the additional cake resistance of the catalyst coating. Dye adsorption played a major role at higher catalyst loading where as photodegradation was significant at lower catalyst concentration. Although G-400 could completely remove the dye, it exhibited the lowest flux and greater dye adsorption. G-100 membrane showed the best result with comparatively higher flux and better photodegradation. Photocatalyst reuse cycles revealed that higher TNS-GO loaded membranes could maintain dye removal capacity since the flux decline provided sufficient time for photocatalytic degradation.

CHAPTER 8

Ag-TiO₂ NANOSHEET (Ag-TNS) PHOTOCATALYTIC HIERARCHICAL MEMBRANE FOR SOLAR WATER PURIFICATION

Abstract

Solar photocatalytic degradation of contaminants from water has much potential as a sustainable means for water treatment. The major challenges in using nano size photocatalysts is catalyst recovery and the rising concern over the toxicity of various nanomaterials. In the present work the problem of catalyst recovery is mitigated by immobilizing the photocatalyst on the surface of a membrane by pressurized ultrafiltration method. The hierarchical membrane thus synthesized is capable of simultaneously degrading and filtering pollutants. The photocatalyst employed is silver doped TiO₂ nanosheets, their ultra-thin structure and larger size favor stable film formation on the membrane surface. The nanosheets were synthesized via hydrothermal route and their photocatalytic efficiency was further enhanced by doping with silver. The nanosheets were characterized using SEM, XRD and EDS. Photocatalytic degradation studies were conducted using Congo red dye as the model pollutant. The effect of varying catalyst loading on permeation properties and dye removal were studied under ultra violet and solar light irradiation. Reuse cycles were conducted to analyze the effect of dye adsorption on the membrane performance. Multiple passage studies were carried out to determine the optimum Ag-TNS loading for superior flux and dye removal.

8.1 INTRODUCTION

In Chapter 7, the use TNS along with graphene oxide (GO) sheets as a novel material for hierarchical membranes was discussed. Although TNS/GO composite hierarchical membranes exhibited good pollutant removal capabilities, the permeate flux obtained was less. GO sheets when used as modifier owing to their larger size of about 3-4 μm resulted in pore blockage, when embedded on top of a membrane with pore size of 0.2 μm . In this chapter an attempt to mitigate this drawback by using silver instead of GO as a modifier along with TiO₂ nanosheets to improve the photocatalytic

performance is discussed. Photodeposition method was used to deposit silver on top of TNS surface; without any significant change in the size of the resultant Ag- TNS nanosheets, and the overall size is in the range of 100-200 nm. Since, the size of the photocatalyst used for coating the membrane is comparable to the pore size of the base membrane, lesser pore blockage occurs. Therefore when compared to GO the use of silver as dopant does not considerably affect the size of the resultant photocatalyst material. Thus using silver as a modifier can nullify additional pore blockage and the flow resistance developed due to the modifier. The uses of silver as dopant has shown to significantly improve the photocatalytic activity in case of TiO₂ nanofibers. Also, silver doped TiO₂ has been proven to exhibit good performance under visible radiation; hence the membranes were studied for potential application in solar water treatment (Tang et al. 2016). A comprehensive study involving parameters such as photocatalyst loading, permeate flux, dye adsorption and reuse cycles were performed to optimize Ag-TNS loading for the process.

8.2 MATERIALS AND METHODS

8.2.1 Materials

Cellulose acetate membrane (diameter - 47 mm and pore size - 0.2 μm) was obtained from Sartorius stedim biotech, Bangalore, India. Congo red dye, silver nitrate and ammonium hydroxide were procured from Nice chemicals Pvt Ltd, Cochin, India.

8.2.2 Synthesis of Ag-TNS composite

1 g of TNS and 427 mg of AgNO₃ were added to 200 mL water under constant stirring. The pH of the solution was adjusted to 11 via adding ammonium hydroxide. The dispersion was exposed to UV light for 4 h under constant stirring. A dark purple colored residue of Ag-TNS was thus obtained (Souwmya& Meenakshi, 2015).

8.2.3 Synthesis of Ag-TNS Hierarchical Membrane

A suitable quantity of Ag-TNS as given in Table 8.1 were dispersed in 100 mL of distilled water and loaded into a filtration assembly (Tarsons-50021). Cellulose acetate membrane of diameter 4.7 cm and pore size 200nm was used as the support membrane. The vacuum was applied using a vacuum pump (Technic-TID-75-S, Pressure- 0.379 MPa) connected to the filtration setup. Water passed through the

membrane as permeate, leaving behind a layer of Ag-TNS on the membrane surface (Bai et al. 2010).

Table 8.1 Photocatalyst loading of various membranes

Membrane	B-50	B-100	B-200	B-300	B-400	B-500
Ag-TNS Loading (mg)	50	100	200	300	400	500
Ag-TNS Loading per unit area (g m ⁻²)	34.24	68.49	136.98	205.47	273.97	342.46

8.3 CHARACTERIZATION

8.3.1 XRD analysis

XRD was done using Rigaku Miniflux 6000, X-ray diffractometer. The diffractograms were obtained at 0.16°/s in the 2θ range of 10-70°. Accelerating voltage was set to 30 kV and a current of 20 mA. Powder samples of TNS and Ag-TNS were examined for their crystalline phases.

8.3.2 SEM analysis

Morphology of synthesized nanosheets and membrane samples were analyzed using JEOL (JSM-6380LA)SEM.

8.3.3 TEM analysis

The Ag-TNS was examined using Transmission electron microscopy (TEM, JEOL, JEM-2100). All the TEM samples were prepared by the deposition of a drop diluted suspensions on a carbon film coated copper grid.

8.3.4 Performance study of membranes under UV radiation

A custom-made dead-end filtration cell with quartz glass window was used to study the performance of the membranes under UV radiation (Fig. 5.1). The effective membrane area of the unit was 14.6 cm². The permeate sample was taken after exposure to 0.1 MPa TMP. The permeate flux (J_w) was determined by the below equation:

$$J_w = \frac{Q}{\Delta t A} \quad (1)$$

Congo red dye solution (50 ppm) was prepared and filtered through the membranes to study the pollutant removal capabilities. Permeate collected was subjected to UV-Vis spectroscopy to estimate residual pollutant concentration at a wavelength of 498 nm.

Percentage removal of dye was calculated using above equation 2, where C_p (mg/L) and C_f (mg/L) are the dye concentrations in permeate and feed respectively.

$$\%R = \left(1 - \frac{C_p}{C_f}\right) \times 100(2)$$

8.3.5 Performance study of membranes under solar radiation

In order to study the performance of the membranes for solar water purification a setup as shown in Fig. 8.1 was used.

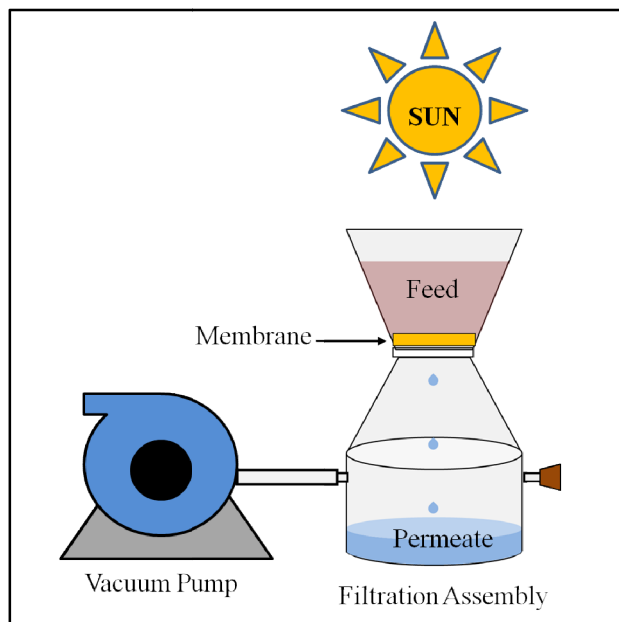


Fig. 8.1 Schematic representation of solar water purification setup

The setup consisted of a transparent 500 mL membrane filtration assembly made of polyester staple fiber which was used to synthesize the hierarchical membranes. The pressure of 0.379 MPa was applied across the membrane via a vacuum pump connected to the filtration assembly. The setup was open at the top to enable good exposure to Sun light and air. No aeration was supplied artificially. The synthesized hierarchical membranes were loaded in the setup and dye solution was feed from the top. After filtration, the collected permeate was subjected to UV-Vis spectroscopy to estimate dye concentration.

8.4 RESULTS AND DISCUSSION

8.4.1 Characterization of Ag-TNS

Fig. 8.2 shows the SEM and TEM image of Ag-TiO₂ nanosheets. The nanosheets exhibited fairly rectangular geometry with very small thickness. Energy dispersive X-ray spectroscopy (EDS) study revealed the presence of silver (2.57 atomic %) in Ag-TiO₂ nanosheets (Fig. 8.3). X-ray diffraction (XRD) pattern of Ag-TNS showed (Fig. 8.4) major peaks at 25.14°, 37.68°, 47.86° and 55.08° corresponding to anatase TiO₂. The smaller peaks at 26.28°, 32.04° and 46.3° indicate the presence of silver.

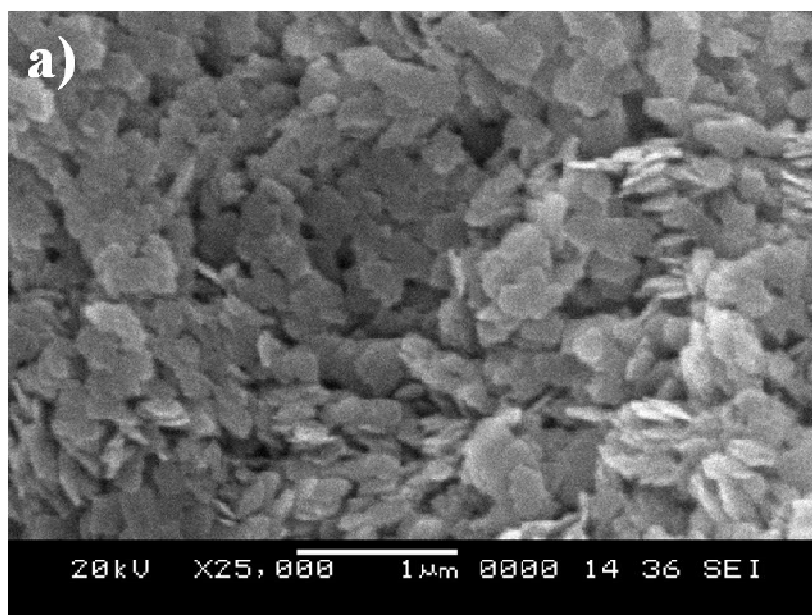


Fig. 8.2 a) SEM image of Ag-TNS

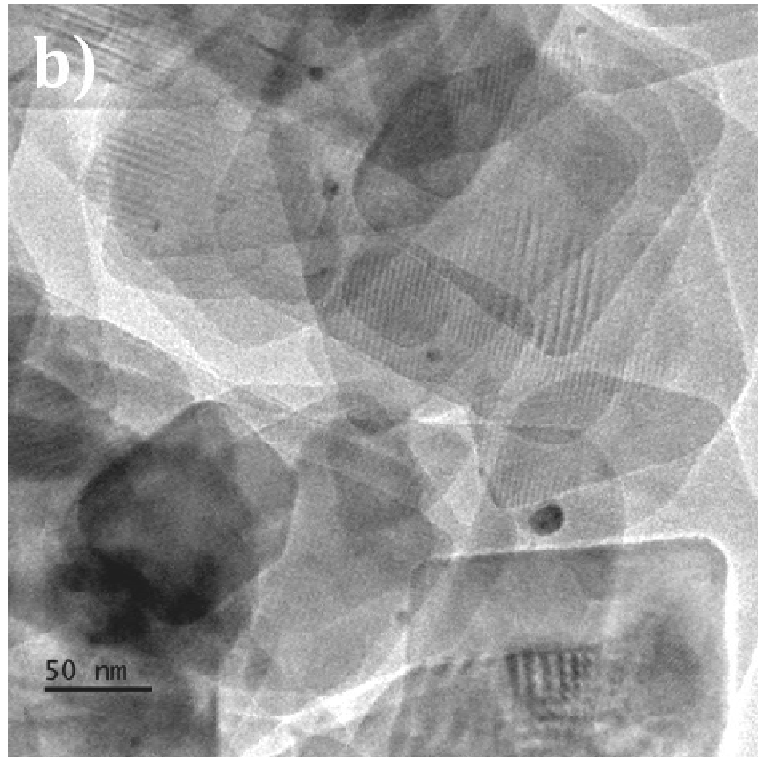


Fig. 8.2 b) TEM image of Ag-TNS

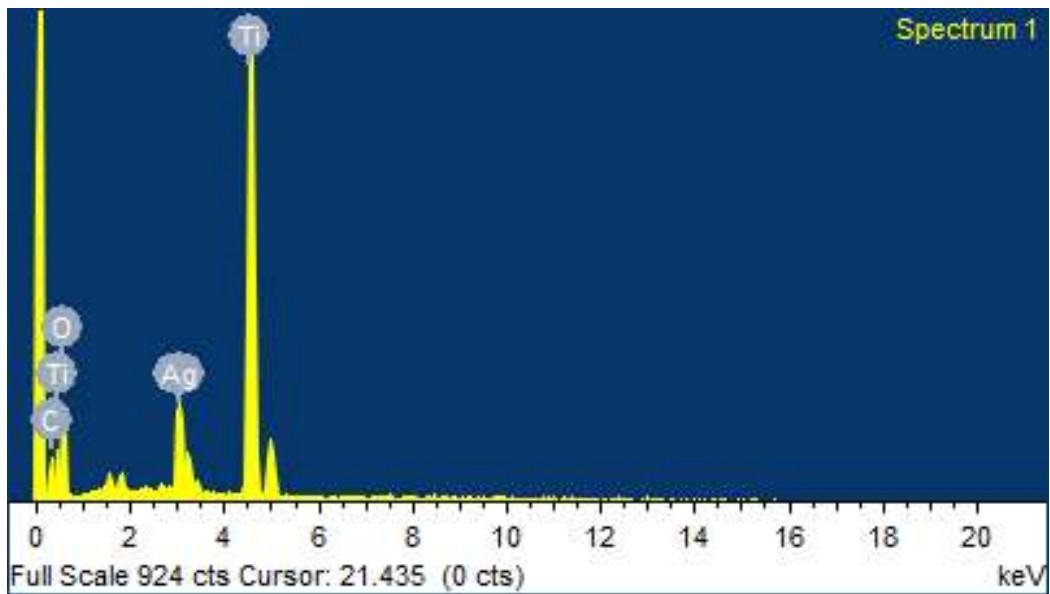


Fig. 8.3 EDS of Ag-TNS

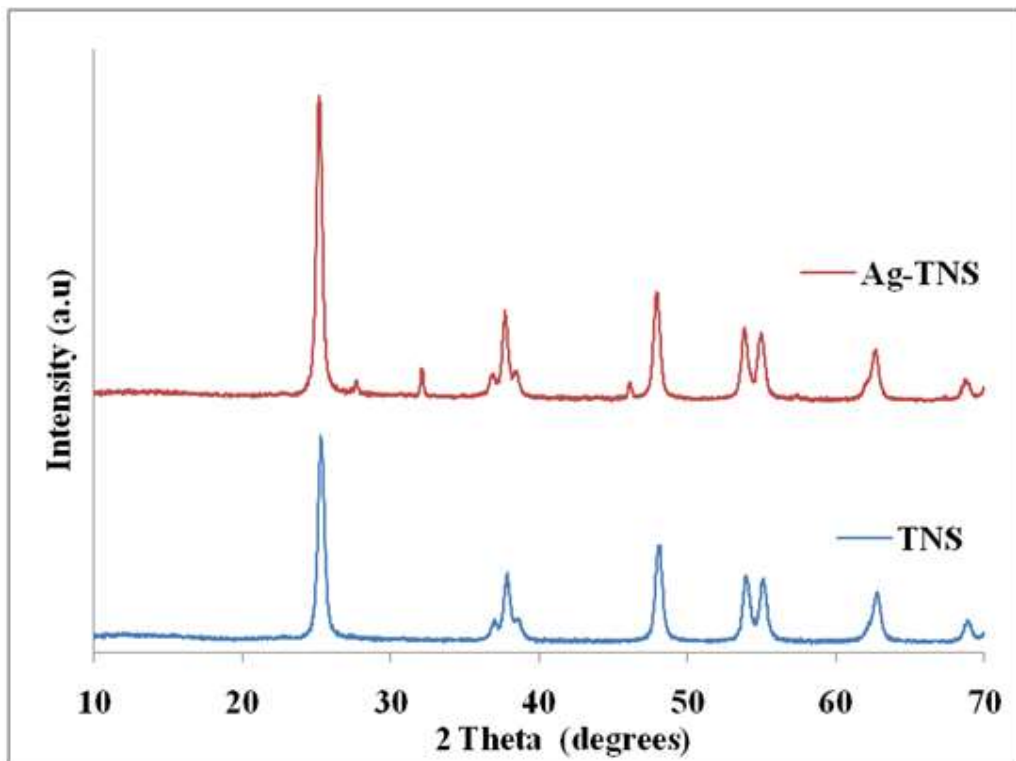


Fig. 8.4 XRD pattern of Ag-TNS

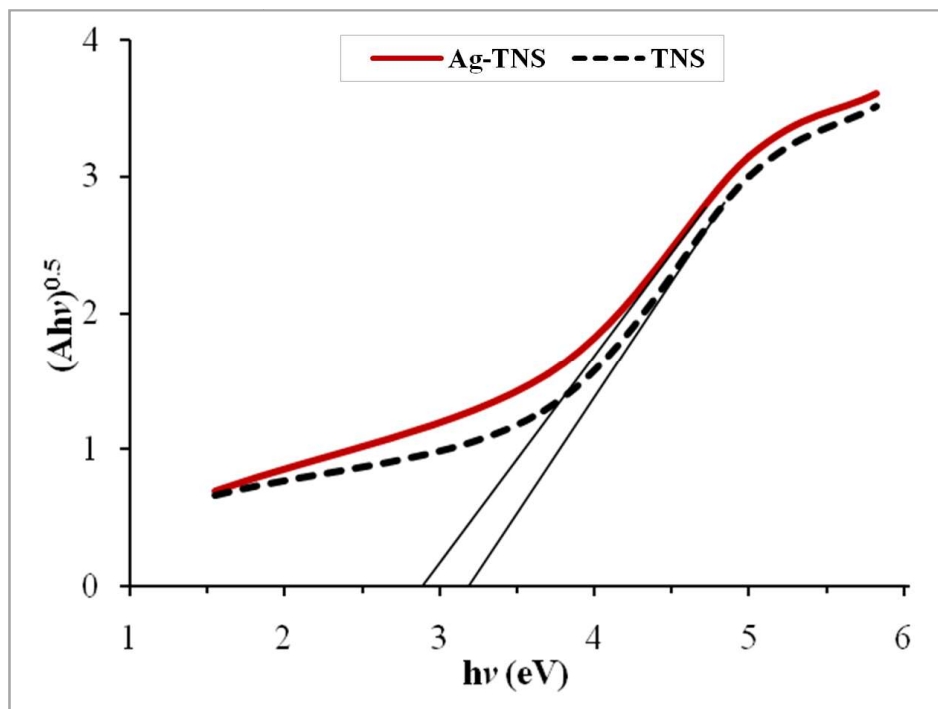


Fig. 8.5 Tauc plots for band gap estimation of TNS and Ag-TNS.

Energy band gap evaluation of the photocatalysts; TNS and Ag-TNS was analyzed via UV–Vis spectral absorption peaks as reported in the literature (Uddandaraao et al. 2016). The Tauc plots showed a decrease in band gap from 3.2 eV to 2.95 eV for Ag doped TNS (Fig. 8.5). Addition of Ag has improved the photocatalytic efficiency of the catalyst. Due to the lower band gap, Ag-TNS can be activated by a wider spectral range including visible light; this can significantly improve photocatalytic performance under sunlight (Liu et al. 2013).

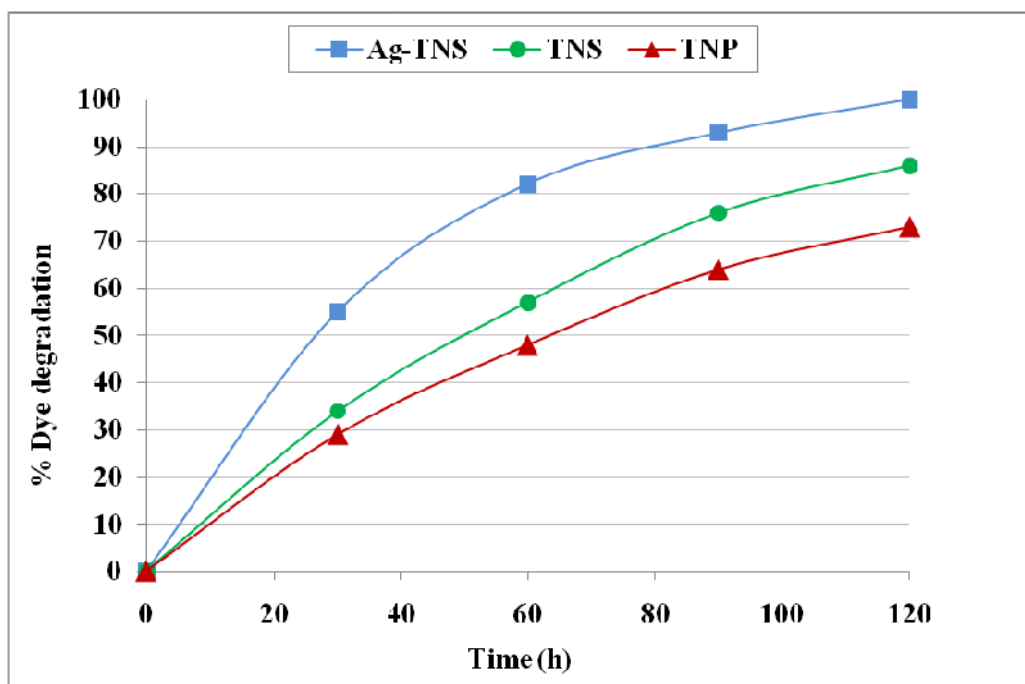


Fig.8.6 Dye degradation by various powder photocatalysts under solar radiation

The photocatalytic activity of TNP, TNS and Ag-TNS were tested under sun light and results are shown in Fig 8.6. TNP showed low performance since it is active only under UV radiation and the UV content of Sun light is less. TNS showed slightly better performance than TNP, which is due to their defect free surfaces that retard faster recombination of charge carriers. Ag-TNS showed superior photocatalytic activity under sun light, clearly due to its lower band gap enabling photocatalytic active under a wider range of solar spectra as revealed from energy gap results. Transfer of electrons to silver enables TiO_2 to improve charge separation and hence

delay the recombination of charge carriers, thereby improve the photocatalytic activity.

8.4.2 Characterization of Ag-TNS Hierarchical Membranes

As shown in Fig. 8.7, Ag-TNS formed a stable coating on the membrane surface and due to the stacking of nanosheets better stability is imparted to the photocatalyst layer.

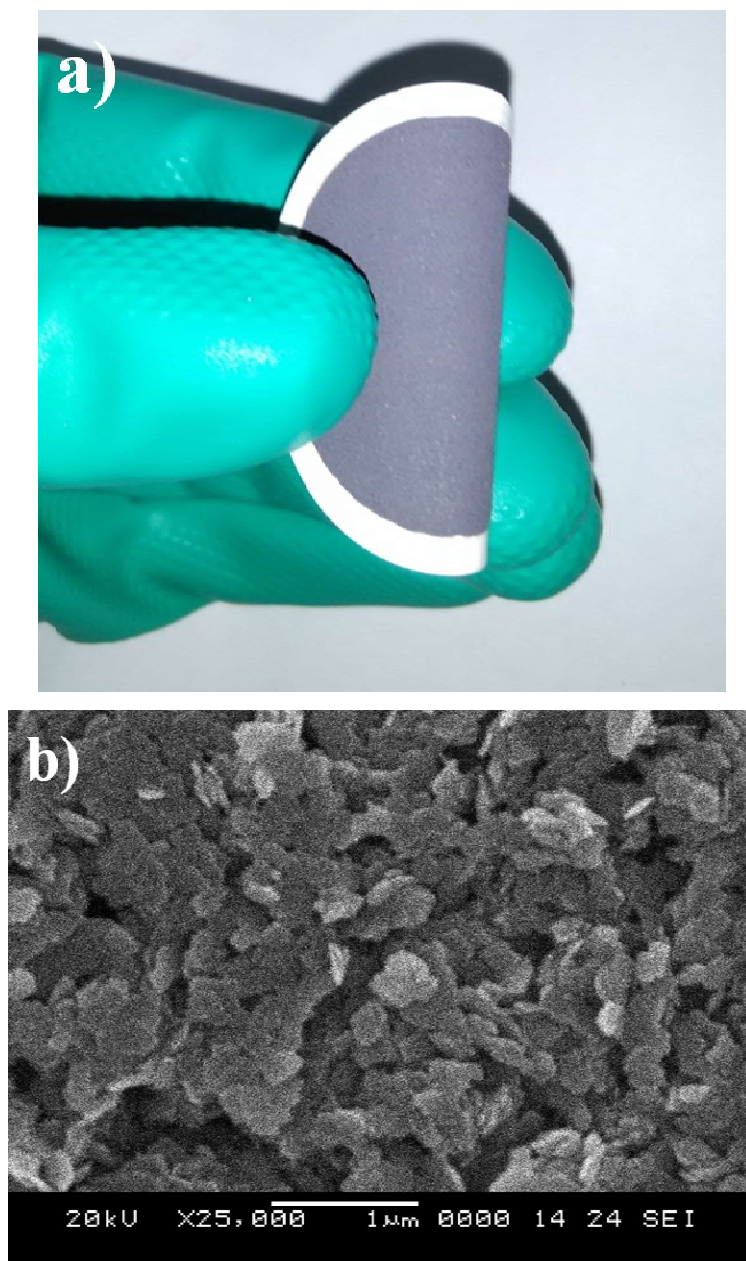


Fig. 8.7 a) Digital image of Ag-TNS hierarchical membrane b) SEM image of Ag-TNS hierarchical membrane surface

As seen from the SEM image (Fig. 8.7b), Ag-TNS on the membrane surface seems to be more uniform and compact when compared to Ag-TNS powder (Fig. 8.2a) which is uneven and loosely held. This is because Ag-TNS is coated on to the membrane surface using pressurized ultra filtration, wherein deposition of Ag-TNS on membrane surface is facilitated by a water based high-pressure filtration process resulting in a uniform compacted layer of Ag-TNS on the membranesurface. The membranes were tested using a UV irradiated membrane cell to study the effect of catalyst loading on permeation properties and dye removal.

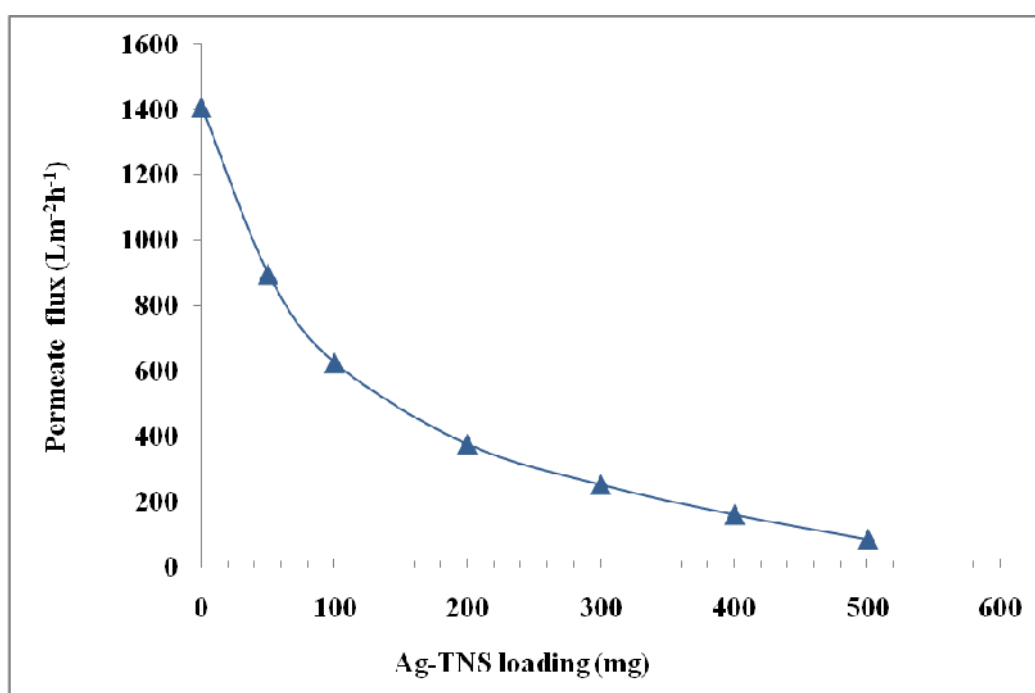


Fig.8.8 Permeate flux of membranes.

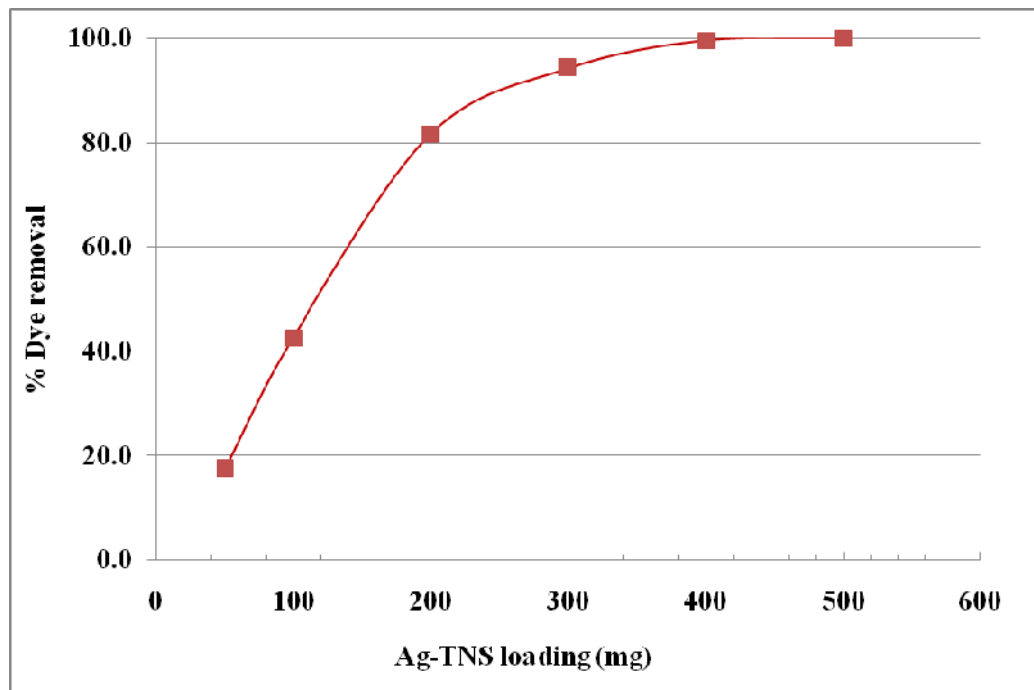


Fig.8.9 Dye removal by membranes under UV radiation.

Fig. 8.8 shows the effect of Ag-TNS loading on permeate flux, a decrease in permeate flux is observed as Ag-TNS loading increases. As more Ag-TNS is deposited on the membrane surface, the thickness of the photocatalyst layer increases, which results in increased resistance to flow. At lower Ag-TNS loading, the flux reduced drastically due to initial pore blockage happening at the membrane-photocatalyst interface (Dipreaza et al. 2008). Flux decline becomes gradual at higher loading due to increasing resistance to flow arising due to the increased thickness of the Ag-TNS layer. The Greater thickness of photocatalyst layer and the decreased permeate flux provide higher residence time and contact area for the feed to interact with the Ag-TNS present on the membrane surface, which results in better dye removal at higher Ag-TNS loading (Fig. 8.9).

Dye removal increased with greater Ag-TNS loading and reached a maximum at 500 mg loading. B-500 showed complete removal of dye with a flux of $86.7 \text{ Lm}^{-2}\text{h}^{-1}$, which is three times higher than the flux observed in case of TNS-GO. Higher flux is an important factor for reducing the time of operation. The use of silver as modifier

mitigated the extra resistance and pore blockage produced in case of GO, hence higher flux is obtained.

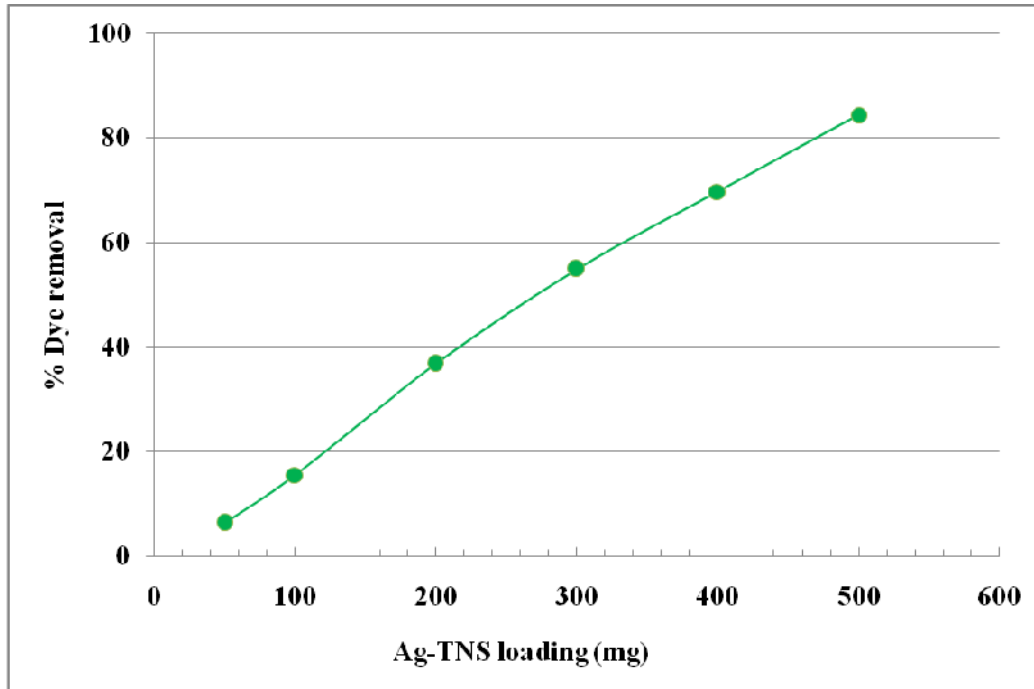


Fig.8.10 Dye removal by membranes in absence of UV radiation.

When dye comes in contact with Ag-TNS both adsorption and photocatalytic degradation can take place (Kordouli et al. 2015). Typically the top layer of the photocatalyst takes part in photocatalytic degradation and as the dye permeates inside the catalyst layer a portion of dye gets adsorbed. Thus, dye adsorption also contributes to dye removal, but as more and more dye gets adsorbed, the catalyst gets exhausted. Permeate flux is also a very important phenomenon affecting the adsorption since lower flux gives ample time for dye adsorption. The ability of the membranes to adsorb dye was accessed by simply passing the dye solution through the membranes in absence of UV radiation (Bai et al. 2015). It was observed that the Ag-TNS catalyst layer could adsorb significant quantity of dye; a maximum of 84.3 % was obtained in case of B-500 (Fig. 8.10). In order to find out the impact of dye adsorption on the dye removal capabilities of the membrane, reuse of the membranewas performed as shown in Fig. 8.11. It was observed that at lower Ag-TNS loading reduction in membrane reusability is observed. On continuous reuse, the lower layers of the Ag-

TNS catalyst coating gets exhausted after dye adsorption and dye removal becomes completely dependent on the photocatalytic degradation. Since the flux is much higher at lower Ag-TNS loading, no sufficient time for efficient photocatalysis is available.

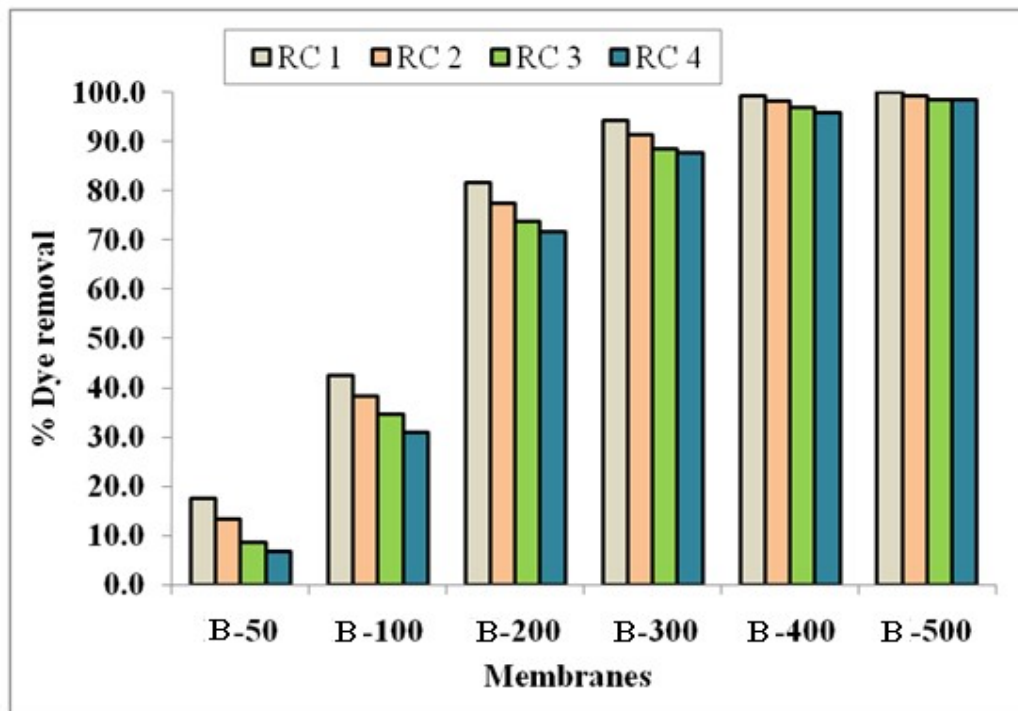


Fig.8.11 Reuse cycles (RC) of various membranes for dye removal under UV radiation.

In case of higher Ag-TNS loaded membranes, the drop in the dye adsorption doesn't significantly affect the performance, since sufficient time for photocatalytic degradation is available due to the lower flux, providing enough residence time for the feed. It is clear that there exists a standoff between permeate flux and dye removal capability of the membrane. But as mentioned earlier lower flux provides more time for photocatalytic degradation but increases the processing time. Hence, it is important to find the optimum catalyst loading for better flux and maximum dye removal. In order to find the optimum catalyst loading multiple passage studies were conducted (Fig. 8.12). Permeate obtained after one passage was again feed through the membranes for the second time. B-500 was able to give the maximum dye

removal in the first pass, interpolating the data showed that 420 mg catalyst loading is the minimal loading needed to achieve complete dye removal in a single pass. By interpolating the flux values given in Figure 8.8, the estimated flux value for 420 mg catalyst loading is $146.5 \text{ Lm}^{-2}\text{h}^{-1}$ (processing time 4.67 hL^{-1}).

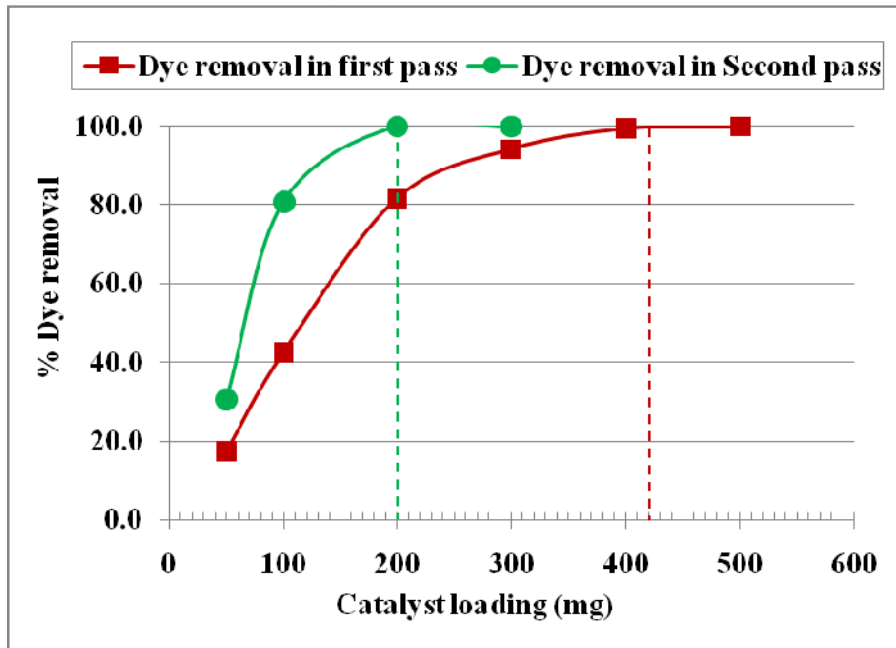


Fig.8.12 Dye removal in multiple passages of feed recycles through membranes under UV radiation.

During the second pass of feed recycle, all the membranes with a catalyst loading of B-200 and above could remove the dye completely. B-200 had a flux of $376.8 \text{ Lm}^{-2}\text{h}^{-1}$ and a total processing time of 3.63 hL^{-1} for two passes. Therefore the flux of B-200 is significantly higher than B-400 (flux $161.5 \text{ Lm}^{-2}\text{h}^{-1}$, processing time 4.24 hL^{-1}) and B-500 (flux $86.7 \text{ Lm}^{-2}\text{h}^{-1}$, processing time 7.89 hL^{-1}) and the time required to obtain complete dye removal is lesser for B-200 in multiple passages. Thus multiple passage studies reveal that better flux and good dye removal could be obtained faster in case of B-200 (catalyst loading of 136.98 gm^{-2}). The excess Ag-TNS in case of B-400 and B-500 was unnecessarily delaying the permeate flux due to added resistance.

The performance of the optimal B-200 membrane obtained from the studies of UV radiation was tested for solar water purification and results are shown in Fig. 8.13. Since, the trans-membrane pressure applied was significantly higher than the pressure used in case of UV irradiated membrane cell, a very high flux of $376.8 \text{ Lm}^{-2}\text{h}^{-1}$ was

observed. Since the flux was high, the feed wouldn't get sufficient residence time for entire dye removal to take place. Complete dye removal was hence possible only after 3 subsequent recycles of the feed through the membrane within an appreciable total processing time of 1.61 hL^{-1} .

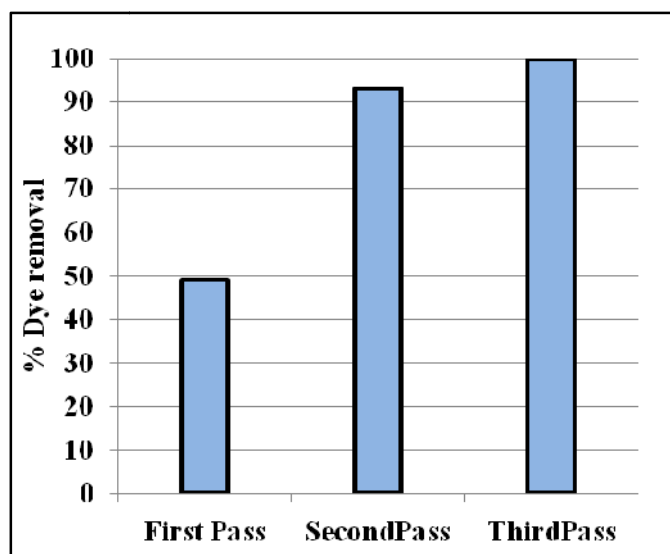


Fig.8.13 Dye removal in multiple passages of feed recycles through B-200 membrane under solar radiation.

8.5 CONCLUSION

Ag-TiO₂ nanosheets were successfully synthesized as confirmed from SEM and EDS. Ag-TNS could form stable photocatalyst coating on the support membrane. The membranes exhibited high flux drop due to increased resistance, due to the Ag-TNS coating. All membranes showed good dye removal traits under UV radiation. The decreased flux, in turn, favored greater contact between catalyst and dye, resulting in better dye removal. Under UV radiation, B-500 showed complete dye removal with an appreciable flux of $86.7 \text{ Lm}^{-2}\text{h}^{-1}$. Reuse cycles revealed that dye adsorption was affecting dye removal significantly at lower Ag-TNS loaded membranes. Multiple passage studies for optimizing the permeate flux and dye removal indicated an optimal performance for B-200 membrane with an Ag-TNS loading of 136.98 gm^{-2} . Under solar radiation B-200 membrane could obtain complete removal obtained in three passages within a short processing time of 1.61 hL^{-1} , exhibiting good flux and dye removal traits.

CHAPTER 9

Ag-TiO₂ NANOSHEET/POLYSULFONE (Ag-TNS/PSF) NANOCOMPOSITE FLOATING PHOTOCATALYSTS FOR SOLAR DEGRADATION OF POLLUTANTS

Abstract

Floating photocatalyst are viable options for degradation of pollutants using solar radiation. The presence of photocatalyst floating on top of water body can enable better exposure to Sunlight and also better air contact for photo-degradation. Direct use of powder photocatalyst in water bodies is impracticable. In the present work silver doped TiO₂ nanosheets were immobilized in polysulfone matrix and coated on low density polyethylene beads to develop a floating photocatalyst. The performance of the floating photocatalyst for degrading pollutants under solar radiation was evaluated using Congo red dye as a model pollutant. The Ag doped TiO₂ nanosheet based floating photocatalyst showed good performance in degradation Congo red dye. XRD and FESEM were used to characterize the floating photocatalyst.

9.1 INTRODUCTION

Sun light is one of the most abundant and constant sources of energy on earth and using solar energy for water treatment are foremost sustainable. But all photocatalyst used in water treatment is in powder form and cannot be dispersed into any water body, also catalyst recovery becomes impossible. There is an alarming concern for the potential toxicity of these nanomaterials as well which must also be considered, hence the photocatalyst need to be immobilized. Typically in a water body, the top surface receives maximum solar radiation and air supply. Therefore the photocatalyst will be most efficient if deployed at the surface or made to float. It would be an additional advantageous if the photocatalyst is highly porous in order to enable ample contact with water. Recently, nanocomposite membranes with polymers blended with photocatalytic nanoparticles especially TiO₂ nanomaterials have shown good performance in degrading organic pollutants in UV assisted membrane filtration. Although most of the polymers employed in membrane synthesis are vulnerable to

UV radiation, the incorporation of nano-TiO₂ has been proven to stabilize the nanocomposite. UV assisted membrane filtration can be converted to solar but the energy required for pumping and pressuring the feed and the large capital cost of setting up the unit is unavoidable. Also, it is doubtful that sun light can be effectively used in membrane modules except in flat sheet configuration. In the current study, we have developed a photocatalytic nanocomposite membrane material and used it as a floating photocatalyst instead of conventional UV assisted membrane filtration. The photocatalyst was subjected to dye degradation studies under sun light to assess its performance.

9.2 MATERIALS AND METHODS

9.2.1 Materials

Polysulfone (PSF, $M_w \sim 35000$ Da), low-density polyethylene (LDPE, the approximate diameter of 3 mm) were purchased from Sigma-Aldrich Co, Bangalore. Congo red dye was obtained from Nice chemicals, Kochi. 1-methyl-2-pyrrolidine (NMP) and polyethylene glycol (PEG, $M_w \sim 600$ Da) were purchased from Merck specialties private ltd., Mumbai.

9.2.2 Preparation of Ag-TNS/PSF floating photocatalyst

2 g of PSF was added to 8 mL of NMP and stirred for 5 h at 65 °C. To the obtained polymer solution 1 g of Ag-TNS was added and stirred for 30 min (Nair et al. 2013). PE beads (size) were immersed into the above polymer solution and dropped individually into 1 L beaker containing distilled water. The polymer coating on the bead surface immediately solidified due to phase inversion. The beaker containing the beads was stirred vigorously at 900 rpm for 24 h.

9.3 CHARACTERIZATION

9.3.1 XRD analysis

XRD was done using Rigaku Miniflux 6000, X-ray diffractometer. The diffraction patterns were obtained at 1°/min in the 2θ range of 10-70°.

9.3.2 FESEM analysis

The morphology of the nanosheets and bead samples were analyzed using FESEM (Zeiss Sigma). All samples were sputtered with gold before analysis. EDS was also done the same equipment.

9.3.3 Dye degradation studies

Solar dye degradation studies of the beads were carried out using Congo red dye. Varying concentrations of congo red dye solutions (10 ppm, 20 ppm, 30 ppm) were prepared. 100 mL of dye solution was taken in a transparent 100 mL glass beaker. 2.4 grams of Ag-TNS/PSF coated beads were added to the solution, such that the beads cover the top of the solution completely. These beakers were then placed in Sun light for 8 hours (9:00 Am to 5 PM). 2 mL samples were collected 2 hours UV-Vis spectroscopy to estimate dye concentration. Evaporation loss of water was neglected throughout the study. The wavelength for Congo red analysis was 498 nm. Percentage degradation was calculated using below equation 1, where C_i (mg/L) and C_f (mg/L) are initial and final dye concentrations respectively.

$$\%R = \left(1 - \frac{C_i}{C_f}\right) \times 100 \quad (1)$$

9.4 RESULTS AND DISCUSSION

9.4.1 Characterization of Ag-TNS

The Ag doped TiO₂ nanosheets are 150-200 nm in size and nearly rectangular in shape as seen from the FESEM images (Fig. 9.1). Fig. 9.2 shows the EDS of Ag-TNS, spectra confirmed the presence of 3.76 wt% silver depositions on the TiO₂ nanosheets.

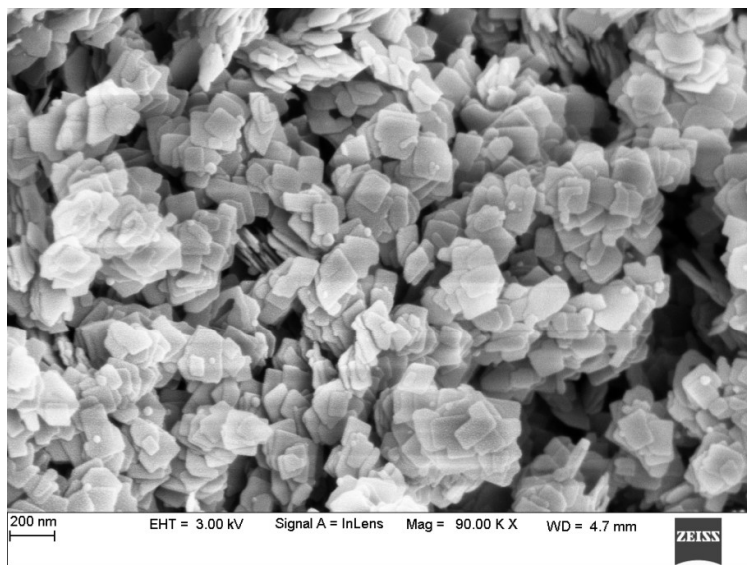


Fig. 9.1 FESEM image of TNS

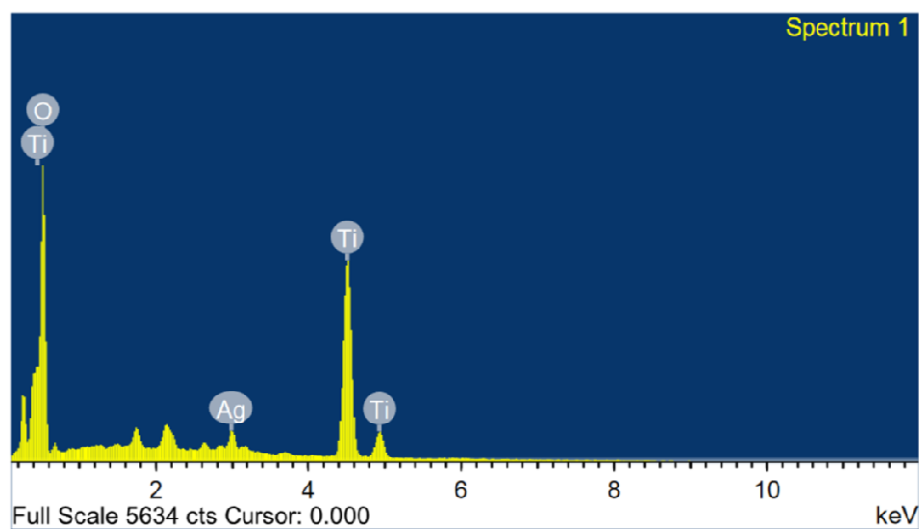


Fig. 9.2 EDS of Ag-TNS

Energy band gap of TNS and Ag-TNS was evaluated using UV-Vis spectral absorption peaks using Tauc plot method (Fig. 9.3). The Tauc plots revealed a decrease in EG from 3.2 eV to 2.95 eV with Ag doping of TNS. The decrease in band gap suggests the shift in photocatalytic activity under visible light and higher photocatalytic efficiency. Hence Ag-TNS is a good photocatalyst under solar radiation.

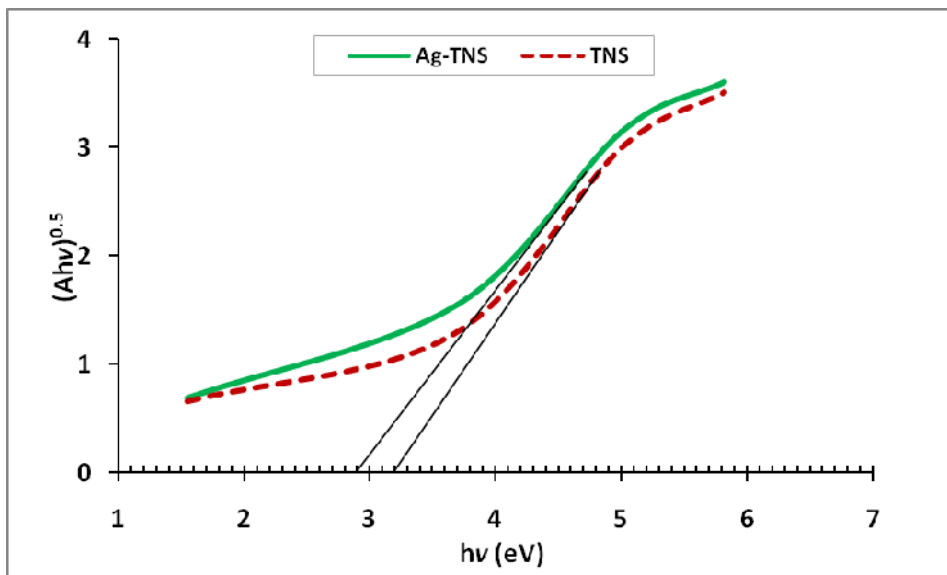


Fig. 9.3. Tauc plots for band gap estimation of Ag-TNS and TNS.

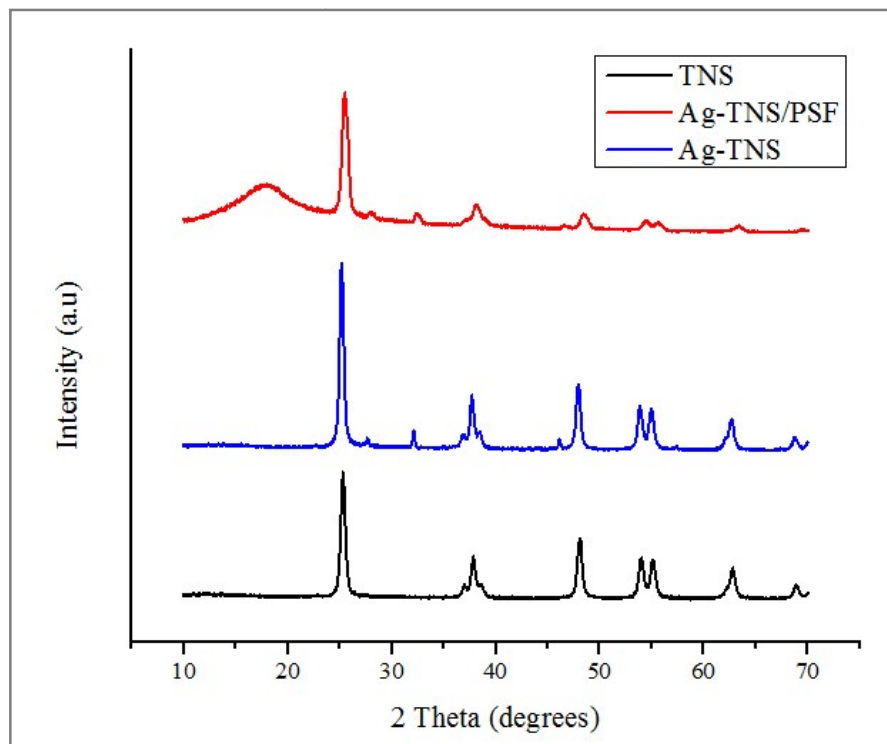


Fig. 9.4 XRD patterns of TNS, Ag-TNS, and Ag-TNS/PSF.

9.4.2 XRD analysis

The XRD patterns of TNS, Ag-TNS and Ag-TNS/PSF are compared in Fig 9.4. The major XRD peaks at 25.2° , 37.72° , 47.98° and 54.98° show that the TNS obtained are of anatase phase. Similar anatase peaks are observed in the case of Ag-TNS as well. The smaller peaks at 26.28° , 32.04° and 46.3° in Ag-TNS XRD pattern indicate the presence of silver. The Ag-TNS/PSF composite also shows the peaks of Ag-TNS although at a lower intensity (Soumya & Meenakshi, 2015).

9.4.3 Characterization of Ag-TNS/PSF coated LDPE bead

Fig. 9.5a shows the cross section of Ag-TNS/PSF coated bead. Ag-TNS/PSF has formed an unbroken coating around the polyethylene bead as seen from the figure. The Ag-TNS/PSF coating is in contact with the LDPE bead surface forming a stable coating (Fig. 9.5b). The Ag-TNS/PSF coating showed good porous structure due to phase inversion occurring during precipitation of the polymer. The solvent NMP diffuses out of the coating and the non-solvent water enters in creating porosity in the coating. Porosity can enable better wettability and contact with aqueous media (Dong et al. 2012).

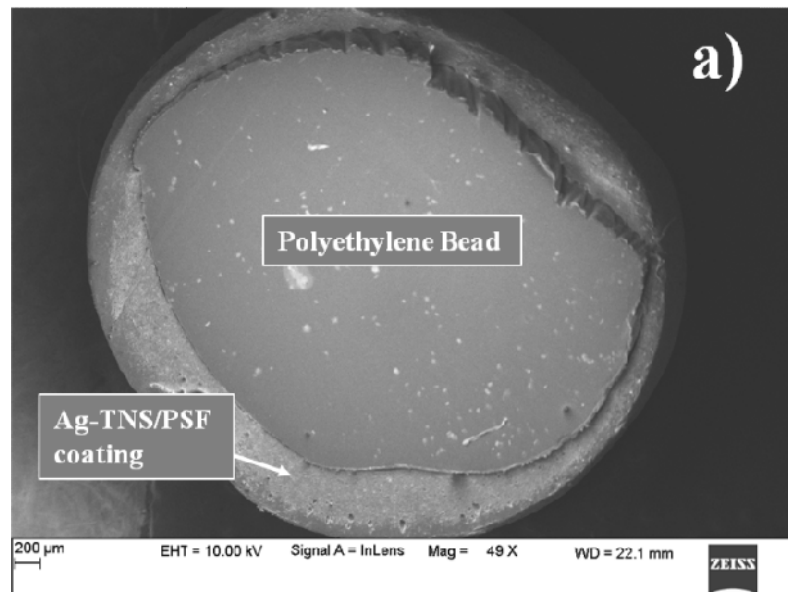


Fig. 9.5 FESEM image a) Ag-TNS/PSF coated bead b) Magnified image of Ag-TNS/PSF coating

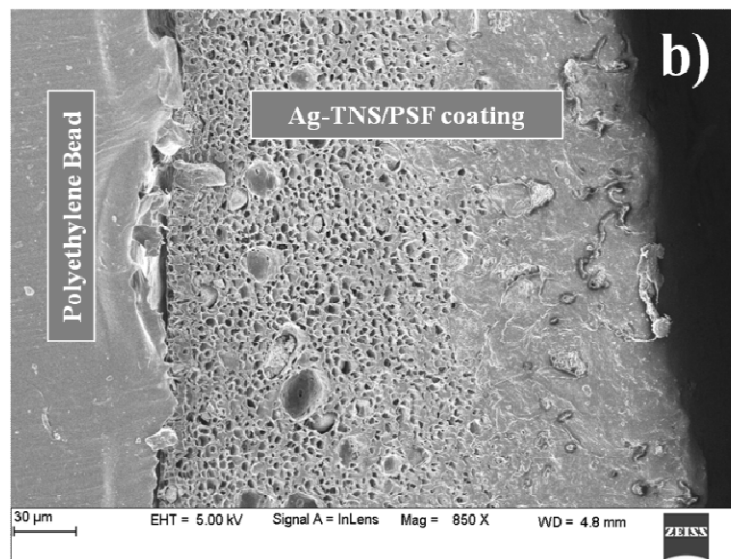


Fig. 9.5 FESEM image a) Ag-TNS/PSF coated bead b) Magnified image of Ag-TNS/PSF coating

9.4.3.1 Dye degradation studies

The schematic representation of dye degradation experiment is given in Fig. 9.6. The Ag-TNS/PSF coated bead floats on the surface of the water and receives maximum solar radiation and air contact. When solar radiation reaches the bead, the photocatalyst gets activated. Electrons and holes get generated, which further react with water to give rise to hydroxyl radical and super oxide radical anion by reacting with dissolved oxygen. These reactive species carry out the degradation process (Kordouli et al. 2015).

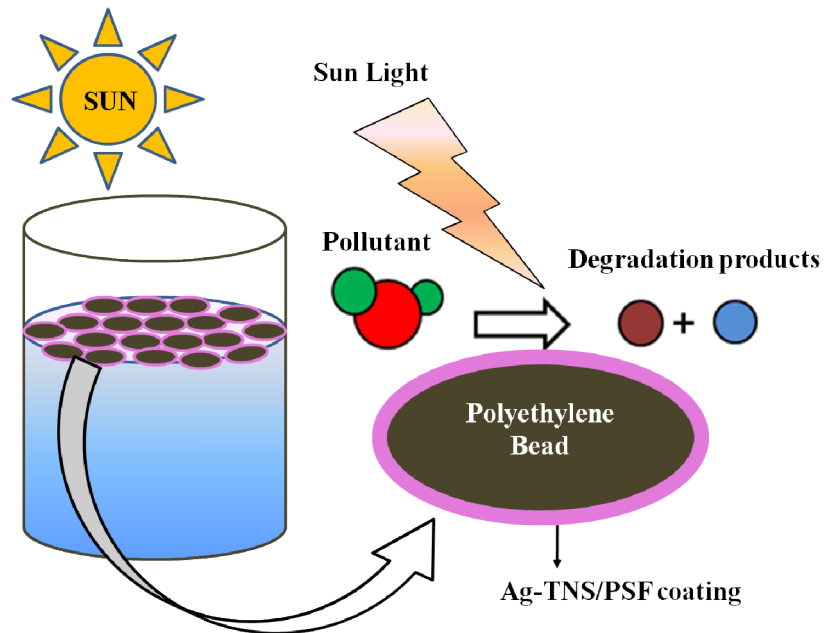


Fig. 9.6 Schematic representation of Ag-TNS/PSF floating photocatalyst

Congo red dye degradation studies at varying concentrations were carried out and the observations are given in Fig. 9.7. It was observed that, at lower Congo red dye concentration of 10 ppm, complete degradation could be achieved in 8 h. When the concentration of dye was increased, the degradation achievable was lesser. 88 % degradation was achieved for 20 ppm dye solution and 74 % in case of 30 ppm. The exposed catalyst surface of the photocatalyst is limited, so degradation performance will decline and more time would be needed with increased concentration of the pollutants. But considering the fact that the pollutant in open water bodies are in much-diluted form and also looking at the energy less and maintenance free aspects, using floating photocatalyst can be a good method for water treatment.

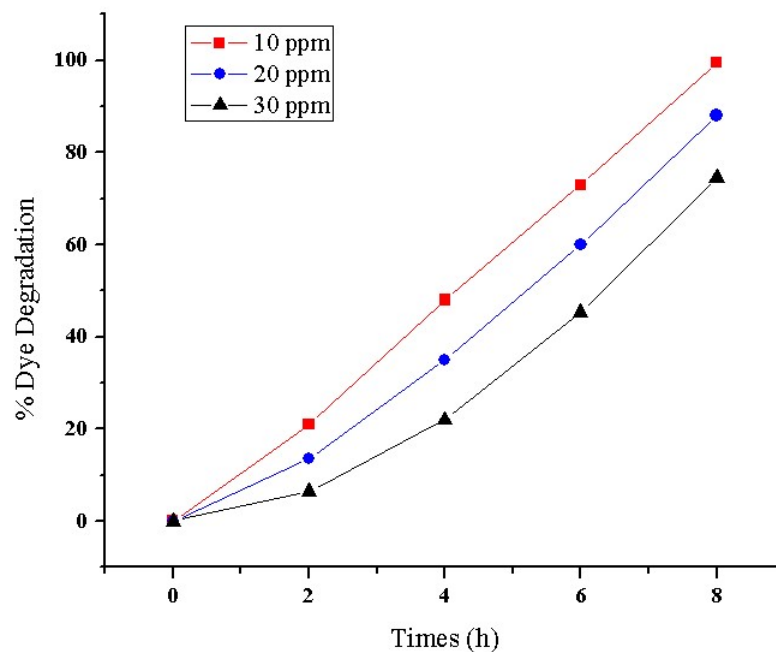


Fig. 9.7. % Dye degradation at different dye concentrations.

5. CONCLUSION

Ag-TNS/PSF was successfully coated on LDPE beads. The coating was found to be unbroken and it held firmly to the LDPE bead. The coating had a porous structure as a result of diffusion of solvents during phase inversion. The Ag-TNS/PSF coated beads showed good dye degradation traits, complete dye degradation of 10 PPM Congo red dye solution could be achieved in 8 hours. 88 % and 74 % dye degradation was observed in case of 20 ppm and 30 ppm dye solutions respectively. Ag-TNF/PSF nanocomposite floating photocatalyst can be a potential energy less solar based approach for water purification.

SUMMARY AND OVER ALL CONCLUSIONS

Various TiO₂ based nanomaterials namely; TiO₂ nanofibers, TiO₂ nanosheets, Ag doped TNF, Ag doped TNS and TNS-GO composite were successfully synthesised, characterized and used for various water purification applications.

TNF/PSF nanocomposite membranes were successfully synthesised. The hydrophilic nature of TiO₂ played a major role in improving the permeate flux and antifouling property. The membrane maximum TNF addition which is with 10 wt% addition showed the highest value of 336.4 Lm⁻²h⁻¹ for pure water flux. The antifouling study showed improved performance with higher TNF concentration. 10 wt% TNF additions showed a maximum FRR of 76%.

- TNS/PSF nanocomposite membranes were synthesised. The additions of TNS showed some remarkable trends in permeate flux. At lower concentrations the flux reduced and improved only after a significant amount of TNS was added. This is a deviation in trend when compared to TNF. This clearly indicates that not only the hydrophilic nature but also the morphology of the nanoadditive has an important role in determining the properties of the composite. Three times rise in PWF was seen at high concentration of TNS addition in S-15 membrane. A maximum of 70.3 % flux recovery was obtained for S-12 membrane. Best results for Congo red rejection were obtained for S-12 and S-15 membranes with dye rejection above 94% and 5 to 6 times increase in permeate flux. S-7 and S-10 membranes were found optimal for Rhodamine-B rejection, with dye rejections above 85% and comparatively higher permeate fluxes.
- Ag-TNF hierarchical photocatalytic membranes were synthesized. Silver doping could significantly improve the photocatalytic activity of TNF. The fibre structure of Ag-TNF enables the easy formation of stable hierarchical membrane. The increase in catalyst loading resulted in a decrease in flux which in turn provided additional time for degradation. Complete degradation of rhodamine B dye was obtained in case of 250 mg Ag-TNF loaded membrane. 250 mg Ag-TNF loaded membrane could maintain dye removal efficiency up to 90.01 % in the third reuse cycle indicating consistent performance and reusability.

- TNS-GO coated hierarchical membranes were successfully. GO sheets when used with TiO₂ exhibited better photocatalytic activity and also the sheet structure of both the materials enabled better mechanical stability to the hierarchical membranes. Synthesised. Although G-400 could completely remove the dye, it exhibited lowest flux and greater dye adsorption. G-100 membrane showed better result with comparatively higher flux 483.5 Lm⁻²h⁻¹ of and better dye removal of 80.1 %. Photocatalyst reuse cycles revealed that higher TNS-GO loaded membranes could maintain dye removal capacity.
- Ag-TNS photocatalytic hierarchal membranes were synthesized. In order to mitigate the additional resistance due to modifier in case GO sheets Ag was used as modifier since it did not cause any significant size increase in the resulting photocatalyst. Therefore Ag-TNS hierarchal membranes exhibited greater permeate flux when compared to GO-TNS. Under UV radiation B-500 showed complete dye removal with an appreciable flux of 86.7 Lm⁻²h⁻¹. Under solar radiation, better result of 63.4 % dye removal in a single pass was observed in case of B-500. Multiple passage studies for optimizing the permeate flux and dye removal indicated an optimum Ag-TNS loading of 200 mg with a flux of 376.8 Lm⁻²h⁻¹.
- Ag-TNS/PSF coated LDPE floating beads was synthesised for photocatalytic applications. The Ag-TNS/PSF coated beads showed good solar dye degradation performance for congo red dye. The degradation performance reduced at higher dye concentration. Under 8 hours solar radiation exposure complete degradation of 10 ppm congo red dye sample was obtained.

SCOPE FOR FUTURE WORK

The synthesis of TiO₂nanomaterials and their application for water purification in various modes have been studied in this work. In a similar way the other nanostructures like nano-thorns, nano-whiskers and so on can also be studied.

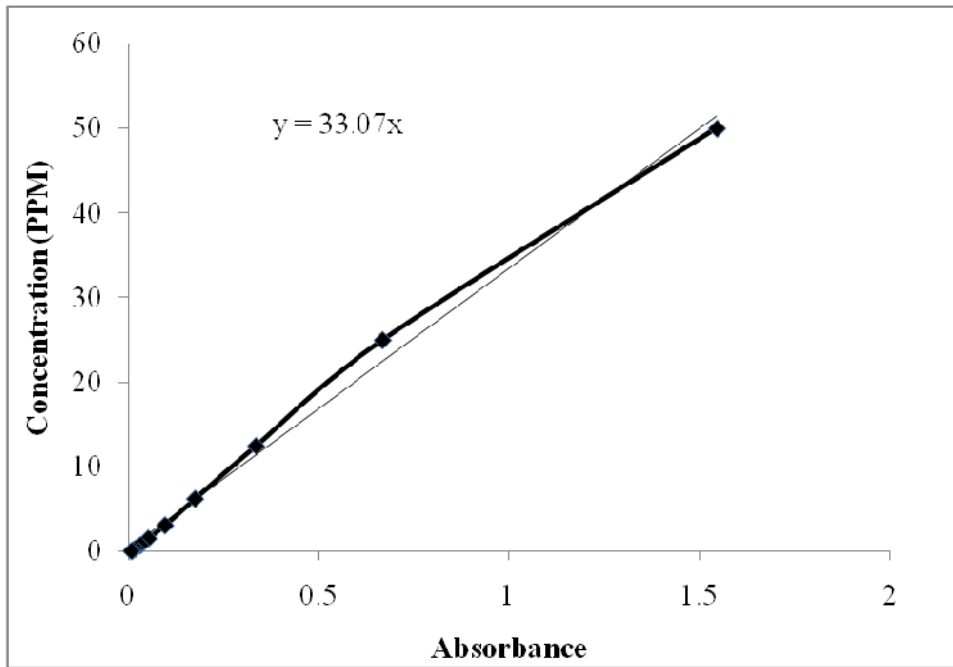
Since shape and morphology of nano-additive greatly influences the performance of nanocomposite membranes, each different nanostructure will produce a different effect in property variation in a polymer matrix. This in itself opens avenues for future research, since there are so many polymers available for study.

Coming to photocatalysis, the performance of the various nanostructures of other photocatalyst material can be studied. Also there is an endless future scope for photocatalytic activity enhancement using various other modifiers.

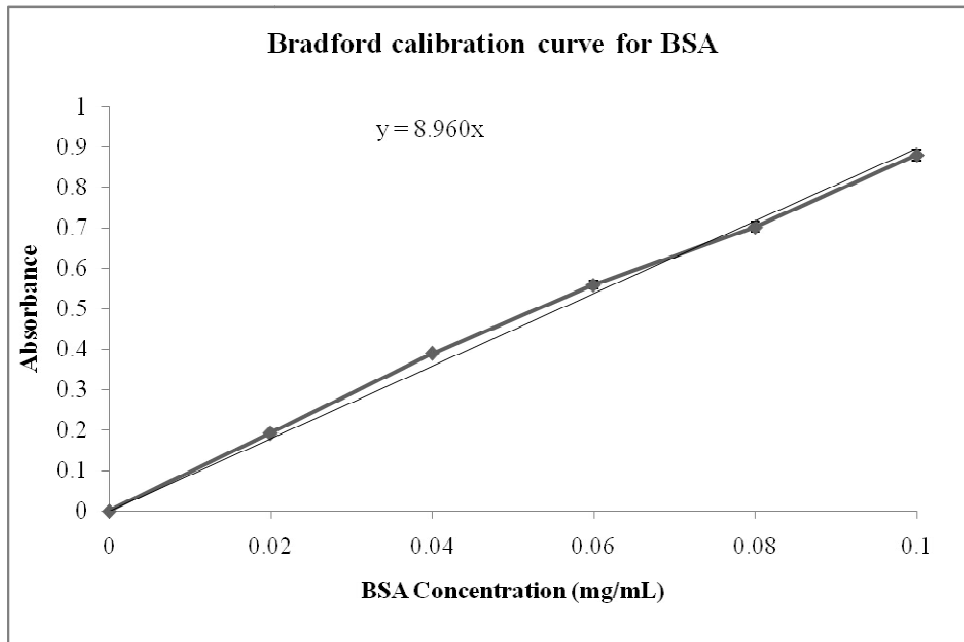
The hierarchical membrane configuration used in this work can be used for other photocatalyst material as well. Also future research can be taken up on embedding of photocatalyst on membrane surface.

APPENDIX-I

CONGO RED DYE CALIBRATION CURVE



APPENDIX-II
BSA CALIBRATION CURVE



REFERENCES

- Ahmad, A. L., Majid, M.A., Ooi, B. S., (2011). "Functionalized PSf/SiO₂ nanocomposite membrane for oil-in-water emulsion separation." *Desalination*, 268, 266–269.
- Ahmad, A. L., Abdulkarim, A. A., Ooi, B. S., Ismail, S. (2013). "Recent development in additives modifications of polyethersulfone membrane for flux enhancement." *Chemical Engineering Journal*, 223, 246-267.
- Akpan, U. G., and Hameed, B. H. (2009). "Parameters affecting the photocatalytic degradation of dyes using TiO₂-based photocatalysts: a review." *J. Hazard. Mater.*, 170(2–3), 520–9.
- Amin, I. N. H. M., Mohammad, A. W. (2015). "Adsorptive fouling of organic solutes simulating sweet water solutions on ultrafiltration membranes." *Chemical Engineering Journal*, 264, 470-478.
- Akbarnezhad, S., Mousavi. S.M. and Sarhaddi, R. (2010). Sol-gel synthesis of alumina-titania ceramic membrane: preparation and characterization." *Indian J. Sci. Technol.*, 3, 1048-1051.
- Alem, A., Sarpoolaky, H. and Keshmiri, M. (2009). "Sol-gel preparation of titania multilayer membrane for photocatalytic applications." *Ceram. Int.*, 35, 1837-1843.
- Alem, A., Sarpoolaky, H. and Keshmiri, M. (2009). "Titania ultrafiltration membrane : Preparation , characterization and photocatalytic activity." *J. Eur. Ceram. Soc.*, 29, 629-635.
- Anderson, M.A., Gieselmann, M.J., and Xu, Q. (1988). "Titania and alumina ceramic membranes." *J. Membr. Sci.*, 39, 243-258.

Arthanareeswaran, G., and Thanikaivelan, P. (2010). "Fabrication of cellulose acetate – zirconia hybrid membranes for ultrafiltration applications : Performance, structure and fouling analysis." *Sep. Purif. Technol.*, 74(2), 230–235.

Bai, H., Liu, Z., and Sun, D. D. (2010). "Hierarchically multifunctional TiO₂nanothorn membrane for water purification." *ChemComm.*, 46, 6542–6544.

Bai, H., and Sun, D. D. (2012). "Hierarchical ZnO nanostructured membrane for multifunctional environmental applications." *Colloids Surf. A Physicochem. Eng. Asp.*, 410, 11–17.

Bai, H., Zan, X., Juay, J., and Delai, D. (2015). "Hierarchical heteroarchitectures functionalized membraneforhigh efficient water purification." *J. Membr. Sci.*, 475, 245–251.

Benfer, S., Popp, U., Richter, H., Siewert, C. and Tomandl, G. (2001). "Development and characterization of ceramic nanofiltration membranes." *Sep. Purif. Technol.*, 23, 231-237.

Bosc, F. and Guizard, C. (2005). "Mesoporous anatase coatings for coupling membrane separation and photocatalyzed reactions." *J. Membr. Sci.*, 265, 13-19.

Bosc, F., Lacroix-desmazes, P. and Ayral, A. (2006). "TiO₂ anatase-based membranes with hierarchical porosity and photocatalytic properties." *J. Colloid Interface Sci.*, 304, 545-548.

Caldeira, L., Vasconcelos, D.C.L., Nunes, E.H.M., Costa, V.C., Musse, A.P., Hatimondi, S.A., Nascimento, J.F., Grava, W. and Vasconcelos, W.L. (2012). "Processing and characterization of sol-gel titania membranes." *Ceram. Int.*, 38, 3251-3260.

Chang, C.H., Gopalan, R. and Lin, Y.S. (1994). "A comparative study on thermal and hydrothermal stability of alumina, titania and zirconia membranes." *J. Membr. Sci.*, 91, 27-45.

Chen, K., Jiang, Z., Qin, J., Jiang, Y., Li, R., Tang, H., and Yang, X. (2014). "Synthesis and improved photocatalytic activity of ultrathin TiO₂ nanosheets with nearly 100 % exposed (001) facets." *Ceram. Int.*, 40(10), 16817–16823.

Debnath, S., Maity, A., and Pillay, K. (2014). "Impact of process parameters on removal of Congo red by graphene oxide from aqueous solution." *J. Environ. Chem. Eng.*, 2(1), 260–272.

Ding, X., Fan, Y. and Xu, N. (2006). "A new route for the fabrication of TiO₂ ultrafiltration membranes with suspension derived from a wet chemical synthesis." *J. Membr. Sci.*, 270(5), 179-186.

Djafer, L., Ayril, A. and Ouagued, A. (2010). "Robust synthesis and performance of a titania-based ultrafiltration membrane with photocatalytic properties." *Sep. Purif. Technol.*, 75, 198-203.

Doke, S. M. and Yadav, G. D. (2014). "Process efficacy and novelty of titania membrane prepared by polymeric sol-gel method in removal of chromium (VI) by surfactant enhanced microfiltration." *Chem. Eng. J.*, 255, 483-491.

Duo, F., Wang, Y., Fan, C., Mao, X., Zhang, X., Wang, Y. and Liu, J. (2015). "Materials Characterization Low temperature one-step synthesis of rutile TiO₂/BiOCl composites with enhanced photocatalytic activity." *Mater. Charact.*, 99, 8-16.

Dipareza, A., Lin, C., and Wu, C. (2008). "Removal of natural organic matter by ultrafiltration with TiO₂-coated membrane under UV irradiation." *J. Colloid Interface Sci.*, 323, 112–119.

Dong, C., He, G., Li, H., Zhao, R., Han, Y., and Deng, Y. (2012). "Antifouling enhancement of poly(vinylidene fluoride) microfiltration membrane by adding Mg(OH)₂ nanoparticles." *J. Memb. Sci.*, 387–388, 40–47.

Fujishima, A., Zhang, X., and Tryk, D. (2008). "TiO₂ photocatalysis and related surface phenomena." *Surf. Sci. Rep.*, 63(12), 515–582.

Ganesh, B. M., Isloor, A. M., Padaki, M. (2012). "Preparation and characterization of polysulfone and modified poly isobutylene-alt-maleic anhydride blend NF membrane." *Desalination*. 287, 103–108.

Ganesh, B. M., Isloor, A. M., Padaki, M. (2012). "Preparation and characterization of polysulfone and modified poly isobutylene-alt-maleic anhydride blend NF membrane." *Desalination*, 287, 103-108.

Gu, Y., Xing, M. and Zhang, J. (2014). "Applied Surface Science Synthesis and photocatalytic activity of graphene based doped TiO₂ nanocomposites." *Appl. Surf. Sci.*, 319, 8-15.

Gude, K., Gun'ko, V. M. and Blitz, J. P. (2008). "Adsorption and photocatalytic decomposition of methylene blue on surface modified silica and silica-titania." *Colloids Surf. A*, 325(1-2), 17-20.

Gupta, S., Bhatiya, D., Murthy, C. N. (2015). "Metal Removal Studies by Composite Membrane of Polysulfone and Functionalized Single-Walled Carbon Nanotubes." *Separation Science and Technology*, 50(3), 421-429.

Gao, P., Liu, Z., Tai, M., Delai, D., and Ng, W. (2013). "Applied Catalysis B: Environmental Multifunctional graphene oxide–TiO₂ microsphere hierarchical membrane for clean water production." *Applied Catal. B, Environ.*, 138–139, 17–25.

Gao, Y., Hu, M., Mi, B. (2014) "Membrane Surface Modification With TiO₂-graphene Oxide for Enhanced Photocatalytic Performance." *J. Membr. Sci.* 455, 349–356.

Gorska, P., Zaleska, A., Kowalska, E., Klimczuk, T., Sobczak, J.W., Skwarek, E., Janusz, W., and Hupka, J. (2008). "TiO₂ photoactivity in vis and UV light: the influence of calcination temperature and surface properties." *Appl. Catal. B: Environ.* 84, 440–447.

Hamid, N. A. A., Ismail, A. F., Matsuura, T., Zularisam, A. W., Lau, W.J., Yuliwati, E., Abdullah, M. S. (2011). "Morphological and separation performance study of polysulfone/titanium dioxide (PSF/TiO₂) ultrafiltration membranes for humic acid removal." *Desalination*, 273(1), 85-92.

Habibpanah, A.A., Pourhashem, S. and Sarpoolaky, H. (2011). "Preparation and characterization of photocatalytic titania-alumina composite membranes by sol-gel methods." *J. Eur. Ceram. Soc.*, 31, 2867-2875.

Ho, S., Kwak, S., Sohn, B. and Hyun, T. (2003). "Design of TiO₂ nanoparticle self-assembled aromatic polyamide thin-film-composite (TFC) membrane as an approach to solve biofouling problem." *J. Membr. Sci.*, 211, 157-165.

Hong, Y., Qin, X. and Yao, G. (2008). "Preparation and properties of supported 100% titania ceramic membranes." *Mater. Res. Bull.*, 43, 1480-1491.

Hu, C., Zhang, X., Li, W., Yan, Y., Xi, G., Yang, H., Li, J., Bai, H. (2014) "Large-scale, ultrathin and(001) facet exposed TiO₂ nanosheet superstructures and their applications in photocatalysis" *J. Mater. Chem. A* 2, 2040-2043.

Kim, J., Lee, K., Effect of PEG additive on membrane formation by phase inversion." *J. Membr. Sci.* 138 (1998) 153–163.

Kordouli, E., Bourikas, K., Lycourghiotis, A., and Kordulis, C. (2015). "The mechanism of azo-dyes adsorption on the titanium dioxide surface and their photocatalytic degradation over samples with various anatase/rutile ratios." *Catal. Today*, 252, 128–135.

Kumar, R., Isloor, A. M., Ismail, A. F., Rashid, S. A., and Al, A. (2013). "Permeation , antifouling and desalination performance of TiO₂ nanotube incorporated PSf/CS blend membranes." *Desalination*, 316, 76–84.

Kumar, R., Isloor, A. M., Ismail, A. F. Matsuura, T. (2013). "Performance improvement of polysulfone ultrafiltration membrane using N-succinyl chitosan as additive." *Desalination* 318 1–8.

Kumar, R., Isloor, A. M., Ismail, A. F., Matsuura, T. (2013). "Synthesis and characterization of novel water soluble derivative of Chitosan as an additive for Polysulfone ultrafiltration membrane" *J. Membr. Sci.* 440, 140–147.

Li, J., Xu, Y., Zhu, L., Wang, J. and Du, C. (2009). "Fabrication and characterization of a novel TiO₂ nanoparticle self-assembly membrane with improved fouling resistance." *J. Membr. Sci.*, 326, 659-666. Li, K. (2007). "Ceramic Membranes for Separation and Reaction." *John Wiley & Sons Ltd*, Chichester, England.

Li, Z., Hou, B., Xu, Y., Wu, D. and Sun, Y. (2005). "Hydrothermal synthesis, characterization, and photocatalytic performance of silica-modified titanium dioxide nanoparticles." *J. Colloid Interface Sci.*, 288(1), 149-54.

Li, Z., Qiu, N. and Yang, G. (2009). "Effects of synthesis parameters on the microstructure and phase structure of porous 316L stainless steel supported TiO₂ membranes." *J. Membr. Sci.*, 326, 533-538.

Liu, L., Bai, H., Liu, J., and Sun, D. D. (2013). “Multifunctional graphene oxide-TiO₂-Ag nanocomposites for high performance water disinfection and decontamination under solar irradiation.” *J. Hazard. Mater.*, 261, 214–223.

Ma, Y., Shi F., Wang, Z., Wu, M., Ma, J., Gao, C. (2012) “Preparation and characterization of PSf/clay nanocomposite membranes with PEG 400 as a pore forming additive.” *Desalination* 286, 131–137.

Ma, Y., Shi, F., Ma, J, Wu, M. M., Zhang, J. , Gao, C. (2011) “ Effect of PEG additive on the morphology and performance of polysulfone ultrafiltration membranes.” *Desalination* 272, 51–58.

Masuda, Y., and Kato, K. (2009). “Synthesis and phase transformation of TiO₂nanocrystals in aqueous solutions.” *J. Ceram. Society Japan*, 117(3), 373–376.

Muhammad, A. S. K., (2015) “Photocatalytic degradation of congo red dye using TiO₂, PANI and PANI/TiO₂ nanoparticles.” M.Tech. Thesis, NITK, Surathkal, India.

Mahmoudi, F., Saljoughi, E. (2013). “Promotion of polysulfone membrane by thermal-mechanical stretching process.” *J. Polym. Res.* 20 (96), 1–10.

Nabe, A. ,Staude, E., Belfort, G., (1997). “Surface modification of polysulfone ultrafiltration membranes and fouling by BSA solutions.” *J. Membr. Sci.* 133, 57–72.

Nair, A. K., Isloor, A. M., Kumar, R., and Ismail, A. F. (2013). “Antifouling and performance enhancement of polysulfone ultrafiltration membranes using CaCO₃ nanoparticles.” *Desalination*, 322, 69–75.

Nakata, K., and Fujishima, A. (2012). “TiO₂ photocatalysis: Design and applications.” *J. Photochem. Photobiol. C Photochem. Rev.*, 13(3), 169–189.

Patterson V.A., Krieg H.M., Kriek R.J., Bisset H.(2006) “Direct synthesis of a titania membrane on a centrifugally casted tubular ceramic support.” *J. Membr. Sci.*, 285, 1–3.

Puhlfürß, P., Voigt, A., Weber, R. and Morbé, M. (2000). “Microporous TiO₂ membranes with a cut off < 500 Da.” *J. Membr. Sci.*, 174, 123-133.

Richards, H. L., Baker, P. G. L., and Iwuoha, E. (2012). “Metal Nanoparticle Modified Polysulfone Membranes for Use in Wastewater Treatment: A Critical Review.” *J. Surf. Eng. Mater. Adv. Technol.*, 2, 183–193.

Reinsch, V. E., Greenberg, A. R., Kelley, S. S., Peterson, R., Bond, L. J., (2000). “A new technique for the simultaneous, real-time measurement of membrane compaction and performance during exposure to high-pressure gas.” *J. Membr. Sci.* 171, 217–228.

Ren, S., Zhao, X., Zhao, L., Yuan, M., Yu, Y., Guo, Y. and Wang, Z. (2009). “Preparation of porous TiO₂/silica composites without any surfactants.” *J. Solid. State. Chem.*, 182(2), 312-316.

Sinha, M. K., Purkait, M. K. (2013). “Increase in hydrophilicity of polysulfone membrane using polyethylene glycol methyl ether.” *J. Membr. Sci.* 437, 7–16.

Santos, T. D., Pacheco, K. A., Poletto, P., Meireles, C. S., Grisa, A. M. C., Zeni, M. (2012). “Effect of cellulose fibers on morphology and pure water permeation of PSF membranes.” *Desalin. Water Treat.* 27, 1–3.

Shi, H., Magaye, R., Castranova, V., and Zhao, J. (2013). “Titanium dioxide nanoparticles: a review of current toxicological data.” *Part. Fibre Toxicol.*, 10(1), 1–33.

Singh, B., Kochkodan, V., Hashaikeh, R., and Hilal, N. (2013). "A review on membrane fabrication: Structure, properties and performance relationship." *Desalination*, 326, 77–95.

Sowmya, A., and Meenakshi, S. (2014). "Photocatalytic reduction of nitrate over Ag–TiO₂ in the presence of oxalic acid." *J. Water Process Eng.*, 8, e23–e30.

Tang, C., Bai, H., Liu, L., Zan, X., Gao, P., Delai, D. (2016). "A green approach assembled multifunctional Ag/AgBr/TNF membrane for clean water production & disinfection of bacteria through utilizing visible light." *Applied Catal. B, Environ.* 196, 57–67.

Tajer-kajinebaf, V., Sarpoolaky, H. and Mohammadi, T. (2014). "Sol-gel synthesis of nanostructured titania-silica mesoporous membranes with photo-degradation and physical separation capacities for water purification." *Ceram. Int.*, 40(1), 1747-1757.

Uddandarao, P., B, R.M. (2016). "ZnS semiconductor quantum dots production by an endophyticfungus *Aspergillus flavus*." *Mater. Sci. Eng. B* 207, 26–32.

Vatanpour, V., Madaeni, S. S., Khataee, A. R., Salehi, E., Zinadini, S., Monfared, H. A. (2012). "TiO₂ embedded mixed matrix PES nanocomposite membranes: Influence of different sizes and types of nanoparticles on antifouling and performance." *Desalination*, 292, 19-29.

Wang, Y. H., Liu, X. Q. and Meng, G. Y. (2007). "Preparation of asymmetric pure titania ceramic membranes with dual functions." *Mater. Sci. Eng. A.*, 446, 611-619.

Wang, Y. H., Tian, T. F., Liu, X. Q. and Meng, G. Y. (2006). "Titania membrane preparation with chemical stability for very harsh environments applications." *J. Membr. Sci.*, 280, 261-269.

Wu, L., Huang, P., Xu, N. and Shi, J. (2000). "Effects of sol properties and calcination on the performance of titania tubular membranes." *J. Membr. Sci.*, 173, 263-273.

Wu, M. C., Sápi, A., Avila, A., Szabó, M., Hiltunen, J., Huuhtanen, M., Tóth, G., Kukovecz, Á., Kónya, Z., Keiski, R., Su, W.-F., Jantunen, H., and Kordás, K. (2011). "Enhanced photocatalytic activity of TiO₂ nanofibers and their flexible composite films: Decomposition of organic dyes and efficient H₂ generation from ethanol-water mixtures." *Nano Res.*, 4(4), 360–369.

Xie, R. C., and Shang, J. K. (2007). "Morphological control in solvothermal synthesis of titanium oxide". *Journal of Materials Science*, 42(16), 6583-6589.

Yang, Y., Wang, P., and Zheng, Q. (2006). "Preparation and properties of polysulfone/TiO₂ composite ultrafiltration membranes." *J. Polym. Sci. Part B Polym. Phys.*, 44(5), 879–887.

Yang, X. H., Li, Z., Liu, G., Xing, J., Sun, C., Yang, H.G., Li, C. (2011). "Ultra-thin anatase TiO₂ nanosheets dominated with {001} facets: thickness-controlled synthesis, growth mechanism and water-splitting properties." *CrystEngComm*, 13(5), 1378-1383.

Yang, Y., Zhang, H., Wang, P., Zheng, Q. (2007). "The influence of nano-sized TiO₂ fillers on the morphologies and properties of PSF UF membrane." *J. Membr. Sci.* 288, 231–238.

Yuan, Z., and Su, B. (2004). "Titanium oxide nanotubes, nanofibers and nanowires." *Colloids Surf., A Physicochem. Eng. Asp.*, 241, 173–183.

Zhang, X., Shi, B., Liu, X. (2012). "Preparation of Polysulfone ultrafiltration membranes modified by silver particles." *Desalin. Water Treat.* 51, 19–21.

Zhang, Q., Gao, L. and Guo, J. (2000). "Effects of calcination on the photocatalytic properties of nanosized TiO₂ powders prepared by TiCl₄ hydrolysis." *Appl. Catal., B.*, 26, 207-215.

Zou, Y., Kang, S. Z., Li, X., Qin, L., Mu, J. (2014). "TiO₂ nanosheets loaded with Cu: A low-cost efficient photocatalytic system for hydrogen evolution from water." *International Journal of Hydrogen Energy*, 39(28), 15403-15410.

PUBLICATIONS FROM THE RESEARCH WORK

JOURNAL PUBLICATIONS

1. Abhinav K. Nair, B. Vinay Kumar, Gopinath Kalaiarasan P.E. JagadeeshBabu, TiO₂ nanosheet incorporated polysulfone ultrafiltration membranes for dye removal, *Desalin. Water Treat.* 107 (2018) 324-331.
2. Abhinav K. Nair, P.E. JagadeeshBabu, (2017), TiO₂ nanosheet-graphene oxide based photocatalytic hierarchical membrane for water purification, *Surf. Coatings Technol.* 320, 259-262.
3. AbhinavK. Nair, P.E. JagadeeshBabu, (2017), Ag-TiO₂ Nanosheet Embedded Photocatalytic Membrane for Solar Water Treatment, *J. Environ. Chem. Eng.* doi.org/10.1016/j.jece.2017.07.046
4. AbhinavK. Nair, P.M. Shalin, P.E. JagadeeshBabu, (2016), Performance enhancement of polysulfone ultrafiltration membrane using TiO₂ nanofibers, *Desalin. Water Treat.* 57 (23), 10506-10514.
5. Abhinav K. Nair, P.E. JagadeeshBabu, Ag-TiO₂ nanofiber membranes for photocatalytic degradation of dyes, *Adv. Sci. Lett.* 24 (2018) 5764-5767.
6. S.D. Neelapala, A.K. Nair, P.E. JagadeeshBabu, (2017), Synthesis and characterization of TiO₂nanofibre/cellulose acetate nanocomposite ultrafiltration membrane, *J. Exp. Nanosci.*, 8080 doi:10.1080/17458080.2017.1285446.
7. S.S. Kola, A. K. Nair, P.E. JagadeeshBabu, (2017), Synthesis and characterization of silver decorated polysulfone/cellulose acetate hybrid ultrafiltration membranes using functionalized TiO₂ nanoparticles, *Desalin. Water Treat.*, 76 112-120.

BOOK CHAPTER

1. AbhinavK. Nair, V.K. Bandaru, and P.E. JagadeeshBabu. (2016), Photocatalytic Degradation of Congo Red Dye Using Silver Doped TiO₂ Nanosheets' *Recent Advances in Chemical Engineering*, Springer doi: 10.1007/978-981-10-1633-2_23.

MANUSCRIPTS UNDER PROCESSING

1. Manuscript entitled 'Ag-TiO₂ Nanosheet/Polysulfone Nanocomposite Floating Photocatalysts for Solar Degradation of Pollutants. (Under Preparation)

CONFERENCE PRESENTATIONS

1. Presented a paper titled 'Ag-TiO₂ nanosheet photocatalytic hierarchical membrane for water treatment' in the *69th Chemical engineering Congress (Chemcon-2016)* organized by the Indian Institute of Chemical Engineers (IIChe), Chennai Regional Centre, Chennai, (December, 2016).
2. Presented a paper titled 'Ag-TiO₂ nanofiber membranes for photocatalytic degradation of dyes' in the *International Conference on Nanoscience and Nanotechnology* organized by the Center for Nanotechnology, Vellore Institute of Technology, Vellore (October, 2016).
3. Presented a paper titled 'TiO₂ nanosheet-graphene oxide based photocatalytic hierarchical membrane for water purification' in the *International Conference on Technological Advances of Thin Films and Surface Coatings (Thinfilms-2016)* organized by the Thinfilm society, Nanyang Technological University (NTU), Singapore (July, 2016).
4. Presented a paper titled 'Photocatalytic degradation of congo red dye using silver doped TiO₂ nanosheets' in the *International conference on advances in chemical engineering, organized by the Department of Chemical engineering, National Institute of Technology Karnataka, Surathkal* (December, 2015).

BIODATA

ABHINAV K NAIR

Email ID: akn2411@gmail.com

Contact no: +91-8792706002

Current position: Assistant Professor, Department of Chemical Engineering, Amal Jyothi College of Engineering, Kottayam, Kerala

Educational qualification:

- Ph.D. (Pursuing) in Chemical Engineering, 2013-2018 (Expected)
Department of Chemical Engineering,
National Institute of Technology Karnataka,
Surathkal, Mangalore, Karnataka.
- M.Tech in Nanotechnology (CGPA – 7.75), 2011-2013
National Institute of Technology Karnataka,
Surathkal, Mangalore, Karnataka.
- B.Tech in Chemical Engineering (66%), 2005-2009
Government Engineering College, Kozhikode
Calicut Dist. Kerala

Research papers published:

1. Abhinav K. Nair, P.E. JagadeeshBabu, TiO₂ nanosheet-graphene oxide based photocatalytic hierarchical membrane for water purification, *Surf. Coat. Technol.*, (2017) doi:10.1016/j.surfcoat.2017.01.022.
2. Abhinav K. Nair, P.E. JagadeeshBabu, Ag-TiO₂ Nanosheet Embedded Photocatalytic Membrane for Solar Water Treatment, *J. Environ. Chem. Eng.* (2017) doi.org/10.1016/j.jece.2017.07.046.
3. Abhinav K. Nair, P.E. JagadeeshBabu, Ag-TiO₂ nanofiber membranes for photocatalytic degradation of dyes, *Adv. Sci. Lett.* 24 (2018) 5764-5767..
4. Abhinav K. Nair, B. Vinay Kumar, Gopinath Kalaiarasan P.E. JagadeeshBabu, TiO₂ nanosheet incorporated polysulfone ultrafiltration membranes for dye removal, *Desalin. Water Treat.* 107 (2018) 324-331.
5. S.S. Kola, Abhinav K. Nair, P.E. JagadeeshBabu, Synthesis and characterization of silver decorated polysulfone/cellulose acetate hybrid ultrafiltration membranes using functionalized TiO₂ nanoparticles, *Desalin. Water Treat.*, 76 (2017) 112-120.
6. S.D. Neelapala, Abhinav K. Nair, P.E. JagadeeshBabu, Synthesis and characterization of TiO₂nanofibre/cellulose acetate nanocomposite ultrafiltration membrane, *J. Exp. Nanosci.*, 8080 (2017) doi:10.1080/17458080.2017.1285446.

7. Abhinav K. Nair, P.M. Shalin, and P.E. JagadeeshBabu, Performance Enhancement of Polysulfone Ultrafiltration Membrane using TiO₂ Nanofibers, *Desalin. Water Treat.*, 57, (2015) 10506-10514.
8. Abhinav K. Nair, Arun M. Isloor, Rajesha Kumar, and Ahmad Fauzi Ismail, Antifouling and performance enhancement of polysulfone ultrafiltrationmembranes using CaCO₃nanoparticles, *Desalination*, 322, (2013) 69-75.

Achievements:

- Recipient of ITS-SERB (International Travel Support funding) from Science and Engineering Research Board, Department of Science and technology (DST), GOI.
- Recipient of Best Paper Award for paper presentation in the 69th Chemical engineering Congress (Chemcon-2016).

Personal Details:

Father's name : Krishnan P Nair
Date of birth : 24 November, 1987
Gender : Male
Nationality : Indian
Permanent address :Chaithram, near arpanthode railway gate, P.OChirakkal R.S, Kannur, Kerala, India Pin- 670011

Declaration:

I hereby declare that the above particulars are true to the best of my knowledge.

Place: Surathkal, India

Date: 24.09.2018

Abhinav K Nair